TABLE OF CONTENTS

Page

LIST OF TABLES

Page

LIST OF FIGURES

Page

LIST OF ABBREVIATIONS

3P3W	Three-phase three-wire system
3P4W	Three-phase four-wire system
AC	Alternating current
AF	Active filter
ANSI	American National Standards Institute
APF	Active power filter
ASDs	Adjustable speed drives
CSAF	Current source active filters
CSC	Current source converter
CSI	Current source inverter
CT	Current transformer
DC	Direct current
DQ	Synchronous reference frame
EPLL	Enhanced phase locked loop
FLL	Frequency locked loop
FMV	Filter Multi-variable
GDT	Gas discharge tube
GTO	Gate turn-off thyristor
IDMT	Inverse Definite Minimum Time
IEEE	Institute of Electrical and Electronics Engineers
IEC	International Electrotechnical Commission

IGBT	Insulated gate bipolar transistor
MIMO	Multiple-input and multiple-output system
MOV	Metal oxide varistor
OCR	Overcurrent relay
PCC	Point of common coupling
PI	Proportional integral
PLL	Phase-locked loop
PQ	Instantaneous reactive power theory
PWM	Pulse width modulation
rms	Root mean square
SAF	Shunt active filters
SAPF	Shunt active power filter
SF6	Sulfur hexafluoride
SISO	Single input and single output system
SMC	Sliding mode control
SOGI	Second order generalized integrator
SPWM	Sinusoidal pulse width modulated
SPD	Surge Protection Devices
SRF	Synchronous reference frame
THD	Total harmonic distortion
TVSS	Transient Voltage Surge Suppressors
UPQC	Unified power quality conditioner
UPS	Uninterruptable power supplies

VSAF	Voltage source active filters
VSC	Voltage source converter
VSI	Voltage source inverter
ZnO	Zinc oxide

LIST OF SYMBOLS

a,b,c	Axes of the ‘abc’ plane
d,q	Direct axis, axis in quadrature of the synchronous rotating plane ‘dq’
$C_{plane-y}^{plane-x}$	Matrix transformation of coordinates of plan x to plan y
ω	Fundamental electric pulsation, rad/sec
η	Internal dynamics parameter
τ_n	Individual harmonic rate n
σ	Switching function
C	Capacitor of the active filter
C_k	Modulation function of leg k of the converter
d_{nk}	Sequential function of the k-axis
f	Fundamental frequency, Hz
h	Harmonic component
i	Instantaneous current , A
I	Average value of i, A
Î	Peak value of i, A
i_{dc}	DC side current of source current type active filter, A
K	Gain, Constant
N	Neutral point of the source
P	Average active power, W
p	Instantaneous active power, W
Q	Average reactive power, VAR

q	Instantaneous reactive power, VAR
S	Apparent power, VA
s	Complex operator of the Laplace transformation
t	Time, sec
v	Instantaneous voltage, V
Vdc	DC bus voltage of the active filter, V
x^*	Reference value of variable x
$\tilde{x}$	Error value of variable x
$\bar{x}$	Stationary plane vector
$\bar{x}^e$	Rotating plane vector
X	Reactance
Z	Impedance

INTRODUCTION

In recent years the subject of power quality has been a major concern since the introduction of power electronics. According to the international standards, power quality is identified as "the physical characteristics of the electrical supply provided under normal operating conditions that do not disrupt or disturb the user's processes" (Khadkikar, 2008). The proliferation of power electronics employed in many harmonics producing loads; deteriorate the quality of power in distribution systems, and more severely at the end users network. Typical examples of such loads include household appliances, office equipment and computers, in addition to adjustable speed drives (ASDs), uninterruptible power supplies (UPS), arc furnaces at the industrial level. The generated harmonic currents from these converters cause malfunction of protection systems, equipment overheating, noise, vibration and interference with communication systems. As a result and in order to alleviate the harmonic pollution in the power system, the IEEE (Institute of Electrical and Electronics Engineers) and IEC (International Electrotechnical Commission) have introduced regulating guidelines and standards IEEE 519 and IEC 61000 to govern the accepted limits of injected harmonics.

A number of mitigation techniques have also been developed to reduce harmonics and improve the power quality. These include passive filters, active filters (AF), universal power quality conditioner (UPQC) and hybrid filters. Passive filters are widely utilized and considered a viable solution due to their simplicity, high efficiency and low cost.

Generally, passive filters are used to compensate harmonic currents and reactive power of the AC network. Passive elements such as inductors and capacitors are tuned to the system impedance where they are intended to be installed to reduce harmonics. In fact, passive filters are designed to shunt harmonics or block them from flowing through the power system by providing low impedance paths for specific harmonic frequencies. However, passive filtering performance has limitations, that they cannot be adjusted once they are tuned and installed in a system, and hence cannot react instantaneously to varying load conditions.

The change in operating conditions of the system may result in detuning of the filter, which could cause additional distortion. Moreover, a common problem of passive shunt filtering is that they resonate with the supply system as a result of the change in the load impedance. However, most of the problems related to the drawbacks of the passive filter could be addressed by using active filtering.

Thanks to the advances in power electronics, active power filters have now become an alternative to passive harmonic filtering. The existing active harmonic filters have a remarkable filtering performance, unlike conventional passive filters. Active filters are actively capable of providing compensation for current related distortions represented in harmonic currents, reactive power, and neutral current. AFs are also applied to eliminate voltage harmonics, regulate voltage, improve voltage balance and voltage flicker suppression.

Active filters can be classified based on the supply system in single phase and three phase three-wire (3P3W) or four-wire (3P4W) active filters. Single phase configuration is used to compensate power quality issues of single-phase loads, such as household appliances, DC power supplies, fluorescent lights, and office equipment. Whereas three-phase active filters are employed for three-phase nonlinear loads such as adjustable speed drives (ASDs) and AC/DC converters.

Moreover, active filters are classified according to the converter type. Active filters employ either current source inverter (CSI) using inductive storage element or voltage source inverter (VSI) with a DC capacitor. The voltage source inverter has become more dominant and it is more favored than the current source inverter due to its cost, size and efficiency (Akagi, 2005). Many configurations such as shunt (parallel) active filters (SAF), series active filters, unified power quality conditioners (UPQC) that uses a combination of both, and hybrid filter which is a combination of active series and passive shunt, have been developed and are commercially available for many applications.

Shunt active filters are among the most widely used to compensate for current harmonics and reactive power of nonlinear loads. Whereas series active filters are used to remove voltage harmonics and to regulate and balance terminal voltage. The UPQC is considered the optimum solution to provide compensation for both current and voltage harmonics. However hybrid filters are more popular in harmonic filtering due to their feasibility and low cost. Many control schemes are used in the AFs both in the frequency domain and time domain, such as Fourier series analysis, instantaneous reactive power *pq* theory, synchronous *dq* reference frame, sliding mode controller and PI controller, etc.

Nowadays, shunt active filters are among the most commonly used types of active power filters. The shunt active filter topology is ideal for the compensation of current related harmonics. As the name implies the shunt active filter is connected in parallel across the nonlinear load or across the point of common coupling (PCC), it is usually compromised of an IGBT based voltage source converter (VSC) controlled by a pulse width modulation PWM current control. With appropriate control algorithm, it can determine in real time the compensating reference current which makes the converter act dynamically and tracks load variations. It generates equivalent compensating currents, that are opposite in phase to cancel the harmonics of the nonlinear load at the PCC, so the load current becomes sinusoidal.

Since the active power filters are extensively utilized in many industrial applications, their reliability becomes extremely important. As such a protection scheme is developed for three phase three wire shunt active filter. The proposed protection system is intended to protect shunt active filters when faults occur.

The work presented in this project concerns particularly the development of a design procedure, control, safe operation mechanism and a fault protection scheme for a three-phase shunt active filter to eliminate harmonics. This thesis is organized as follows:

In the first chapter, presentation of a literature review for different harmonic mitigation techniques, active filter topologies and control, and the different faults and protection of active filter is provided.

The second chapter analyzes the modeling of a three phase three wire voltage source based shunt active filter, using nonlinear control system design with anti-windup PI controller, In addition to a study of the stability of the control system.

In the third chapter design procedures showing the selection of filter's various power components such as the link inductor, DC bus voltage, and DC bus capacitor are included.

The fourth chapter covers the application of the different protection methods and a presentation of the simulation results, which allows the validation of the proposed protection scheme. Finally, the project is concluded with a general conclusion about simulation results.

CHAPITRE 1

LITERATURE REVIEW

1.1 Introduction

The mitigation of current and voltage harmonics in distribution power systems has always been a significant concern following the power electronics introduction. Harmonics could create many problems for both end users and utilities. The generated harmonic currents can cause overheating of equipment, malfunction of protection systems and potential damage of several electronic types of equipment. In order to overcome the harmonic pollution associated problems, many filtering solutions and mitigation techniques have been developed.

1.2 Background

The increasing use of power converters and harmonic producing loads in both residential and commercial installations is known to contribute a considerable deterioration in the electrical power quality. Despite the advantages obtained in employing converter based equipment to process power flow, the use of power electronic devices has a significant drawback. These converters draw distorted (non-sinusoidal) currents from the power system, which causes serious issues for utility interface, in addition to degradation of power quality. These harmonic distortions could be particularly damaging to both the load side and to the utility. Hence, harmonics generated by nonlinear loads have become a major issue. The harmonic distortion sources in power systems can be categorized into two types:

1.2.1 Nonlinear loads of Current source type

Thyristor controlled converter loads are a typical source of harmonic currents. The operation of such loads generates harmonic currents at the grid side of the rectifier. The distortion of the current waveform is a direct result of switching. These nonlinear loads behave like a current source type of load. Therefore, it is defined as a current source nonlinear load and generally modeled as a current source.

1.2.2 Nonlinear loads of Voltage source type

The other source of harmonics is a diode rectifier with DC bus capacitor. Such loads generate voltages on the supply side of the rectifier for their operation. Harmonic currents on the grid are caused because of harmonic voltages, which are determined by the impedance of the grid. Therefore, the diode rectifiers behave like a voltage source, rather than a current source.

1.2.3 Harmonic standards

Due to the increase of power electronic based equipment used in power systems, several international organizations have established limits on the amplitude of the injected harmonic current into the distribution system to maintain the quality of power. These standards and measures identify the limits and level of harmonic voltage and current disturbances at different frequencies of harmonics. The most renowned are IEEE-519 standards in North America and IEC-61000-3 in Europe. The IEC-61000-3-2 describes the general requirements for harmonic current emissions and voltage fluctuations of equipment connected to the supply with line currents lower than 16A per phase. For the purpose of harmonic current limitation, the standard IEC 61000-3-4 is applied for line currents greater than 16A per phase.

The IEEE 519-1992 recommended practice covers the problem of harmonic distortion at the point of common coupling (PCC) for power systems with nonlinear loads as shown in table 1.1 and 1.2. The harmonic limits of IEC 61000-3 are based on product level at the terminals of end-user equipment while those of IEEE 519 are based on the interactions between facilities and the public distribution system. To meet the terms of the IEC standard, equipment design is often involved. However, complying with the IEEE recommendations could be accomplished using filters and active filters in particular. The main reason for these harmonic standards which are still evolving is to limit harmonic emissions from electronic equipment in order to protect other loads and components of the power system (IEEE Recommended Practices and Requirements for Harmonic Control in Electrical Power Systems, 1993);(Standard, 2004);(Kim, 2002);(Haddad, 1996).

Table 1.1 IEEE 519 harmonic current limits

I_{SC}/I_{L1}	h <11	11 ≤ h< 17	17 ≤ h < 23	23 ≤ h < 35	35 ≤ h	THD (%)
< 20	4.0	2.0	1.5	0.6	0.3	5.0
20 - 50	7.0	3.5	2.5	1.0	0.5	8.0
50 - 100	10.0	4.5	4.0	1.5	0.7	12.0
100 - 1000	12.0	5.5	5.0	2.0	1.0	15.0
> 1000	15.0	7.0	6.0	2.5	1.4	20.0

Table 1.2 IEEE 519 voltage distortion limits

Bus voltage at PCC	Maximum individual Harmonic component (%)	Maximum THD (%)
69kV and below	3.0	5.0
69.00kV through 161kV	1.5	2.5
161.00kV and above	1.0	1.5

1.3 Harmonic Filtering Solutions

Harmonic filtering involves the selective absorption of undesired harmonic currents generated by non-linear loads. The two basic harmonic filtering techniques are passive filtering and active filtering. These two techniques are also combined to form various hybrid active filter solutions.

1.3.1 Passive filtering

Shunt passive filtering is still the most dominant and cost-effective technology, in spite of their serious drawbacks (Bhattacharya, 2003). Passive filters use reactors and capacitors to stop the flow of harmonic currents into the power system by means of creating a low impedance path in order to divert them using a parallel passive filter, or by creating a high series impedance to block them using a series passive filter, so as to provide sinusoidal currents from the utility. Therefore, they are used to reduce voltage distortion resulting due to non-linear loads, and they are also effective in improving power factor. However, there are some concerns in the use of passive filtering. Such as series and parallel resonance with grid impedance could increase the harmonic voltage and current at specific frequencies. Additionally, the harmonic mitigation is dependent on the source impedance and is not decided only by the passive filter (Haddad, 1996).

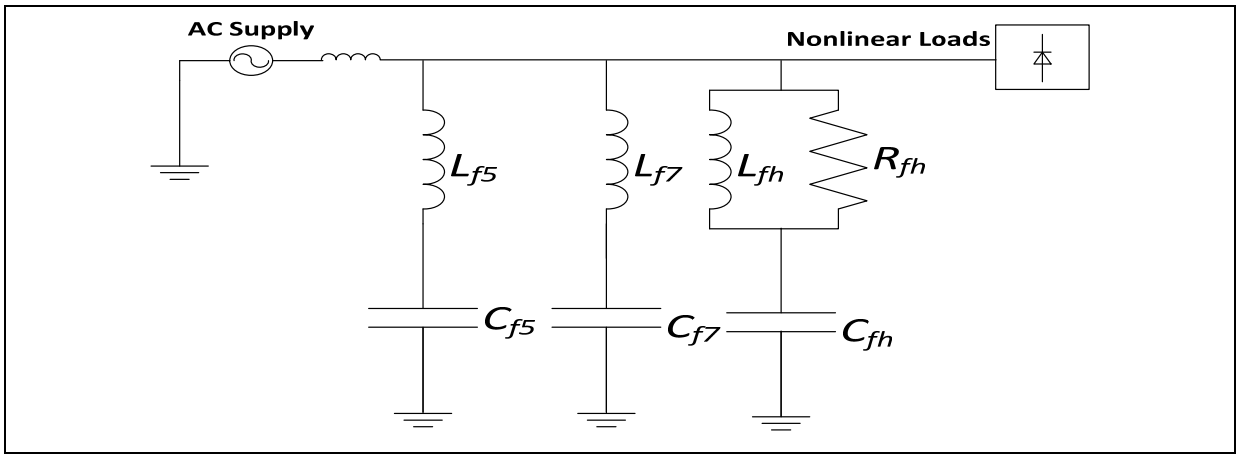

Figure 1.1 Tuned passive harmonic filters

Moreover, the passive filter cannot adapt to changing load harmonics and reactive power requirement. To compensate for major harmonics (e.g. 5^{th} , 7^{th} , 11^{th} , 13^{th} , etc.), several separate passive filters may be required as shown in figure1.1(Kim, 2002). Furthermore, with the extensive usage of nonlinear loads, the harmonic reference extraction is not effectively accomplished. Besides, resonance conditions are more likely increased with more connected filtering elements. Therefore, the conventional use of tuned passive filters has limited effectiveness. Hence, active filtering has been developed to take control of the complications related to passive filtering.

1.3.2 Active filtering

Active filtering solutions have recently emerged as popular techniques to remove current harmonics. They have reduced size and could offer further solutions to issues of power quality, such as correction of power factor, load balancing, reduction of voltage flicker and regulation, harmonic damping and harmonic isolation (Hasan et Mahedi, 2013). Different configurations of active filters for different systems have been reported in the literature.

1.4 Active power filter topologies

Several active harmonic filtering solutions such as shunt, series, and hybrid active power filters, are reviewed and their advantages and disadvantages are discussed. The active power filter can be connected to the point of common coupling (PCC) either in series or in parallel. Active filters can be classified according to their topology, voltage source and current source. Current source active filters use inductive element for DC energy storage. Whereas voltage source active filters employ a DC capacitor for the energy storage. VSAFs are light in size, not costly, and can be controlled with ease compared to CSAFs. In addition, active filters can be classified on the basis of grid system such as single-phase or three-phase, three wire or four wire.

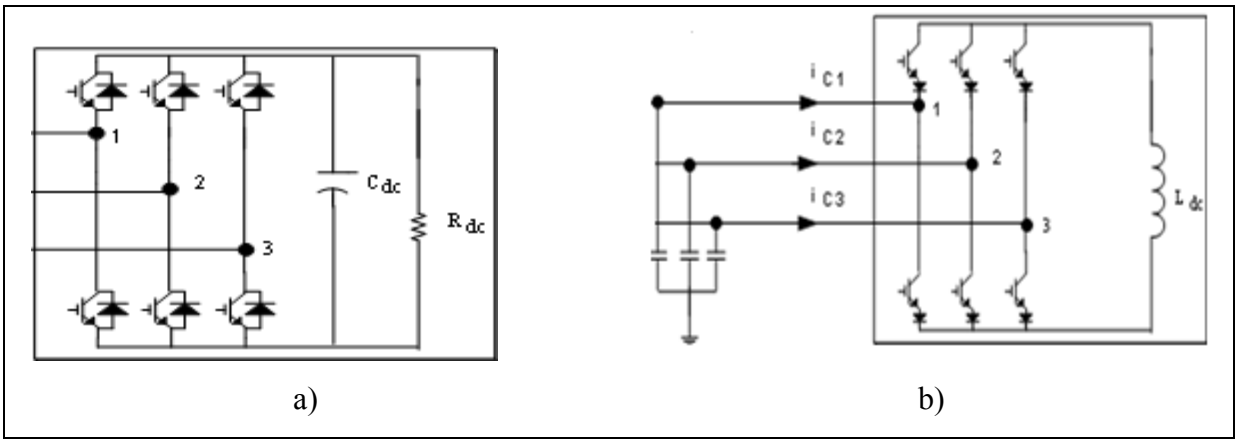

Figure 1.2 a) PWM voltage source inverter, b) PWM current source inverter

Figure 1.2.a illustrates a Pulse Width Modulation (PWM) Voltage Source Inverter (VSI) with a DC bus capacitor and Figure 1.2.b illustrates a PWM Current Source Inverter (CSI) with a DC link inductor. The VSI utilizes IGBTs with anti-parallel diodes, while CSI utilizes IGBTs with series connected diodes for reverse-blocking capability, which have higher conduction and switching losses than IGBTs with antiparallel diodes. Moreover, the DC link inductor for the CSI makes the inverter more bulky and costly compared to the DC bus capacitor for the VSI. The protection circuitry for CSI is more complicated than the one of VSI. Therefore, VSIs are more efficient, more cost-effective, and smaller in size compared to CSIs (Özkaya, 2007).

1.4.1 Shunt active power filter

Shunt active filter (SAPF) shown in Figure 1.3, is the most common style of active filters. These filters work as a current controlled source that is installed in parallel with the nonlinear load. SAPFs are capable to provide the required harmonics by the load; as such the main supply provides only sinusoidal currents.

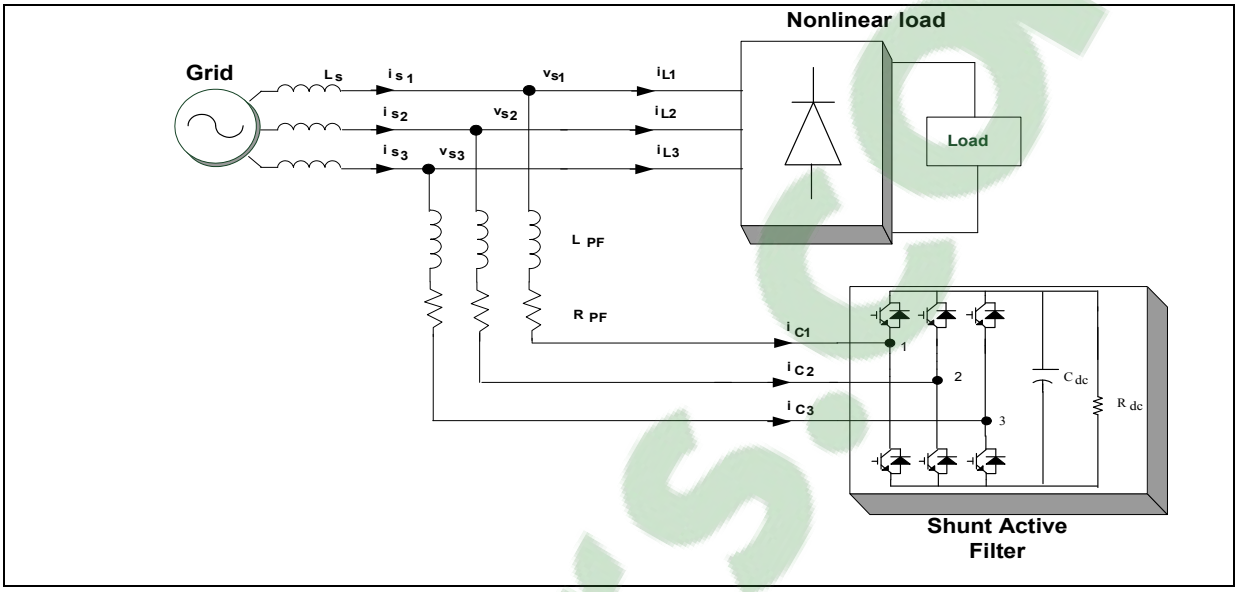

Figure 1.3 Shunt active filter

The main section of the active power filter shown in Figure 1.3 is a force commutated voltage source inverter connected to a DC capacitor. Current harmonic compensation is achieved by generating equivalent but opposite in phase current harmonic components at the PCC, thereby eliminating the harmonic distortion and enhancing the power quality of the power system (Morán, Dixon et Wallace, 1995).

1.4.2 Series active power filter

The series active power filters can also be classified as a single phase or three phase and employs current or voltage source inverters. It is used to compensate voltage type harmonics. Figure 1.4 shows the circuit diagram of a series active filter. This type of filter is connected in series with the AC distribution network and compensates for both the harmonic currents generated by the nonlinear loads and the voltage distortion existed on the AC system (Kim, 2002). Series active power filters are less common due to the main drawback of series circuits in that the transformer must be designed for full load current, which increases their current rating considerably as compared with a shunt active filter. In addition, the coupling transformer can produce a considerable over-voltage with the short circuit on the load side.

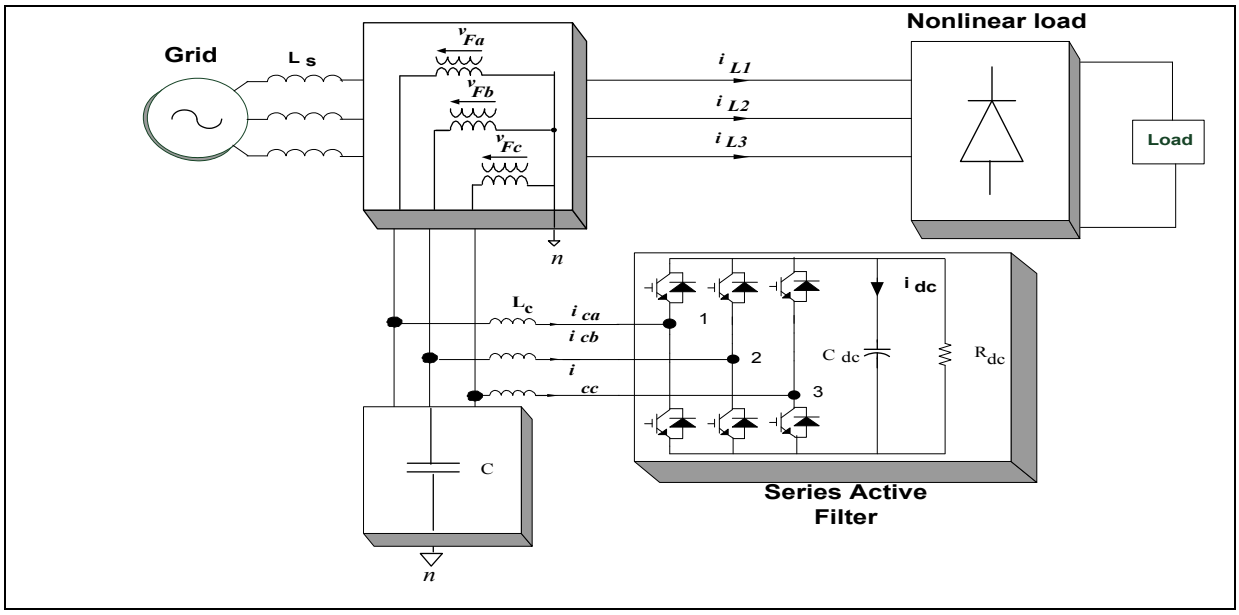

Figure 1.4 Series active filter

1.4.3 Hybrid active power filter

Hybrid active power filters combine passive and active filters in various configurations in order to decrease the value of the filter and to increase the efficiency and reduce active filter rating. The basic principle of hybrid filtering is to improve the filtering capacity of a passive filter and to damp series and parallel resonances with a small rated active filter. Generally, the passive filter is set at a certain frequency to eliminate that frequency and decrease the power capacity of the active filter. The used shunt passive filters have to be of the high-pass type to remove the switching frequency of the active filter and high-order harmonics (Haddad, 1996);(Emadi, Nasiri et Bekiarov, 2004).

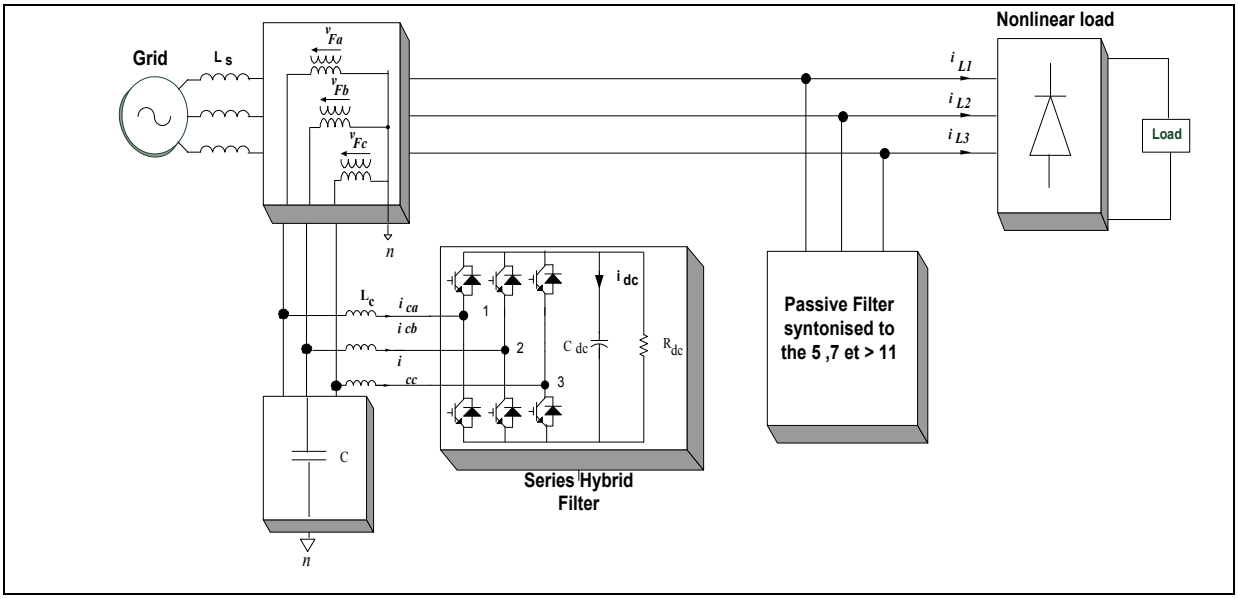

Figure 1.5 Series hybrid filter

1.5 Active power filter control techniques

Several control systems have been designed, developed, and realized for active filters. Compensation of harmonics can be accomplished in the time domain or frequency domain. In time domain the control algorithms are based on the calculation of an instantaneous error function, while frequency domain control uses Fourier analysis of the distorted current or voltage signals. There are several methods of time domain control techniques applied for active power filters control such as the instantaneous active and reactive power 'pq' theory, synchronous dq reference frame, nonlinear control, PI control, sliding mode control to name a few. Similarly, there are also a number of frequency domain control strategies such as Fourier based harmonic extraction methods, Kalman filter control, wavelet transformation theory and others. Using Fourier transformations in the control of active power filters requires substantial computation and has a sluggish response time. Therefore, time domain control strategies are preferable for real-time control of active power filters (Singh, Al-Haddad et Chandra, 1999). The control strategies mentioned above are all employed for the control of APFs. However, for brevity, only some of time domain techniques are discussed hereafter.

1.5.1 PQ direct Control

The instantaneous reactive power theory developed by (Akagi, Kanazawa et Nabae, 1983) shown in figure 1.6 below is based on Clarke transformation of the three phase voltages and currents. The instantaneous active and reactive power could be calculated as transformed voltages and currents. Using low pass and high pass filters, the harmonic active and reactive powers can be extracted from instantaneous active and reactive powers.

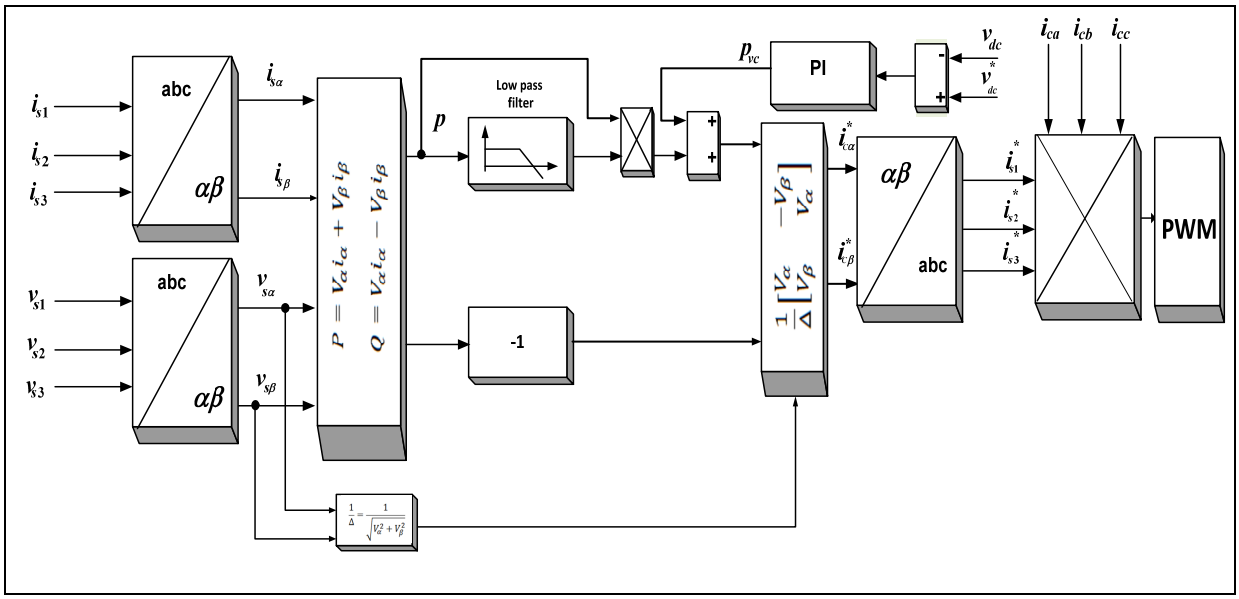

Figure 1.6 Control of SAPF using PQ direct control

1.5.2 Synchronous reference frame control

In the synchronous '*dq'* reference frame control strategy as shown in figure 1.7, the load currents are transformed from the *'abc'* stationary reference frame to the '*dq0'* synchronously rotating frame using the Park's transformation. The DC link voltage is measured as feedback to maintain a constant DC bus. In addition, a phase-locked loop (PLL) is applied to sync the signals with the grid voltages. Using low-pass filters the DC components (i_{ld}, i_{lq}) are extracted from '*dq'* current components. As such the AC quantities (harmonics) are removed from the reference signals.

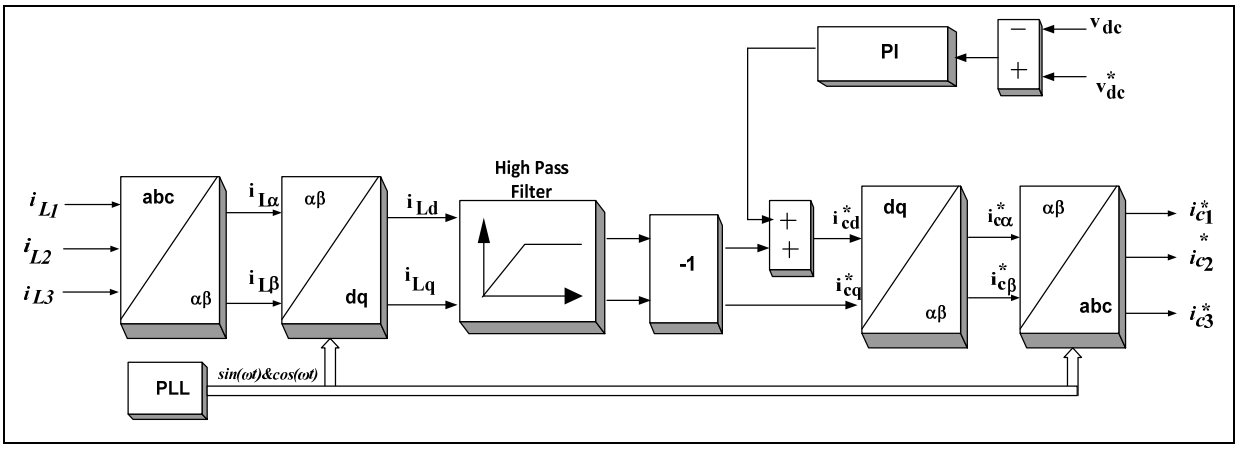

Figure 1.7 SRF 'dq' based control

1.5.3 Indirect control

In the indirect control approach, the three-phase supply voltages are measured and the DC bus of the active power filter is kept regulated to estimate the reference values for the magnitudes of the source currents. With the help of PI voltage controllers, the amplitude of the in-phase components of reference supply currents is estimated. In subtracting load currents from reference supply currents, the compensation commands can be derived.

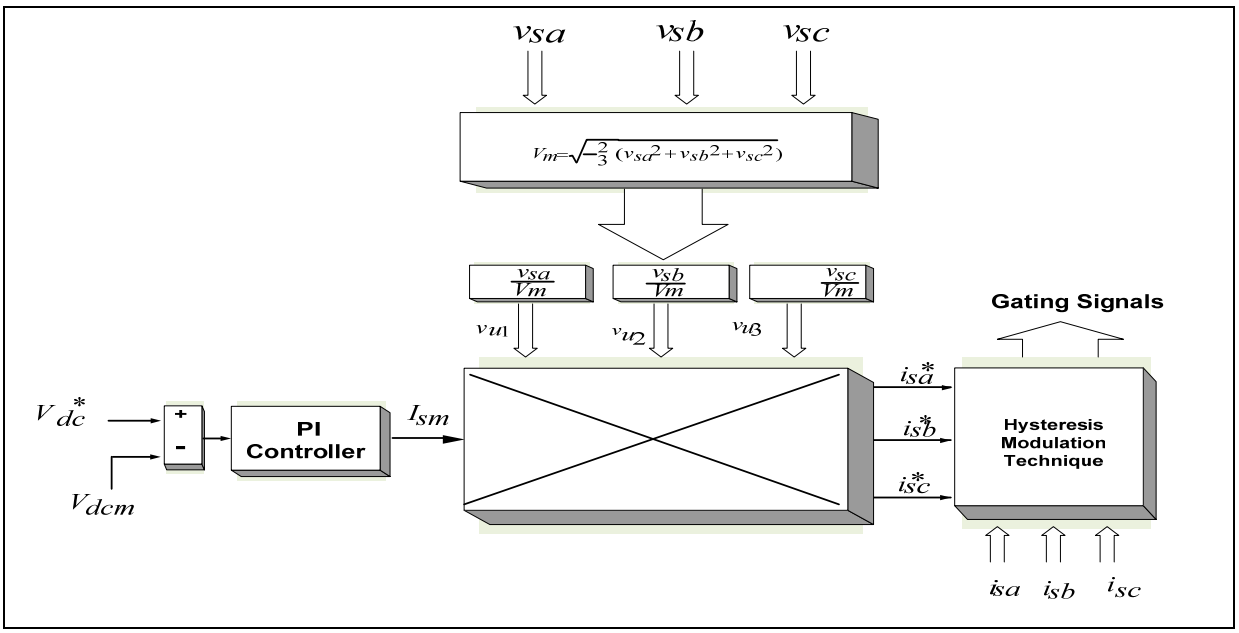

Figure 1.8 Indirect control based system

1.5.4 Sliding mode control

Sliding mode control (SMC) is one of the nonlinear control techniques that present significant qualities in terms of robustness, accuracy, simple implementation and easy tuning. The controller is also insensitive to variation of the system parameters. SMC systems are designated to drive the system trajectories onto a specific surface in the state space, namely sliding surface. The sliding surface can be chosen by subtracting load currents from reference supply currents or by additional mathematical processing of the error. When the sliding surface is achieved, sliding mode control keeps the states on the close neighborhood of the sliding surface. Design of SMC includes two phases, initial design of the appropriate sliding surface and then a control law to force the system trajectories to reach and stay on the sliding surface (Mane et Namboothiripad, 2016). Furthermore, sliding mode control has two fundamental benefits. First, the dynamic performance of the system could be customised by the specific selection of the sliding function. Secondly, the response of the closed loop becomes completely insensitive to many system disturbances. An APF based on sliding mode control is shown in the following figure.

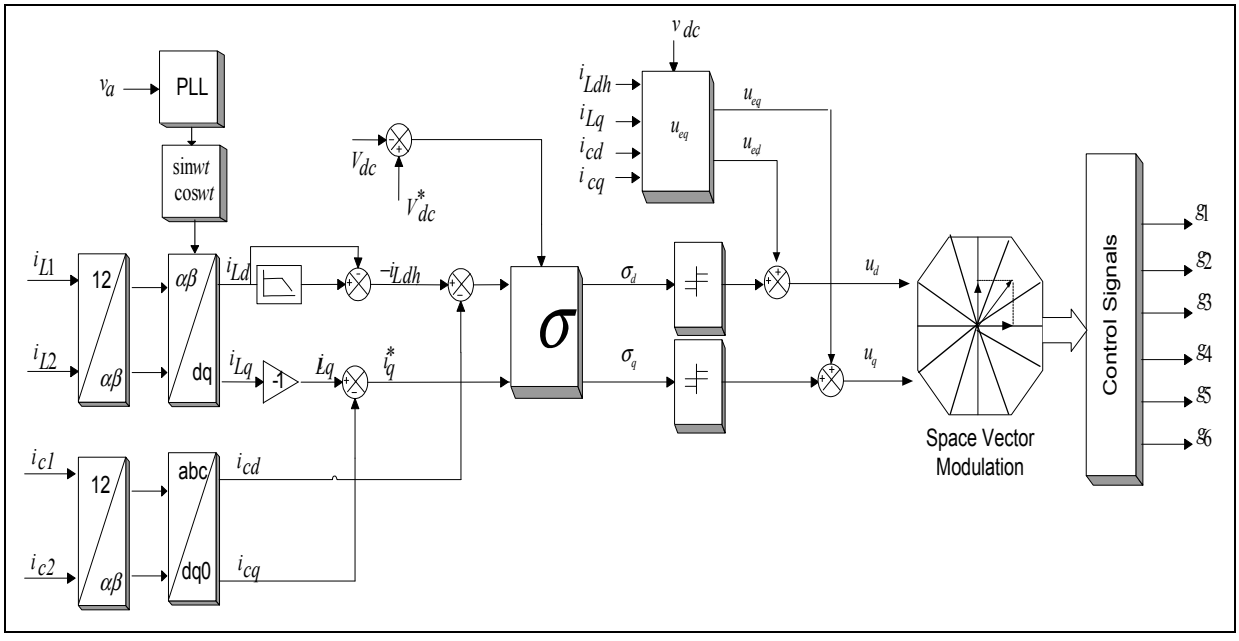

Figure 1.9 Sliding mode control for shunt active filter

1.5.5 PQ Indirect Current Control

The indirect current control is simple and offers a good performance and does not require much hardware compared to other control methods such as direct current control technique. In indirect current control, the source currents are taken as the reference current components for comparison, and an active power average component only flow through control scheme and reactive component is zero. As such the switching commands are derived. The indirect current control technique is shown in Figure 1.10 (Gotherwal et al., 2016).

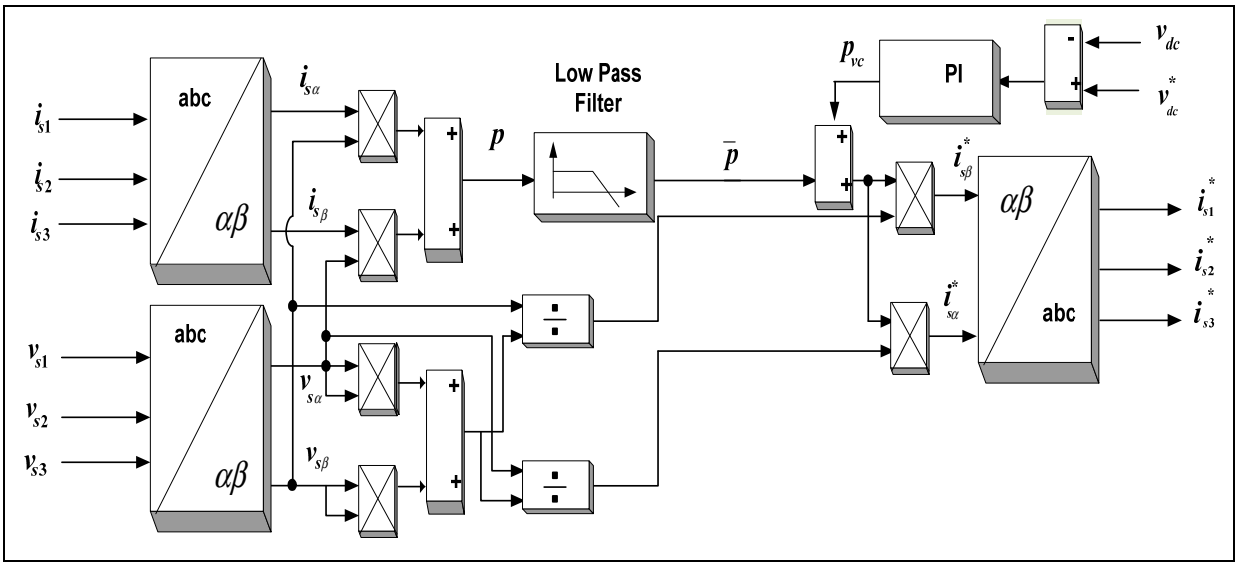

Figure 1.10 PQ Indirect current control

1.6 Protection of active power filter

These filters as many other power electronics are vulnerable to various faults due to components failure; overload and control faults. Therefore, the reliability of shunt active filters becomes extremely important in industrial applications. Protection of active power filters against potential problems, such as overcurrent, overvoltage, undervoltage, and overload, arising in the process of its operation is extremely significant, to minimize the disturbances caused by any failure in the system and to ensure continuous operation of the active filter. SAPFs are used intensively in industry and power quality applications, and their failures can be generally categorized as short circuit fault, overvoltage, ground faults and overload. Various detection and protection methods have been developed over the years. In this chapter, a comprehensive review of these works is investigated.

1.6.1 Shunt active filter faults and protection

A voltage source inverter based shunt active power filter can develop various types of faults that can be classified as follows:

Table 1.3 Types of active power filter faults

Protection	Description
DC overvoltage	The DC overvoltage protection has been triggered.
DC undervoltage	The DC under voltage protection has been triggered.
Ground fault	A ground fault has been detected.
Loss of phase	The system has detected a loss of supply on at least one phase.
Overvoltage transient	The transient network overvoltage protection has been triggered.

Protection	Description
Overvoltage RMS	The RMS value of the supply voltage measured with the AC voltage measurement board is higher than the acceptable maximum value.
Overcurrent peak	The peak current protection has been triggered.
Preload problem	The DC capacitors could not be preloaded at startup.
Preload time-out	The DC capacitors could not be charged.
Unbalanced supply level	The supply network imbalance is out of range.
Under voltage RMS	The RMS value of the supply voltage measured with the AC voltage measurement board is lower than the acceptable maximum value.
Unstable mains frequency	The network frequency is varying too fast.
Wrong phase rotation	The supply network feeding the filter has the wrong phase rotation.
Over temperature	The system detected an over temperature of the main controller board.
High frequency resonance	High Frequency Resonance on IGBT Power Converter Module output current. active filter shutdown
THDu resonance	APF has been stopped due to exceeding of THDu limit (line resonance)

Faults may also occur inside the power device of the converter, the “IGBTs”. Some common IGBTs failures are catastrophic failure and wear out failure. IGBT wear out failure is a result of components aging, while catastrophic failure is caused by incidents, such as overvoltage, overcurrent, overheat and so on (Wu et al., 2013). The detection and protection methods of voltage source inverter systems have been covered in many publications. However, most of the work concentrated on the applications of induction motor drive.

1.6.2 Over-current and short circuit fault

A short circuit fault in the distribution system normally results in an excessive current which is significantly higher than the operational or nominal current, that could cause an overcurrent to the shunt active filters (SAF) installed in the distribution system to mitigate the current harmonic (Sheng, 2016). Hence, overcurrent protection procedures need to be considered to prevent the disruption of the active filter. The conventional protection is usually achieved by a combination of fuses and circuit breakers which are triggered by various types of relays such as the overcurrent relay.

The overcurrent relays (OCRs) have been most commonly used as an efficient device for the overcurrent protection to minimize fault duration and damage of equipment. This relay uses current inputs from a CT and compares the measured values with pre-set values. If the input current value exceeds the pre-set value, the relay detects an overcurrent and issues a trip command to the breaker which releases its contact to disconnect the protected equipment (Almas, Leelaruji et Vanfretti, 2012). The relay can send a trip signal with or without an intended time delay, this time delay is known as the operation time of the relay, and is computed by the relay on the basis of the incorporated protection algorithm.

1.6.2.1 Overcurrent Relay classification

There are several types of overcurrent relays with different operating times and in this paragraph, a comparison between three categories of OCRs is presented. Overcurrent relays can be categorized based on the operation time as in the following order:

- **Instantaneous Overcurrent Relay**

This type of relay can promptly generate a trip command to the associated circuit breaker once the fault is sensed. The time delay is not defined for these relays. They are typically installed in proximity of the supply, where the level of current fault is considered particularly high and a slight delay in relay response could severely damage the equipment.

- **Definite Time Overcurrent Relay**

The definite time overcurrent relay could be used as a secondary protection for overhead lines where distance relay is applied as the primary source of protection. If the distance relay fails to sense a fault on the line and hence does not issue a trip signal to the circuit breaker, the overcurrent relay will then activate and trigger a trip signal to the breaker. In such circumstances, the time delay of the overcurrent relay is set to be slightly greater than the standard operating time for the distance relay and the operating time of the circuit breaker.

- **Inverse Definite Minimum Time (IDMT) Overcurrent Relay**

The inverse time characteristic of this relay implies that the operating time of the relay is inversely proportional to the level of current fault. In other words, the higher the fault current, the lesser the operating time would be. The IDMT could be rated for a wide range of fault currents and operation times. The characteristics of such relay are governed by the applied standard for the relay operation. These standards could be IEC, IEEE, ANSI or determined by the consumer. The characteristic curves are used to determine the operation time. Figure 1.11 shows the overall Simulink model of the overcurrent relay for different scenarios.

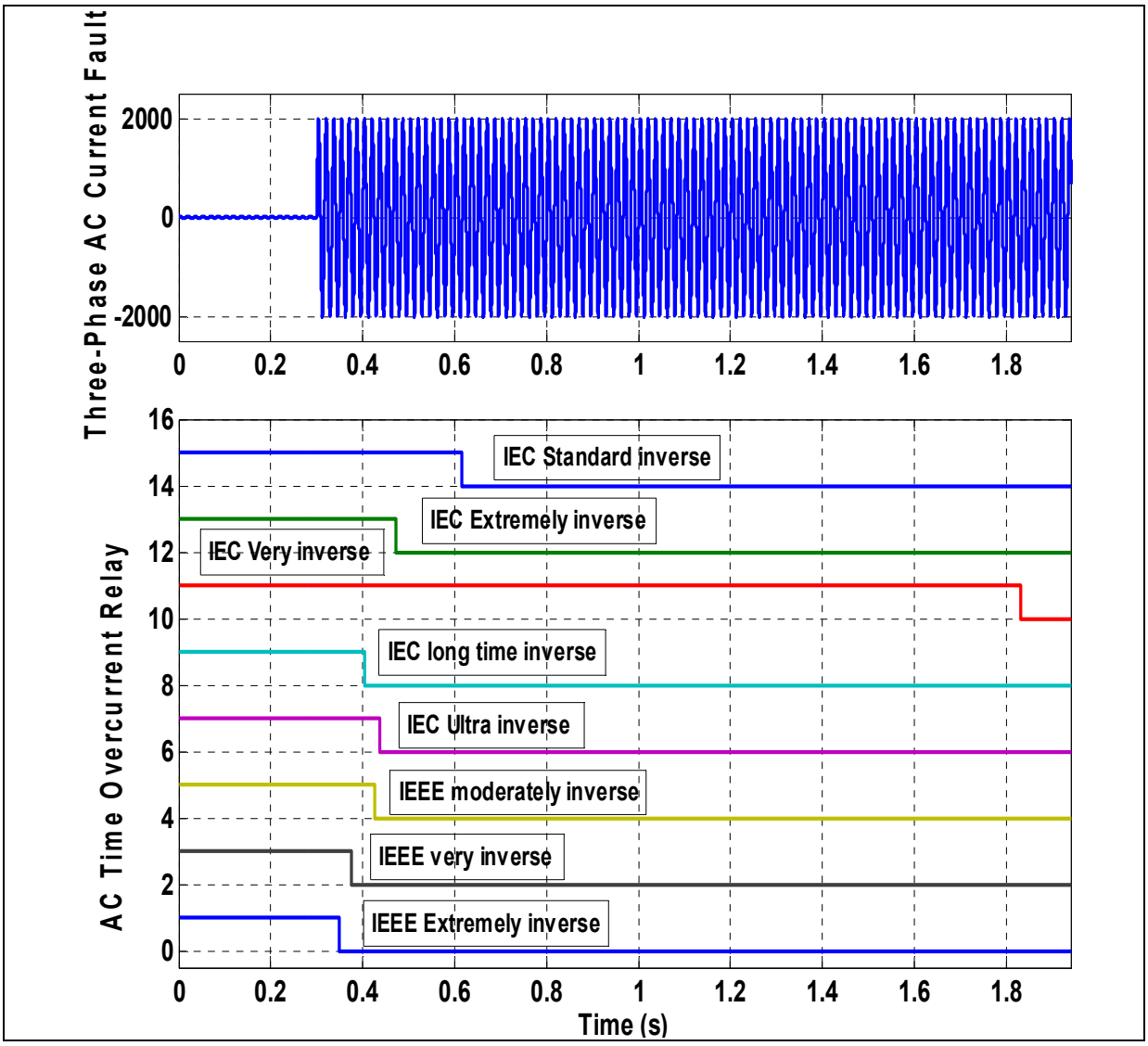

Figure 1.11 Comparison of operation times for several overcurrent relays

1.6.2.2 Shunt Active filter with dynamic output current limitation

Moreover, (Pregitzer et al., 2007) developed a conventional proportional control method for current limiting of a three-phase two level four leg inverter. The controller is able to dynamically limit the output current by restraining the maximum reference currents value allowed by the inverter's IGBTs. Although the technique is proved to be effective, yet it has a response delay of at least a fundamental frequency cycle.

1.6.2.3 Design of security and protection system for shunt active power filter

A similar truncated current limiting control method developed by (Tianyuan et al., 2007) is also applied for the protection of shunt active filters. It is based on the comparison of the compensation reference currents with the maximum permissible instantaneous current. When the reference currents are higher, the additional part of the reference currents will be reduced. Although this technique is straightforward with a better response, the summation of the reference currents does not converge to zero in order to achieve the control of current limiting that could result in more current harmonics to appear in the filter output currents.

1.6.2.4 An improved current-limiting control strategy for shunt active power filter

More recently, (Sheng, 2016) took advantage of the potentials in the previous two techniques of current limiting in (Pregitzer et al., 2007);(Tianyuan et al., 2007) to design an enhanced current limiting scheme applied on a shunt active filter. With this novel control scheme, if one or more phase currents of the compensation reference currents surpass the instantaneous current, the surpassed portion of the phase current with the maximum instantaneous value is cut, while the other phase currents with lesser current values are correspondingly reduced. The developed system has a faster response with no additional current harmonics.

1.6.2.5 Fault protection scheme for series active power filters

Among other short circuit protection schemes in use is the varistor. The work of (Moran et al., 1999), developed a protection scheme focused on series active power filters application. The scheme employs a varistor installed in shunt to the secondary windings of each current transformer (CT) with a pair of thyristors connected in antiparallel. When a short-circuit occurs the CT decreases the magnitude of the secondary current and voltages, and the large voltages at the secondary prompted by the short-circuit currents in the primary are controlled by the varistors. Consequently, the voltage source inverter is bypassed through the antiparallel thyristors. Thus, the PWM-VSI could then be isolated.

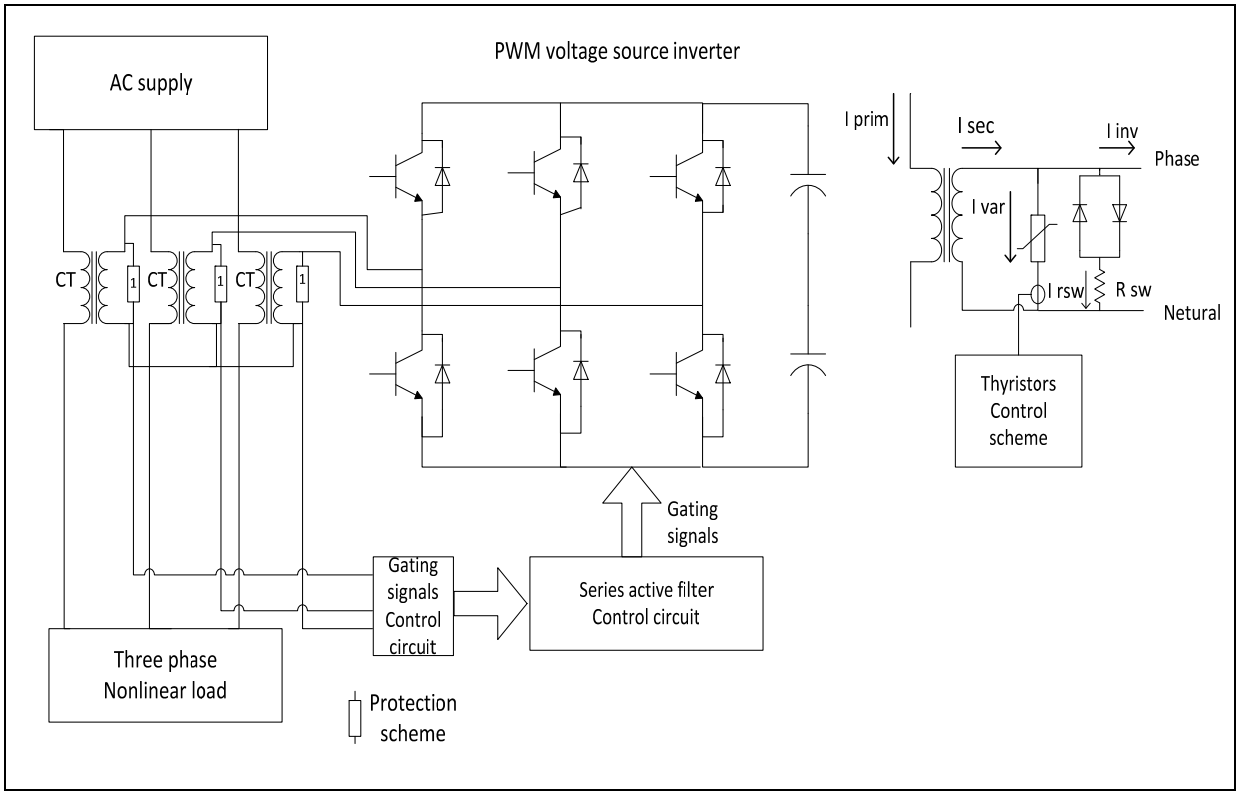

Figure 1.12 Series active power filter and the developed protection scheme

In terms of protection, it is clear that the total dissipated energy in the varistor is decreased. However, there is still a drawback that the protection of the primary windings of the transformer, which cannot withstand short circuit currents for a longer time, is dependent on the circuit breaker's clearing time. In addition, varistors could collapse when exposed to current surge exceeding their maximum ratings, or when normally working at operating voltages surpassing their ratings. Another drawback of this protection scheme is the failure to protect the series VSI from overcurrent in the situation where the short circuit on the load side occurs when the supply system is simultaneously undergoing deep voltage sag (Moran et al., 1999).

1.6.2.6 Fault protection scheme for unified power quality conditioners

A different fault protection scheme based on Unified Power Quality Conditioner (UPQC) is established by (Beom-Seok et al., 2001) to protect the UPQC without using additional protection circuits. The ability of overcurrent protection of UPQC is obtained by series active power filter, which is a high impedance to the fundamentals of the source current, load current, and is obtained by having the series active power filter outputting the reverses of its injected voltage polarity so as to minimise the current flow. However, this protection approach can only be applied when the nominal voltage of the primary winding of the series coupling transformer is close to the nominal voltage at the point of common coupling of the UPQC (Axente et al., 2010).

1.6.3 Frequency deviation

Three phase voltage source converters (VSC) are usually utilized to maintain a continuous output of DC bus voltage, with the least input current harmonic distortion. They are also used as an interface for various systems of power conversion with the AC distribution system. The control of shunt active filters can be carried out using different approaches (Singh, Al-Haddad et Chandra, 1999);(Buso, Malesani et Mattavelli, 1998). Most of them are based on two control loops. The regulation of the output voltage is usually realized by an outer loop of voltage feedback and an inner current loop operating with sinusoidal pulse width modulation (SPWM). However, grid-connected power converter may experience variations in line frequency, which would degrade the compensation performances of the APF (Lanfang et al., 2016). Consequently, if the deviation of the system frequency is critical, the control of the converter must take into consideration its effect to guarantee stability and accurate performance. Traditionally the control of power converters considers a stable supply frequency (Rohten et al., 2012). Otherwise, if the supply frequency is not stable, the model of the system may lose stability. In such conditions, the inconstant frequency of the grid should be considered in the control scheme analysis and design to achieve the required performance.

1.6.3.1 Odd-harmonic repetitive control of an active filter under varying network frequency

Much research effort has been reported in the literature for better performance and stability of three-phase voltage source converters connected to a variable frequency grid supply. A number of these studies are related to control theory of power electronic converters operating in non-ideal network conditions. In (Olm et al., 2010) the authors developed a repetitive control of shunt active filter to operate with fluctuating grid frequency. The design comprises a compensation scheme involving an adaptive change of the controller's sampling time according to the supply frequency variations to preserve the steady-state performance and maintains a low computational cost.

However, this may destabilize the system, which requires the stability of the closed-loop system to be ensured. Thus, a small gain theorem based technique has been used to improve the performance.

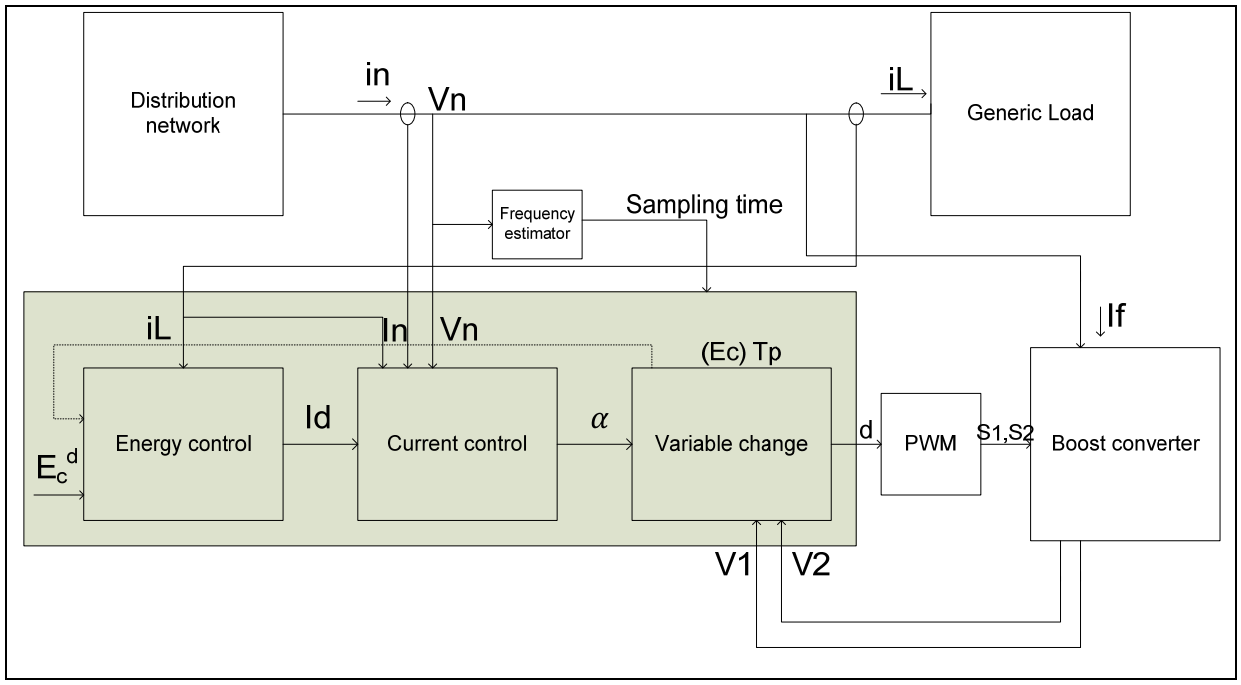

Figure 1.13 Global architecture of the control system

1.6.3.2 Repetitive control implementation with frequency adaptive algorithm for shunt active power filter

Similarly, the work of (Lanfang et al., 2016) proposed an improved repetitive control scheme with frequency adaptive capability for three-phase shunt APF to enhance the tracking performance and reduce the harmonic distortion during grid frequency variation.

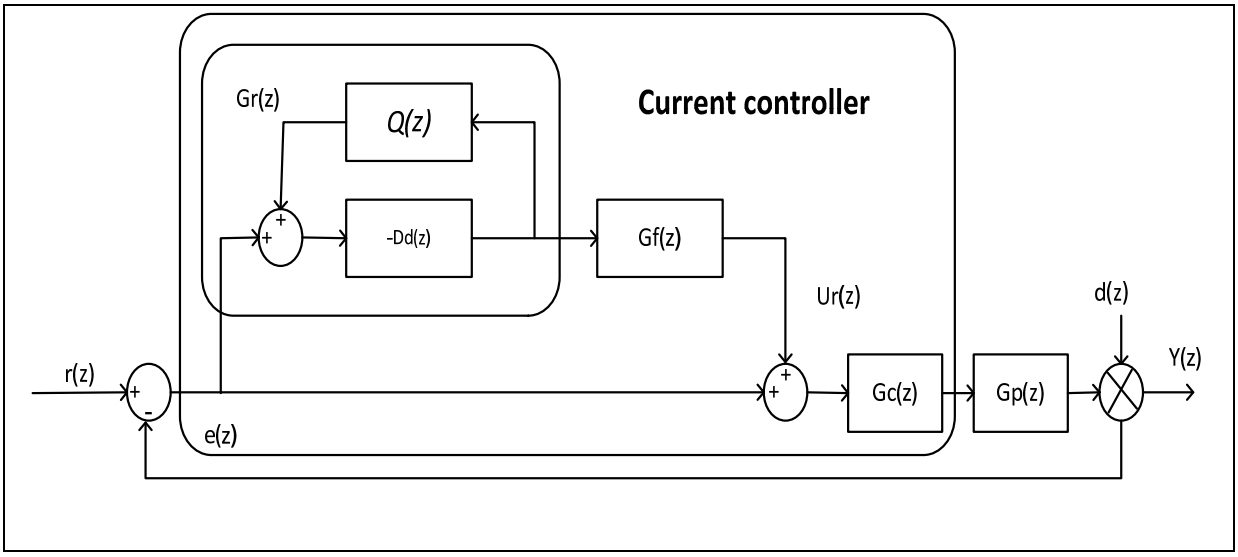

Figure 1.14 Repetitive control with frequency-adaptive capability

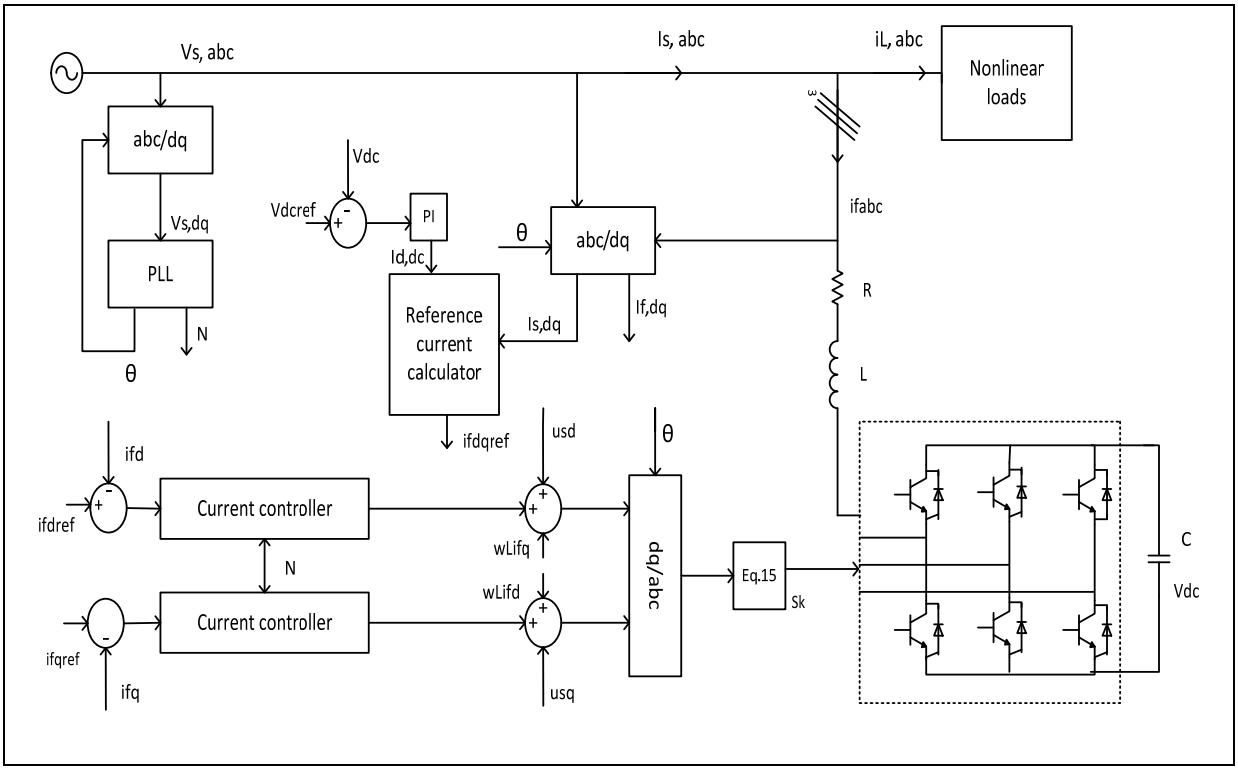

Figure 1.15 Block diagram of the improved repetitive control scheme

1.6.3.3 Design and analysis of hybrid active power filter based on sliding mode control under variable network frequency

Moreover on the subject of control theory, (Wang et al., 2013) designed a hybrid active filter based on sliding mode control working in a varied frequency power system of a civil aircraft. The proposed hybrid APF works fine at different frequencies. However, the total harmonic distortion increases as the frequency increases, which suggest the necessity for a faster current tracking of active power filter for higher fundamental frequency. As the harmonic mitigation effect will decrease as the system frequency will increase.

1.6.3.4 Frequency relaying based on instantaneous frequency measurement

A frequency relay with the capability of detecting over and under frequency and the rate of change of frequency measurements using an instantaneous frequency measuring algorithm is presented in (Moore, Allmeling et Johns, 1996). Similarly, in (Aman et al., 2012) a digital frequency relay simulation model is proposed for synchronous generator protection, where various cases are simulated and adequate responses are obtained from the model.

1.6.4 Grid voltage phase sequence detection

The AC supply voltage phase sequence identification and detection are considered crucial in the proper operation and control of many electrical and electronic applications. Several detection circuits are reported in the literature. However, most of them focus on positive phase sequence detection under unbalanced and distorted grid conditions.

1.6.4.1 Fast extraction of positive and negative sequence voltage components for inverter control

In the work of (Hao et al., 2016), the authors proposed a new algorithm for a fast extraction of the positive and negative sequence voltage components for inverter control operating in unbalanced three phase voltages. Compared to conventional methods such as (SRF-PLL), (DD-SRFPLL) and the second-order generalized integrator based quadrature signal generator FLL (SOGI-QSGFLL), this technique proves to enhance the system response speed using the property of a non-nominal dq transformation, in addition to the capability of rejecting/tracking certain harmonics order. Thus, many unbalanced utility voltage-based control objectives can be achieved with better performance with such faster extraction.

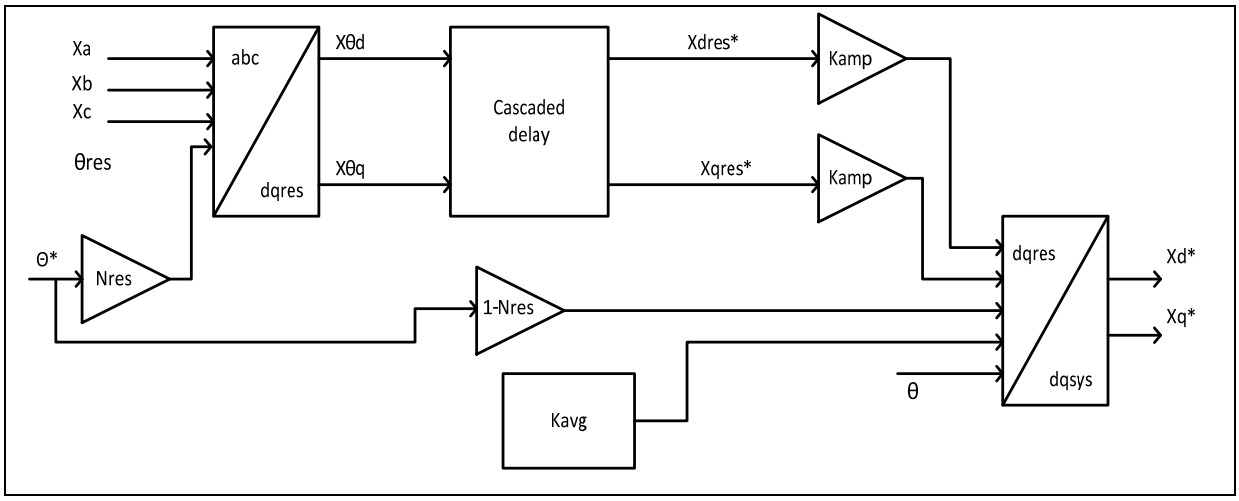

Figure 1.16 Decomposing system for extracting the positive sequence signal

1.6.4.2 A positive and negative sequences detecting method based on an improved PQ theory for power grid synchronization

Furthermore, in (Boussaid et al., 2013) a different detection method based on modified PQ theory for faulty grid conditions is presented. This technique uses the Filter Multi-Variable (FMV) instead of the typical PLL to obtain synchronization information, resulting in less time response.

Additionally, a real-time means value calculation is employed to cancel the alternating components generated as a result of using narrow bandwidth filters to separate the positive and negative components. However, this comes with a compromise in response time and phase delay.

1.6.4.3 Three-phase positive and negative sequences estimator to generate current reference for selective active filters

Moreover, in an attempt to develop an online load current harmonics reference generator for shunt active power filters, the authors (Ronchi et Tilli, 2002b) developed a three-phase positive and negative sequence estimator, based on Luenberger observer model to isolate positive and negative sequences of each harmonic, that can be then managed by APF controller.

1.6.4.4 Comparison of positive sequence detectors for shunt active filter control

The authors (Jamarani et al., 2014) and (Serra, Forchetti et De Angelo, 2010) conducted a comparison between three different positive sequence detector systems for grid-connected SAF. The three structures are based on pq theory, EPLL and SOGI-PLL. From the evaluation of the three analyzed detection systems, the pq-PLL based system offers a better dynamic response than the other two structures for ideal grid voltages. However, under distorted grid conditions, the performance is unsatisfying. Then again, the EPLL performs acceptably in the presence of voltages harmonics but it has a phase error for unbalanced conditions. Finally, SOGI based structure presents a better performance than both pq-PLL and SOGI-PLL.

1.6.5 Protection devices

1.6.5.1 Fuses

The simplest and most commonly used circuit interrupting devices is the fuse. A fuse is an "overcurrent protective device with a circuit-opening fusible part that is heated and severed by the passage of overcurrent through it" (The Authoritative Dictionary of IEEE Standards Terms, Seventh Edition, 2000). Fuses are available in different current ratings, which correspond to the maximum allowable continuous current. These fuses are installed in series with the supply service lines and they carry normal load current without interruption. If the load of the circuit exceeds the rating of the fuse or, if a fault develops in the circuit wiring or a connected appliance, the fuse melts and generates an open circuit at the service entrance.

Fuses are designed for many different applications and with a wide variety of characteristics to meet the requirements for both routine and special situations(Anderson, 1998). An enormous variety of fuses are available today. In terms of quantity, fuses outnumber any other overcurrent protection devices. They provide economy in protection as well as flexibility in rating and time current characteristic. They are used for overcurrent protection of transformers, capacitors and lateral taps in distribution systems.

1.6.5.2 Protection Relays

Relays are available in many different types, serving a host of different purposes and having different design characteristics. They could be categorized in many different ways, for instance, function, performance features, or operating method. The most common categorization is by function, where five forms of functions exist that includes protection, regulation, reclosing and synchronizing, monitoring and auxiliary relays. The IEEE defines a protective relay as "a relay whose function is to detect defective lines or apparatus or other power system conditions of an abnormal or dangerous nature and to initiate appropriate control circuit action" (IEEE 100, 2000).

Protection relays are compressed units of analog, discrete solid state components, operational amplifiers, and digital microprocessor networks connected to the power system to detect problems. These are commonly referred to as relays. Protection relays together with ancillary systems and fuses operate for the detection of intolerable conditions and faults. They are utilized in all units of the power system such as transmission lines, generators, buses, transformers, motors and capacitor banks. The components of a typical relay can be Electromechanical, solid state or numerical. All protection relays were of the electromechanical type, which is still in widespread use. Analog type electronic relays using discrete electronic components were introduced in the 1970s. Recently, microprocessor-based electronic relays have been developed and are being used at an increasing rate (Blackburn et Domin, 2015).

1.6.5.3 Circuit breakers

Protection relays provide the ability to detect the faults in the power system, however, being low power devices; they cannot perform the isolation of the faulted section of the power system. Circuit breakers are then used for this purpose. Hence, circuit breakers and protection relays work simultaneously for the instantaneous isolation of intolerable section or equipment. The power circuit breaker is the main member of the devices family which is intended to open an electric circuit. A power circuit breaker is defined as “a device for closing, carrying, and interrupting a circuit by parting separable contacts under either load or fault conditions”. Circuit breakers are often classified according to the physical mechanism used to interrupt the circuit, this includes oil circuit breakers, air circuit breakers, sulfur hexafluoride (SF6) circuit breakers, and vacuum circuit breakers (Anderson, 1998).

1.6.5.4 Surge Protection Circuits

Switching transients and voltage surges can be a substantial threat to today's semiconductor devices. A surge voltage is an increase in voltage considerably above the rated level, which steps up the electrical charge at some point. Thus, causing an increase in the energy potential, that could increase the line current flow. In general transient surges occur unexpectedly, which could damage many consumers' electrical and electronic devices. Therefore, the protection against transients is essential. This protection depends mostly on controlling the magnitude of the surge to a safe value and diverting the surge currents by employing protection specific devices.

Surge Protection Devices (SPDs) or Transient Voltage Surge Suppressors (TVSSs) are meant to provide protection for electronic equipment against power surges. A great number of surge protection devices employ non-linear components to divert the additional energy carried in via a surge voltage. Diverting voltage transients could be realized by means of a crowbar device or a voltage clamping device. Metal oxide varistors (MOVs) are among the most frequently used semiconductor-based devices, besides thyristors and avalanche-type back to back Zener diodes. Gas discharge tubes (GDTs) are also found in some systems. Thyristors and GDTs are categorized as crowbar devices, whereas MOVs and avalanche-type back to back Zener diodes are voltage clamping devices (James, 2014).

1.6.5.5 Metal Oxide Varistors (MOVs)

The Metal Oxide Varistor (MOV) is the most significant element in the vast majority of surge protection devices (SPDs). Almost over 90% of the modern SPDs designated for the protection of low-voltage AC power equipment and systems are of shunt type employing a (MOV) as the main element in control of the overvoltage suppression (Drabkin, 2002). The MOVs are composed of zinc oxide (ZnO) ceramic semiconductor elements with highly nonlinear V-I characteristics. A MOV basically conducts as a result of the semiconductor P-N junctions at the boundaries of the (ZnO) grains.

A MOV is a multi-junction component with masses of grains performing as a series-parallel combination between the electrical terminals. MOVs are able to suppress a high transient energy for their size and cost, and simultaneously protecting the equipment by maintaining necessarily low clamping voltages. Hence, surge protection devices employing MOV are considered to be the most effective protection technology for industrial applications (Samaras et al., 2007). MOVs are usually molded into a disc form, where the absorbent capability of large transients is accomplished by increasing the disc size. Typical disc diameters range from 3 to 20 mm. In addition; MOVs reacts rapidly in a few nanoseconds with high clamping voltages, in the region of 30V to 1.5kV. Figure 1.17 shows a typical V-I characteristic of a MOV.

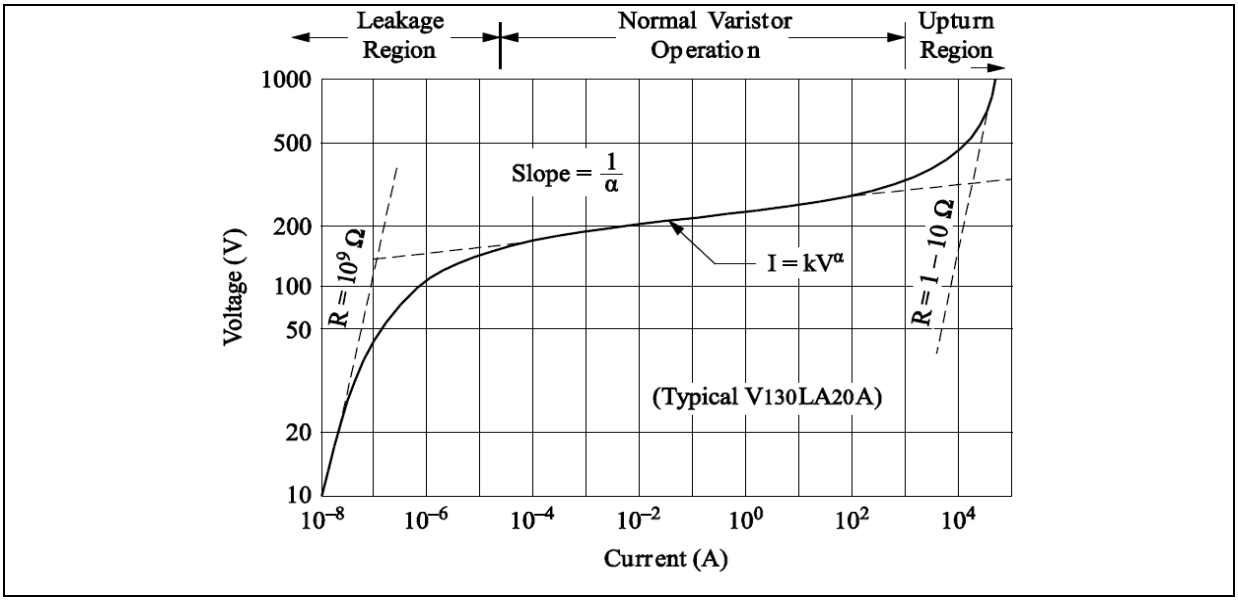

Figure 1.17 Metal oxide varistor V-I characteristic

At low voltage level, the MOV carries very small current in microamperes. As the breakdown voltage approaches, the MOV begins to carry current. At voltages marginally beyond the breakdown, high currents flow, efficiently clamping the output voltage. The clamping permits the high voltage levels to be forced to ground, consequently averting equipment from overvoltage.

Furthermore, exposing MOV to constant conditions of abnormal voltage, instead of short intervals of transients, might drive the MOV into thermal runaway, causing overheat, smoke and may possibly go on fire. To prevent such incident, various contemporary MOVs comprise an internal thermal fuse or a thermal cut-off element.

MOV based SPDs are available for industrial applications in two forms. The first one utilizes small diameter MOVs that are mainly considered to provide protection for different electronic PCBs. These MOVs lacks the essential capability of energy handling to divert high surges from electronic equipment. They usually comprise of an MOV disk with a width of up to 20 mm covered with resin. To overcome such problems, a number of MOVs are parallel connected to improve the capacity of surge current. The other form of surge protection is constructed on the usage of a single MOV disk capable of effectively conducting the surge energy. This can be accomplished by using an industrial MOV material and also by increasing the disk diameter to 80 mm. Resin layers have been exchanged with an aluminum housing that performs as a heat sink to the MOV (Samaras et al., 2007).

1.6.5.6 TVS diodes and thyristors

TVS diodes and TVS thyristors are two basic types of p-n junction devices available for transient surge protection. Both forms are available as back-to-back devices suitable for protection against positive or negative surges occurring at power entry inputs. The TVS diode is a clamping device which suppresses all voltages above its breakdown voltage whereas the TVS thyristors is a crowbar device which switches on when overvoltages rise up to the break-over voltage. Silicon rectifiers, intended for transient suppression, have enhanced the performance of regulator-type Zener diodes to provide TVS diodes. The main advantage of these diodes is their effective clamping, which comes closest to an ideal constant voltage clamp. TVS diodes are specially designed to clamp transient surges, rather than regulate a relatively stable voltage.

Like all clamping devices, it automatically resets when the transient drops below the breakdown voltage but absorbs much more of the transient energy internally than a similarly rated TVS thyristor device. These diodes react almost promptly to transients. Their clamping voltage varies from a few volts to a few hundred volts.

A TVS diode can respond to transients faster than other transient protection components such as MOVs and GDTs. Clamping occurs in picoseconds. The fast reaction time of the TVS diodes means that any overshoot in voltage is mainly caused by lead inductance. When individual excessive surges occur beyond the rating of the TVS diode, it can fail like any other stressed semiconductor component.

TVS thyristors are solid state components built with four alternating layers of p-type and n-type material. The advantage of this device is its low on-state voltage after triggering which provides a capability of a much higher current for a relatively small size chip compared to a clamp device. TVS thyristors are used extensively in surge protection of communication equipment. TVS thyristors are avalanche triggered components and protect sensitive loads by switching to a low on-state of a few volts, thus providing a “crowbar” effect with high current capability. The surge current capability of a TVS thyristor is determined by its structure as well as its size. Operating voltage levels begin at 12V and are available in several increments up through several hundred volts. They do not wear out, but when electrically overstressed fail as a short circuit.

CHAPITRE 2

NONLINEAR CONTROL OF SHUNT ACTIVE FILTER

2.1 Introduction

The idea of shunt active filters is based on the principle of generating harmonic currents in the network, which have the same amplitude and opposite phase of the harmonic currents generated by the nonlinear load. Generally, the harmonic components in the currents of the nonlinear load are extracted to be used as references to the currents of the active filter, and the DC voltage of the active filter is measured to be regulated in a feedback loop. This control loop imposes a low current at the fundamental frequency in phase with the voltages at the point of common coupling in order to compensate for the losses in the elements of the active filter. In addition, thanks to the rapid progress in the technology of power electronics such as IGBT and GTO, shunt active filters have become an effective solution in the compensation of harmonics of low and medium power nonlinear loads.

In this chapter the shunt active filter is modeled based on the matrix transformation of the differential equations and nonlinear control strategy is elaborated and applied in the control of the filter.

2.2 Modeling of shunt active filter

The system shown in Figure 2.1 is a three-phase AC source V_s having an inductor L_s, feeding a nonlinear load consisting of a full diode bridge rectifier supplying an inductive load. The nonlinear load carries currents of low order that are high in harmonics (5^{th}, 7^{th}, 11^{th}, 13^{th} etc.). The Active filter contains a VSC, having inductances (L_c, R_c) at the input and a capacitor C at the output. It is connected in parallel with the load in order to compensate for the harmonic component of the currents $[i_{l123}] = [i_{l1} i_{l2} i_{l3}]^T$, thereby enabling the source to provide quasi-sinusoidal I_{s123} currents. The voltages at the connection point of the active filter are V_{123}.

The currents in the three phases at the input of the filter are i_{123}, and the voltages between the inputs of the converter and the point M are v_{123m}. The voltages v_{dc} and v_{mn} represent the potential differences respectively at the terminals of the capacitor C and between the point M and the neutral point N of the source. The shunt active filter will be modeled in the (abc) reference frame. The obtained model will then be transformed to the rotating reference frame (dq) by applying the transformation matrices directly to the three phase systems (Mendalek, 2003).

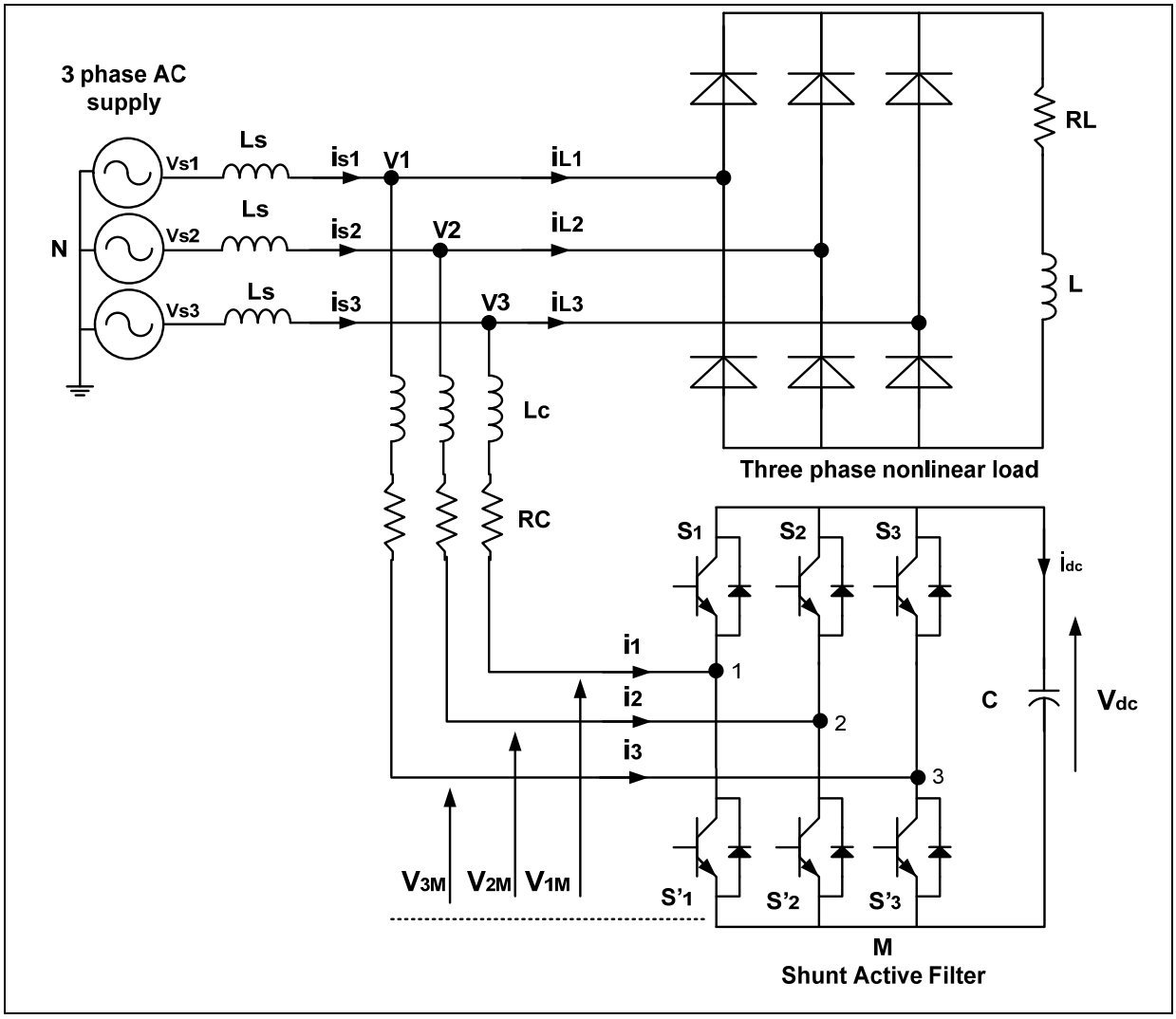

Figure 2.1 Three-Phase Shunt Active Filter

2.2.1 Modeling of shunt active filter in abc frame

By applying Kirchhoff's voltages and currents laws for each phase at the point of common coupling PCC we obtain the following differential equations:

$$\begin{cases} v_1 = L_c \dfrac{di_1}{dt} + R_c i_1 + v_{1M} + v_{MN} \\ v_2 = L_c \dfrac{di_2}{dt} + R_c i_2 + v_{2M} + v_{MN} \\ v_3 = L_c \dfrac{di_3}{dt} + R_c i_3 + v_{3M} + v_{MN} \end{cases} \tag{2.1}$$

By summing the three equations in (2.1) assuming that the three-phase AC supply voltages are balanced and taking into consideration the absence of the zero sequence in the currents of a three wire system, we obtain:

$$v_{MN} = -\frac{1}{3}\sum_{m=1}^{3} v_{mM} \tag{2.2}$$

The switching function C_k of the kth leg of the converter is defined as

$$C_k = \begin{cases} 1, if\ S_k\ is\ On\ and\ S_k'\ is\ Off \\ 0, if\ S_k\ is\ Off and\ S_k'\ is\ On \end{cases} \tag{2.3}$$

Thus we can write $v_{kM} = C_k v_{dc}$, which makes it possible to deduce

$$V_{MN} = -\frac{1}{3}\sum_{m} C_m\, v_{dc} \tag{2.4}$$

The differential equation governing phase k becomes:

$$v_k = L_c \frac{di_k}{dt} + R_c i_k + C_k v_{dc} - \frac{1}{3}\sum_{m=1}^{3} C_m\, v_{dc} \tag{2.5}$$

Or

$$\frac{di_k}{dt} = -\frac{R_c}{L_c} i_k - \frac{1}{L_c}\left(C_k - \frac{1}{3}\sum_{m=1}^{3} C_m\right) v_{dc} + \frac{v_k}{L_c} \tag{2.6}$$

For $k = 1,2,3$.

Knowing that there are eight possible states of operation for the active filter, we can define the state switching function d_{nk} as being:

$$d_{nk} = \left(C_k - \frac{1}{3}\sum_{m=1}^{3} C_m\right)_n \tag{2.7}$$

The value of d_{nk} depends on the switching state n (n = 0, 1, …, 7) of the converter and on the phase k. In other words, d_{nk} simultaneously depends on the switching functions of the three legs of the active filter. This demonstrates the interaction between the three phases. Table 2.1 gives the values of d_{nk} according to the switching state and for each phase of the system. Furthermore, based on equation (2.7) and for the eight possible switching states of the active filter, the conversion of the matrix $[C_k]$ to $[d_{nk}]$ is given by:

$$\begin{bmatrix} d_{n1} \\ d_{n2} \\ d_{n3} \end{bmatrix} = \frac{1}{3}\begin{bmatrix} 2 & -1 & -1 \\ -1 & 2 & -1 \\ -1 & -1 & 2 \end{bmatrix}\begin{bmatrix} c_1 \\ c_2 \\ c_3 \end{bmatrix} \tag{2.8}$$

It should be noted that the rank of the transformation matrix in (2.8) equals 2 and that the system $[d_{nk}]$ has no zero sequence component.

Table 2.1 Value of d_{nk} according to switching state n and phase k

n	**[C_1 C_2 C_3]**	**d_{nk}**		
		K = 1	**K = 2**	**K = 3**
0	[0 0 0]	0	0	0
1	[1 0 0]	2/3	-1/3	-1/3
2	[1 1 0]	1/3	1/3	-2/3
3	[0 1 0]	-1/3	2/3	-1/3
4	[0 1 1]	-2/3	1/3	1/3
5	[0 0 1]	-1/3	-1/3	2/3
6	[1 0 1]	1/3	-2/3	1/3
7	[1 1 1]	0	0	0

Furthermore, on the DC side of the active filter, the following relation holds:

$$\frac{dv_{dc}}{dt} = \frac{1}{c} i_{dc} \tag{2.9}$$

Kirchhoff's law for the currents gives:

$$i_{dc} = c_1 i_1 + c_2 i_2 + c_3 i_3 \tag{2.10}$$

and it can be easily verified that:

$$\sum_{m=1}^{3} d_{nm}\, i_m = \sum_{m=1}^{3} c_m\, i_m \tag{2.11}$$

This allows obtaining the following equation:

$$\frac{dv_{dc}}{dt} = \frac{1}{c} \sum_{m=1}^{3} d_{nm}\, i_m \tag{2.12}$$

Moreover, with the absence of zero sequence in the AC currents and in the $[d_{nk}]$ functions, the following differential equation on the DC side is obtained:

$$\frac{dv_{dc}}{dt} = \frac{1}{C}(2d_{n1} + d_{n2})i_1 + \frac{1}{C}(d_{n1} + 2d_{n2})i_2 \tag{2.13}$$

Consequently, the complete model of the active filter in the 'abc' reference frame is realized by utilizing relation (2.6) for phases 1 and 2 and the relation (2.13):

$$\left\{\begin{array}{l} L_c\frac{di_1}{dt} = -R_c i_1 - d_{n1}v_{dc} + v_1 \\ L_c\frac{di_2}{dt} = -R_c i_2 - d_{n2}v_{dc} + v_2 \\ C\frac{dv_{dc}}{dt} = (2d_{n1} + d_{n2})i_1 + (d_{n1} + 2d_{n2})i_2 \end{array}\right\} \tag{2.14}$$

It should be noted that this model is nonlinear and time-varying and the state space representation of the model is minimal. However, the steady state fundamental components are sinusoidal. Therefore, in order to facilitate the control, the model can be transformed to the synchronous orthogonal frame rotating at the fundamental frequency of the supply (ω). Using this time-varying transformation, the positive sequence component at fundamental frequency becomes constant.

2.2.2 Model conversion into 'dq' reference frame

$$C_{123}^{dq0} = \sqrt{\frac{2}{3}}\begin{bmatrix} 1/\sqrt{2} & \cos\theta & -\sin\theta \\ 1/\sqrt{2} & \cos(\theta - \frac{2\pi}{3}) & -\sin(\theta - \frac{2\pi}{3}) \\ 1/\sqrt{2} & \cos(\theta - \frac{4\pi}{3}) & -\sin(\theta - \frac{4\pi}{3}) \end{bmatrix} \quad (2.15)$$

The inverse conversion is then obtained from the transposed matrix of C_{123}^{dq0}.

where $$C_{dq0}^{123} = \left(C_{123}^{dq0}\right)^{-1} = \left(C_{123}^{dq0}\right)^{T}$$

The third equation of the model (2.14) can be written in the following form:

$$\frac{dv_{dc}}{dt} = \frac{1}{C}\,[d_{n123}]^T\,[i_{123}]$$

Applying the coordinate transformation, the following is obtained:

$$\frac{dv_{dc}}{dt} = \frac{1}{C}\left(C_{123}^{dq0}[d_{ndq0}]\right)^T\left(C_{123}^{dq0}[i_{dq0}]\right)$$

$$= \frac{1}{C}[d_{ndq0}]^T\left(C_{123}^{dq0}\right)^T\left(C_{123}^{dq0}[i_{dq0}]\right) = \frac{1}{C}[d_{ndq0}]^T[i_{dq0}]$$

$$= \frac{d_{nd}i_d}{C} + \frac{d_{nq}i_q}{C} + \frac{d_{n0}i_0}{C}$$

and knowing that $d_{n0} = 0$ and $i_0 = 0$ we obtain:

$$\frac{dv_{dc}}{dt} = \frac{d_{nd}i_d}{C} + \frac{d_{nq}i_q}{C} \quad (2.16)$$

The simplified transformation matrix of the stationary frame 'abc' to 'dq' reference frame becomes:

$$C_{dq}^{12} = \sqrt{2}\begin{bmatrix} \cos(\theta - \frac{\pi}{6}) & \sin\theta \\ -\sin(\theta - \frac{\pi}{6}) & \cos\theta \end{bmatrix} \tag{2.17}$$

and the inverse transformation matrix:

$$C_{12}^{dq} = \sqrt{\frac{2}{3}}\begin{bmatrix} \cos\theta & -\sin\theta \\ \sin(\theta - \frac{\pi}{6}) & \cos(\theta - \frac{\pi}{6}) \end{bmatrix} \tag{2.18}$$

In this way the stationary frame model with state variables as (i_1, i_2, v_{dc}) will be transformed into a synchronous model with variables as (i_d, i_q, v_{dc}), and the relationship between the two groups of variables will be:

$$\begin{bmatrix} i_d \\ i_q \\ v_{dc} \end{bmatrix} = \sqrt{2}\begin{bmatrix} \cos\left(\theta - \frac{\pi}{6}\right) & \sin\theta & 0 \\ -\sin\left(\theta - \frac{\pi}{6}\right) & \cos\theta & 0 \\ 0 & 0 & 1/\sqrt{2} \end{bmatrix}\begin{bmatrix} i_1 \\ i_2 \\ v_{dc} \end{bmatrix} \tag{2.19}$$

The first two equations of the stationary frame model described by (2.14) can be put in the following form:

$$\frac{d}{dt}[i_{12}] = -\frac{R_c}{L_c}\begin{bmatrix} 1 & 0 \\ 0 & 1 \end{bmatrix}[i_{12}] - \frac{1}{L_c}[d_{n12}]v_{dc} + \frac{1}{L_c}[v_{12}] \tag{2.20}$$

where $[i_{12}] = [i_1, i_2]^T$, $[d_{n12}] = [d_{n1}, d_{n2}]^T$ and $[v_{12}] = [v_1, v_2]^T$ are the first two components in the three phase stationary frame 'abc'. That implies:

$$\frac{d}{dt}\left[C_{12}^{dq}[i_{dq}]\right] = -\frac{R_c}{L_c}\begin{bmatrix} 1 & 0 \\ 0 & 1 \end{bmatrix} C_{12}^{dq}[i_{dq}] - \frac{1}{L_c} C_{12}^{dq}[d_{ndq}]v_{dc} + \frac{1}{L_c} C_{12}^{dq}[v_{dq}] \tag{2.21}$$

where $[i_{dq}] = [i_d,\ i_q]^T$, $[d_{ndq}] = [d_{nd}, d_{nq}]^T$ and $[v_{dq}] = [v_d, v_q]^T$ are the vectors of the synchronous 'dq' frame.

Applying the differentiation property:

$$\frac{d}{dt}\left[C_{12}^{dq}[i_{dq}]\right] = C_{12}^{dq}\frac{d}{dt}[i_{dq}] + \left(\frac{d}{dt}C_{12}^{dq}\right)[i_{dq}] \tag{2.22}$$

We can write:

$$\frac{d}{dt}[i_{dq}] = \left(-(C_{12}^{dq})^{-1}\left(\frac{d}{dt}C_{12}^{dq}\right) - \frac{R_c}{L_c}\begin{bmatrix}1 & 0\\ 0 & 1\end{bmatrix}\right)[i_{dq}] - \frac{1}{L_c}[d_{ndq}]v_{dc} + \frac{1}{L_c}[v_{dq}] \tag{2.23}$$

This can be verified that:

$$(C_{12}^{dq})^{-1}\left(\frac{d}{dt}C_{12}^{dq}\right) = \frac{2}{\sqrt{3}}\begin{bmatrix}0 & -\omega\cos(\pi/6)\\ \omega\cos(\pi/6) & 0\end{bmatrix} = \begin{bmatrix}0 & -\omega\\ \omega & 0\end{bmatrix} \tag{2.24}$$

The following relation can be derived:

$$\frac{d}{dt}[i_{dq}] = \begin{bmatrix}\frac{R_c}{L_c} & -\omega\\ \omega & \frac{R_c}{L_c}\end{bmatrix}[i_{dq}] - \frac{1}{L_c}[d_{ndq}]v_{dc} + \frac{1}{L_c}[v_{dq}] \tag{2.25}$$

In conclusion, the representation of the model in the 'dq' frame is obtained as follows:

$$\left.\begin{aligned} L_c\frac{\mathrm{d}i_d}{\mathrm{dt}} &= -R_c i_d + L_c\omega i_q - v_{dc}\,\mathrm{d}_{nd} + \mathrm{V}_d\\ L_c\frac{\mathrm{d}i_q}{\mathrm{dt}} &= -R_c i_q - L_c\omega i_d - v_{dc}\,\mathrm{d}_{nq} + \mathrm{V}_q\\ \mathrm{C}\frac{\mathrm{d}v_{dc}}{\mathrm{dt}} &= \mathrm{d}_{nd}\,i_d + \mathrm{d}_{nq}i_q \end{aligned}\right\} \tag{2.26}$$

This model is nonlinear for the reason of the multiplication terms between the state variables (i_d, i_q, v_{dc}) and the inputs (d_{nd}, d_{nq}). However, this model is time-invariant during given switching state. Moreover, the fundamental concept of the active filter needs that the three state variables have to be controlled independently. Therefore, *id* and *iq* have to follow a varying reference current that is extracted from the nonlinear load currents.

Additionally, the DC bus voltage *vdc* has to be controlled so that it is kept at a fixed value in order to keep the compensation performance of the active filter during dynamic variations. However, the model has only two independent inputs. Therefore, a control strategy based on the decoupling of the current tracking loop and DC voltage regulation loop is used. In this way, the active filter can compensate for the AC currents and the DC bus voltage independently of each other. Yet, the results in either one of the decoupled subsystems would have a dynamic response that is considerably slower than the other one. In order to obtain a fast dynamic response of harmonic compensation, a structure of an inner fast current tracking loop and an outer slow DC voltage regulation loop is implemented.

2.3 Control strategy

2.3.1 Exact Nonlinear control

The exact nonlinear control in the form of input-output linearization is applied for the shunt active filter controller design (Mendalek, 2003). In this approach, the system is represented in two subsystems, one represents the fast dynamics and the other represents slow dynamics. The subsystem of the fast dynamics is multiple input and multiple output system (MIMO), and the slow dynamic is single input and single output system (SISO). The problem of the nonlinear control of the active filter is solved using the feedback linearization technique applied to each of the two subsystems. In this section, a review of the theory related to the nonlinear control of the SISO and MIMO systems is outlined. Thereafter, the decoupling of fast and slow dynamics based on the proposed strategy is carried out.

Review of the Exact Nonlinear control theory

Single input single output systems

A nonlinear system can be linearized by exact linearization control in the input-output technique. Consider the following nonlinear system:

$$\begin{aligned} &\dot{x} = f(x) + \mathrm{g}(x)\, u, \qquad x(t_\mathrm{o}) = x_o \in M \\ &y = h(x) \end{aligned} \tag{2.27}$$

Where M is a smooth manifold, u $\in \mathfrak{R}$, f(x) and g(x) are vectors of smooth functions and h is a smooth function in M. The relative degree r of a system is defined as being the smallest integer k for which the derivative $y^{[k]}$ (t) is an explicit function of the input u. In other words, r is the smallest integer k for which $L_\mathrm{g}\, L_f^{k-1}\, h \neq 0$, or how many times do we need to differentiate the output (y) until the input (u) appears.

Moreover, either the function h : M $\rightarrow \mathfrak{R}$ and the vector field $X(x)$ in M, $L_x\, h(x)$ denotes the derivative of lie of $h(x)$ along $X(x)$ and can also be written in the following form:

$$L_x\, h(x) = \, dh_x \; X(x)$$

The successive derivation of (2.27) gives:

$$\left\{\begin{array}{l} y^{[1]}(t) = d\, h_{x(t)}\, \big(f\big(x(t)\big) + g\big(x(t)\big)\, u(t)\big) \\ \qquad\quad = \, L_f\, g\big(x(t)\big) + L_g\, h\big(x(t)\big)\, u(t) \\ \qquad\quad = \, L_f\, g\big(x(t)\big) \\ \qquad\quad \vdots \\ y^{[r-1]}(t) = \, L_f^{r-1}\, h\big(x(t)\big) \\ y^{[r]}(t) = L_f^{r}\, h\big(x(t)\big) + L_g\, L_f^{r-1}\, h\big(x(t)\big)\, u(t) \end{array}\right\} \tag{2.28}$$

Note that if r is the smallest integer such that $L_g\, L_f^i\, h(x(t)) \equiv 0$ for $i = 1, 2, \ldots, r-2$ and $L_g\, L_f^{r-1}\, h(x(t))$ is bounded and different from zero, then the nonlinear control law:

$$u(t) = \frac{1}{L_g\, L_f^{r-1}\, h(x(t))} \left(-L_f^r\, h(x(t)) + w(t) \right) \tag{2.29}$$

Gives the following linear system

$$y^{[r]}(t) = w(t) \tag{2.30}$$

Having the closed loop linear system in the form (2.30), a linear control strategy can be used to force the output to keep track of the set point $y_d(t)$. The tracking error and its derivative of order r are:

$$e(t) = y(t) - y_d(t) \text{ and } e^{[r]}(t) = y^{[r]}(t) - y_d{}^{[r]}(t). \tag{2.31}$$

By substituting the expressions of the equation (2.28), one obtains;

$$e^{[r]}(t) = L_f^r\, h(x(t)) + L_g\, L_f^{r-1}\, h(x(t))\, u(t) - y_d{}^{[r]}(t) \tag{2.32}$$

The controller design is based on the change of the error e which must be managed by a globally asymptotically stable differential equation of the following form:

$$e^{[r-1]}(t) + k_{r-2}\, e^{[r-2]}(t) + \cdots + k_o\, e(t) = 0 \tag{2.33}$$

Where the parameters $k_{r-2}, \cdots, k_o$ are the coefficients of a Hurwitz polynomial. They can be obtained using the poles placement method.

Multi-input and multi-output system

Consider the following nonlinear multivariable system

$$\left\{\begin{array}{l} \dot{x}(t) = f(x(t)) + \sum_{t=1}^{p} u_i(t)\,.\, g_i(x(t)) = f(x(t)) + g(x(t))\,u(t) \\ y_1(t) = h_1(x(t)) \\ \quad\vdots \\ y_p(t) = h_p(x(t)) \end{array}\right\} \tag{2.34}$$

Where $x(t) \in M$, n-dimensional smooth fields, the control vector $u(t) = [u_1(t), \ldots, u_p(t)]^T \in \Re^p$ and the output $y \in \Re^p$. We suppose that $f(x)$, $g(x)$ and y_j are smooth. By deriving the j^e output y_j as a function of time, one obtains:

$$\dot{y}_j(t) = L_f h_j(x) + \sum_{i=1}^{p} (L_{gi} h_j(x))\, u_i(t) \tag{2.35}$$

In (2.26), if $L_{gi} h_j(x) = 0, \forall\, i = 1, \ldots p$, none of the inputs appear implicitly in $\dot{y}_j$. Therefore we define r_j as the smallest integer such that at least one of the inputs appears in $y_j^{[r_j]}$. It follows:

$$y_j^{[r_j]}(t) = L_f^{r_j} h_j(x) + \sum_{i=1}^{p} L_{g_i} \left(L_f^{r_j-1} h_j(x)\right) u_i(t) \tag{2.36}$$

It is assumed that $L_{g_i} \left(L_f^{r_j-1} h_j(x)\right) \neq 0$ for some $x \in M$.

Let us now define the decoupling matrix $A(x)$ of dimensions $(p \times p)$:

$$A(x) = \begin{bmatrix} L_{g_1} & L_f^{r_1-1} h_1 & \cdots & L_{g_p} & L_f^{r_1-1} h_1 \\ & \vdots & & & \vdots \\ L_{g_1} & L_f^{r_p-1} h_p & \cdots & L_{g_p} & L_f^{r_p-1} h_p \end{bmatrix} \tag{2.37}$$

Using (2.37), the relation (2.36) can be rewritten in the following form:

$$\begin{bmatrix} y_1^{[r_1]} \\ \vdots \\ y_p^{[r_p]} \end{bmatrix} = \begin{bmatrix} L_f^{r_1} h_1 \\ \vdots \\ L_f^{r_p} h_p \end{bmatrix} + A(x) \begin{bmatrix} u_1 \\ \vdots \\ u_p \end{bmatrix} \tag{2.38}$$

For the points $x \in M$ where the matrix A(x) is invertible, the linearizing control law:

$$\begin{bmatrix} u_1 \\ \vdots \\ u_p \end{bmatrix} = -A^{-1}(x) \begin{bmatrix} L_f^{r_1} h_1 \\ \vdots \\ L_f^{r_p} h_p \end{bmatrix} + A^{-1}(x) \begin{bmatrix} w_1 \\ \vdots \\ w_p \end{bmatrix} \tag{2.39}$$

This control law allows to obtain the decoupled multi-input multi-output system and linear system, as follows:

$$\begin{bmatrix} y_1^{(r1)} \\ \vdots \\ y_p^{(rp)} \end{bmatrix} = \begin{bmatrix} w_1 \\ \vdots \\ w_p \end{bmatrix} \tag{2.40}$$

With (2.40), one becomes able to design a linear control for the tracking problem. In fact, suppose the $y_{jd}(t)$ p trajectories of reference for the p outputs.

The tracking error and its derivatives are defined as follows:

$$e_j(t) = y_j(t) - y_{jd}(t) \text{ and } e^{[r_j]}(t) = y_j^{[r_j]}(t) - y_{jd}^{[r_j]}(t). \tag{2.41}$$

By substituting the equation (2.36) in these expressions, we obtain;

$$e_j^{[r_j]}(t) = L_f^{rj} h_j(x) + \sum_{i=1}^{p} L_{gi} \left(L_f^{r_j - 1} h_j(x) \right) u_i(t) - y_{jd}^{[r_j]}(t) \tag{2.42}$$

The multivariable control must be determined based on the change of e_j which is managed by a globally asymptotically stable differential equation of the following form:

$$\begin{bmatrix} e_1^{[r_1-1]}(t) & + k_{r_1-2,1} & e_1^{[r_1-2]}(t) & +\cdots+ & k_{0,1} & e_1(t) \\ e_2^{[r_2-1]}(t) & + k_{r_2-2,2} & e_2^{[r_2-2]}(t) & +\cdots+ & k_{0,2} & e_2(t) \\ \vdots & & \vdots & +\cdots+ & \vdots & \\ e_p^{[r_p-1]}(t) & + k_{r_p-2,p} & e_p^{[r_p-2]}(t) & +\cdots+ & k_{0,p} & e_p(t) \end{bmatrix} = \begin{bmatrix} 0 \\ 0 \\ \vdots \\ 0 \end{bmatrix} \quad (2.43)$$

As already mentioned the parameters of the design $k_{r_j-2,1}, \cdots, k_{o,j}$ can be obtained by the pole placement method.

2.3.2 Application of the exact nonlinear control on the active filter

2.3.2.1 Local approach

In order to apply the theory of exact nonlinear control in the input-output linearization approach, the model will be divided into two subsystems, in particular, a MIMO type subsystem containing the dynamics of the currents of the active filter and a subsystem of the SISO type consisting of the dynamics of the DC voltage. The exact nonlinear control is applied to each of the two subsystems (Mendalek, 2003).

2.3.2.2 Current loop

To design the inner loop of the current, the first two differential equations of the model (2.26) are considered. These will be decoupled by applying the theory of the exact nonlinear control. The first two differential equations are rewritten in the following form:

$$\begin{bmatrix} \frac{di_d}{dt} \\ \frac{di_q}{dt} \end{bmatrix} = \begin{bmatrix} -\frac{R_c}{L_c} i_d + \omega i_q + \frac{v_d}{L_c} \\ -\frac{R_c}{L_c} i_q - \omega i_d + \frac{v_q}{L_c} \end{bmatrix} + \begin{bmatrix} -\frac{v_{dc}}{L_c} & 0 \\ 0 & -\frac{v_{dc}}{L_c} \end{bmatrix} \begin{bmatrix} d_{nd} \\ d_{nq} \end{bmatrix}$$

$$y_1 = h_1(x) = i_d$$
$$y_2 = h_2(x) = i_q \qquad (2.44)$$

This system is a multiple input multiple output MIMO nonlinear type system that has two inputs and two outputs. The relative degrees of the outputs are $r_1 = r_2 = 1$, and we have the following:

$$\begin{bmatrix} L_f^{r_1} h_1 \\ L_f^{r_2} h_2 \end{bmatrix} \triangleq \begin{bmatrix} -\frac{R_c}{L_c} i_d + \omega i_q + \frac{v_d}{L_c} \\ -\frac{R_c}{L_c} i_q - \omega i_d + \frac{v_q}{L_c} \end{bmatrix}, \qquad A(x) = \begin{bmatrix} -\frac{v_{dc}}{L_c} & 0 \\ 0 & -\frac{v_{dc}}{L_c} \end{bmatrix} \qquad (2.45)$$

$$\text{and } \begin{bmatrix} u_1 \\ u_2 \end{bmatrix} = \begin{bmatrix} d_{nd} \\ d_{nq} \end{bmatrix}$$

It is obvious that A(x) is invertible. Therefore, the input signals can be deduced to be modulated by the space vector modulator by:

$$\begin{bmatrix} u_1 \\ u_2 \end{bmatrix} = -A^{-1}(x) \begin{bmatrix} L_f^{r_1} h_1 \\ L_f^{r_2} h_2 \end{bmatrix} + A^{-1}(x) \begin{bmatrix} u_d \\ u_q \end{bmatrix} \qquad (2.46)$$

The control law can be obtained as follows:

$$\begin{Bmatrix} u_1 = d_{nd} = \dfrac{1}{v_{dc}}(-R_c i_d + L_c \omega i_q + v_d - L_c u_d) \\ \\ u_2 = d_{nq} = \dfrac{1}{v_{dc}}(-R_c i_q - L_c \omega i_d + v_q - L_c u_q) \end{Bmatrix} \tag{2.47}$$

Applying these nonlinear controls, the dynamics in the closed loop of the inner loop becomes a set of linear decoupled equations as follows:

$$\begin{bmatrix} \dfrac{di_d}{dt} \\ \\ \dfrac{di_q}{dt} \end{bmatrix} = \begin{bmatrix} u_d \\ \\ u_q \end{bmatrix} \tag{2.48}$$

The currents i_d and i_q will be controlled independently by acting upon the inputs u_d and u_q respectively. An integrator can also be added to eliminate the tracking steady-state error. The expressions of the compensators are then as follows:

$$\begin{Bmatrix} u_d = \dfrac{di_d}{dt} = \dfrac{di_d^*}{dt} + k_p \tilde{i}_d + k_i \int \tilde{i}_d \, dt \\ \\ u_q = \dfrac{di_q}{dt} = \dfrac{di_q^*}{dt} + k_p \tilde{i}_q + k_i \int \tilde{i}_q \, dt \end{Bmatrix} \tag{2.49}$$

Where $\tilde{i}_d = i_d^* - i_d$ and $\tilde{i}_q = i_q^* - i_q$ are the current errors, and i_d^*, i_q^* denote the references of (i_d, i_q). The closed loop current error dynamics are given by:

$$\begin{Bmatrix} \ddot{\tilde{i}}_d + k_p \tilde{i}_d + k_i \tilde{i}_d = 0 \\ \\ \ddot{\tilde{i}}_q + k_p \tilde{i}_q + k_i \tilde{i}_q = 0 \end{Bmatrix} \tag{2.50}$$

In order to obtain asymptotic tracking, the error characteristic equations are compared to the standard second-order equation $s^2 + 2\xi\omega_{ni}s + \omega_{ni}^2 = 0$, where ω_{ni} is the natural frequency and ξ is the damping factor. The proportional gain k_p and the integral gain k_i will be obtained as follows:

$$k_p = 2\xi\omega_{ni} \text{ and } k_i = \omega_{ni}^2 \tag{2.51}$$

For the optimal value of the damping factor $\xi = \sqrt{2/2}$, and the inner loop natural frequency ω_{ni} may be selected to be as high as possible, yet it is limited by the value of the switching frequency.

2.3.2.3 Outer loop

The instantaneous active and reactive power exchanged between the active filter and the AC supply is given by:

$$\mathrm{P} = \mathrm{v_d i_d} \text{ and } \mathrm{Q} = -\mathrm{v_d i_q}$$

since $v_q = 0$ under ideal supply conditions

This shows that in order to maintain the DC voltage value across the DC capacitor of the active filter, the losses through the active filter's resistive inductive components can be compensated by acting on the current i_d. Therefore, an auxiliary input of the output feedback loop is defined as:

$$\mathrm{i_e} = \mathrm{C}\frac{\mathrm{dv_{dc}}}{\mathrm{dt}} = \mathrm{C\,dv_{dc}^*} + \mathrm{k_1\tilde{v}_{dc}} + \mathrm{k_2}\int \mathrm{\tilde{v}_{dc}\,dt} \tag{2.52}$$

where $\mathrm{\tilde{v}_{dc}} = \mathrm{v_{dc}^*} - \mathrm{v_{dc}}$ is the DC voltage error. The closed-loop dynamic voltage error becomes:

$$\ddot{\tilde{\mathrm{v}}}_{\mathrm{dc}} + \frac{\mathrm{k_1}}{\mathrm{C}}\dot{\tilde{\mathrm{v}}}_{\mathrm{dc}} + \frac{\mathrm{k_2}}{\mathrm{C}}\tilde{\mathrm{v}}_{\mathrm{dc}} = 0 \tag{2.53}$$

The proportional gain k_1 and the integral gain k_2 are derived from:

$$k_1 = 2\xi\omega_{nv}C \text{ and } k_2 = \omega_{nv}^2 C \tag{2.54}$$

In the outer loop, the natural frequency ω_{nv} should be selected to be close to the supply fundamental frequency. The control law can be derived using both (2.52) and the third equation in the main model (2.26).

$$\mathrm{i}_{\mathrm{do}}^{*} = \frac{\mathrm{i}_{\mathrm{e}} - \mathrm{d}_{\mathrm{nq}}\mathrm{i}_{\mathrm{q}}}{\mathrm{d}_{\mathrm{nd}}} = \frac{\mathrm{i}_{\mathrm{e}}\mathrm{v}_{\mathrm{dc}} - \mathrm{d}_{\mathrm{nq}}\mathrm{v}_{\mathrm{dc}}\mathrm{i}_{\mathrm{q}}}{\mathrm{d}_{\mathrm{nd}}\mathrm{v}_{\mathrm{dc}}} \tag{2.55}$$

Assuming the inner current loops to be ideal and that the active power filter operates in normal conditions, therefore these properties hold:

$$\mathrm{d}_{\mathrm{nq}}\mathrm{v}_{\mathrm{dc}} \approx \mathrm{v}_{\mathrm{q}} \text{ and } \mathrm{d}_{\mathrm{nd}}\mathrm{v}_{\mathrm{dc}} \approx \mathrm{v}_{\mathrm{d}} \tag{2.56}$$

Assuming also that the supply voltages are given by:

$$\begin{aligned} v_1 &= \hat{V}\cos(\omega t) \\ v_2 &= \hat{V}\cos(\omega t - 2\pi/3\,) \\ v_3 &= \hat{V}\cos(\omega t - 4\pi/3) \end{aligned} \tag{2.57}$$

and considering the transformation to the synchronous reference frame which gives:

$$\begin{bmatrix} \mathrm{v}_{\mathrm{d}} \\ \mathrm{v}_{\mathrm{q}} \end{bmatrix} = \sqrt{2}\begin{bmatrix} \cos(\theta - \pi/6) & \sin\theta \\ -\sin(\theta - \pi/6) & \cos\theta \end{bmatrix}\begin{bmatrix} \mathrm{v}_1 \\ \mathrm{v}_2 \end{bmatrix} = \sqrt{\frac{3}{2}}\begin{bmatrix} \hat{\mathrm{V}} \\ 0 \end{bmatrix} \tag{2.58}$$

This shows that:

$$\mathrm{d}_{\mathrm{nq}}\mathrm{v}_{\mathrm{dc}} \approx \mathrm{v}_{\mathrm{q}} = 0 \text{ and } \mathrm{d}_{\mathrm{nd}}\mathrm{v}_{\mathrm{dc}} \approx \mathrm{v}_{\mathrm{d}} = \sqrt{\frac{3}{2}}\hat{\mathrm{V}} \tag{2.59}$$

Therefore the control law can be given by:

$$i_{do}^{*} \approx \sqrt{\frac{2}{3}} \frac{v_{dc}}{\hat{V}} i_{e} \tag{2.60}$$

The reference current i_{do}^{*} is added to the harmonic reference current of i_{d} loop. The i_{do}^{*} is a DC component, which forces the active filter to draw a current at the fundamental frequency to compensate for the converter switching and conduction losses.

2.3.2.4 Current loop references

Since the fundamental positive sequence components of the nonlinear load currents appear as DC quantities in the synchronous reference frame, they can be simply separated from the actual load current. As shown in figure 2.2, two load currents i_{L1} and i_{L2} are measured and converted to synchronous reference frame i_{Ld} and i_{Lq}. While the current i_{Ld} is processed through a low-pass filter to isolate its DC component and then extract its harmonic componenti_{Ldh}. i_{Lq} is inverted and used as a harmonic and reactive reference component i_{q}^{*}, this requires the generation of in-phase and in-quadrature sinusoidal synchronous signals with the supply voltage, that can be acquired by using a PLL circuit.

The current loop references become:

$$\begin{aligned} i_{d}^{*} &= -i_{Ldh} + i_{do}^{*} \\ i_{q}^{*} &= -i_{Lq} \end{aligned} \tag{2.61}$$

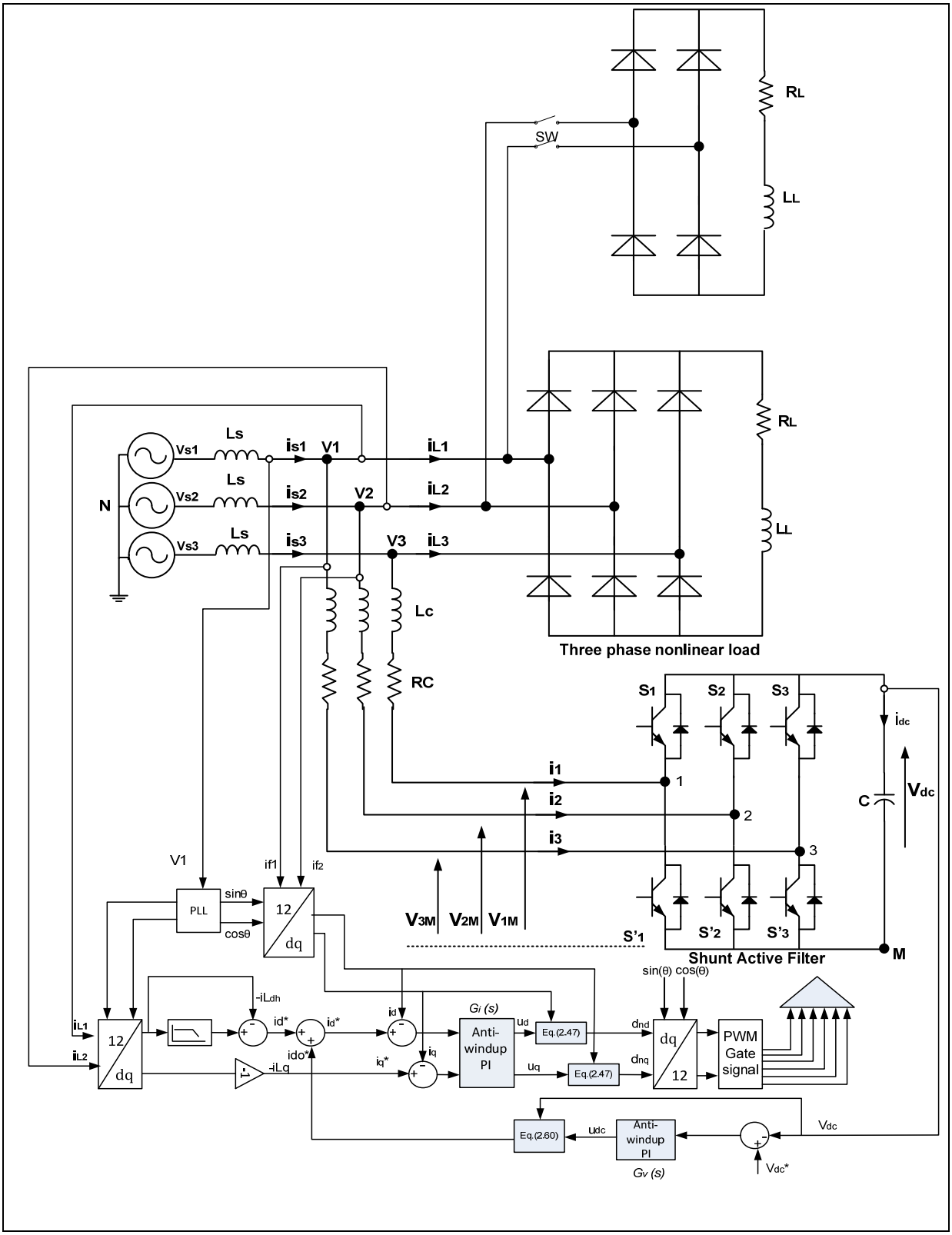

Figure 2.2 Nonlinear control scheme of the SAPF

2.3.3 Determination of internal dynamics

In order to determine the internal dynamics, the state representation of the model in the synchronous "dq" frame obtained during the modeling of this converter (2.26) is used:

$$\begin{cases} L_c \dfrac{di_d}{dt} = -R_c i_d + L_c \omega i_q - v_{dc}\, d_{nd} + V_d \\ L_c \dfrac{di_q}{dt} = -R_c i_q - L_c \omega i_d - v_{dc}\, d_{nq} + V_q \\ C \dfrac{dv_{dc}}{dt} = d_{nd}\, i_d + d_{nq} i_q \end{cases}$$

By observing this state representation, it can be noticed that the state variables i_d and i_q are each found in the dynamics of the other, which means that in this state model there is a coupling between the state variables. Moreover, one can also note that the inputs d_{nd} and d_{nq}, which are in fact the control laws on the d-axis and the q-axis multiply the state variables id, iq or vdc. And since the laws of control are not constant in time, then these products ($vdc \times dnd$, $vdc \times dnq$, $dnd \times id$, or $dnq \times iq$) are not constant but rather variable. Therefore, this state representation is a nonlinear system.

Accordingly, an input-output nonlinear control is developed to determine if internal dynamics exists. For this purpose, from the state model, we define the following state variables:

$$\begin{cases} X_1 = i_d \\ X_2 = i_q \\ X_3 = v_{dc} \end{cases}$$

The state model becomes:

$$\begin{Bmatrix} X_1 = -\frac{R_c}{L_c}X_1 + \omega X_2 - \frac{1}{L_c}X_3 \mathrm{d}_{nd} + \frac{\mathrm{V}_d}{L_c} \\ X_2 = -\frac{R_c}{L_c}X_2 - \omega X_1 - \frac{1}{L_c}X_3 \mathrm{d}_{nq} + \frac{\mathrm{V}_q}{L_c} \\ X_3 = \frac{1}{C}\mathrm{d}_{nd}\, X_1 + \frac{1}{C}\mathrm{d}_{nq} X_2 \end{Bmatrix} \quad (2.62)$$

The model can be written in the following form:

$$\begin{bmatrix} \dot{X}_1 \\ \dot{X}_2 \\ \dot{X}_3 \end{bmatrix} = \begin{bmatrix} -\frac{R_c}{L_c}X_1 + \omega X_2 + \frac{\mathrm{V}_d}{L_c} \\ -\omega X_1 - \frac{R_c}{L_c}X_2 + \frac{\mathrm{V}_q}{L_c} \\ \frac{1}{C}\mathrm{d}_{nd}\, X_1 + \frac{1}{C}\mathrm{d}_{nq} X_2 \end{bmatrix} + \begin{bmatrix} -\frac{1}{L_c}X_3 & 0 \\ 0 & -\frac{1}{L_c}X_3 \end{bmatrix} \begin{bmatrix} d_{nd} \\ d_{nq} \end{bmatrix} \quad (2.63)$$

Thus the system is of the form:

$\dot{X} = F(X) + G(X)U$ (General form of a nonlinear system), with,

$$F(X) = \begin{bmatrix} -\frac{R_c}{L_c}X_1 + \omega X_2 + \frac{\mathrm{V}_d}{L_c} \\ -\omega X_1 - \frac{R_c}{L_c}X_2 + \frac{\mathrm{V}_q}{L_c} \\ \frac{1}{C}\mathrm{d}_{nd}\, X_1 + \frac{1}{C}\mathrm{d}_{nq} X_2 \end{bmatrix};\ G(X) = \begin{bmatrix} -\frac{1}{L_c}X_3 & 0 \\ 0 & -\frac{1}{L_c}X_3 \end{bmatrix} \quad (2.64)$$

and $\mathrm{U} = \begin{bmatrix} \mathrm{d}_{\mathrm{nd}} \\ \\ \mathrm{d}_{\mathrm{nq}} \end{bmatrix}$ the input vector.

The following outputs are selected:

$$\begin{Bmatrix} \mathrm{y}_1 = \mathrm{X}_1 \\ \mathrm{y}_2 = \mathrm{X}_2 \end{Bmatrix}$$

Differentiating the outputs until the inputs appear leads to:

$$\left.\begin{aligned}\dot{y}_1 = \dot{X}_1 = -\frac{R_c}{L_c}X_1 + \omega X_2 + \frac{\mathrm{V}_d}{L_c} - \frac{1}{L_c}X_3\mathrm{d}_{nd}\\ \dot{y}_2 = \dot{X}_2 = -\omega X_1 - \frac{R_c}{L_c}X_2 + \frac{\mathrm{V}_q}{L_c} - \frac{1}{L_c}X_3\mathrm{d}_{nq}\end{aligned}\right\} \quad (2.65)$$

Thus, the system in the matrix form becomes:

$$\begin{bmatrix}\dot{y}_1\\ \dot{y}_2\end{bmatrix} = \begin{bmatrix}-\frac{R_c}{L_c}X_1 + \omega X_2 + \frac{\mathrm{V}_d}{L_c}\\ -\omega X_1 - \frac{R_c}{L_c}X_2 + \frac{\mathrm{V}_q}{L_c}\end{bmatrix} + \begin{bmatrix}-\frac{1}{L_c}X_3 & 0\\ 0 & -\frac{1}{L_c}X_3\end{bmatrix}\begin{bmatrix}d_{nd}\\ d_{nq}\end{bmatrix} \quad (2.66)$$

$\leftrightarrow\ \dot{y} = A(x) + G(x)U$, with

$$A(x) = \begin{bmatrix}-\frac{R_c}{L_c}X_1 + \omega X_2 + \frac{\mathrm{V}_d}{L_c}\\ -\omega X_1 - \frac{R_c}{L_c}X_2 + \frac{\mathrm{V}_q}{L_c}\end{bmatrix};\ G(x) = \begin{bmatrix}-\frac{1}{L_c}X_3 & 0\\ 0 & -\frac{1}{L_c}X_3\end{bmatrix} \quad (2.67)$$

$$\text{and } U = \begin{bmatrix}d_{nd}\\ d_{nq}\end{bmatrix}.$$

For $X_3 \neq 0$ we have $G(x) \neq [0]$ and therefore the relative degree *r* is

$$r = r_1 + r_2 = 1 + 1 = 2$$

$r = 2 < n = 3$ (n = Degree of the system) and therefore we have input-output linearization. In addition, we have $n - r = 3 - 2 = 1 \neq 0$, this means that there is an internal variable(η). In this case, the linearization control is consequently (Slotine et Li, 1991):

$$\mathrm{U} = \begin{bmatrix}\mathrm{d_{nd}}\\ \mathrm{d_{nq}}\end{bmatrix} = \mathrm{G^{-1}(x)} \times \big(\mathrm{v} - \mathrm{A(x)}\big) \quad (2.68)$$

$$\text{with } G^{-1}(x) = \begin{bmatrix} -\frac{L_c}{X_3} & 0 \\ 0 & -\frac{L_c}{X_3} \end{bmatrix} \text{ and } v = \begin{bmatrix} v_1 \\ v_2 \end{bmatrix} \tag{2.69}$$

Consequently, the dynamics of the output becomes

$$\dot{y} = v \leftrightarrow \begin{bmatrix} \dot{y}_1 \\ \dot{y}_2 \end{bmatrix} = \begin{bmatrix} v_1 \\ v_2 \end{bmatrix} \tag{2.70}$$

Here we have:

$$\begin{Bmatrix} v_1 = U_d \\ v_2 = U_q \end{Bmatrix} \tag{2.71}$$

which are the equivalent inputs of decoupling and linearization of the output dynamics. By applying the Laplace transform on (2.70) we obtain:

$$\frac{y}{v} = \frac{1}{s} \tag{2.72}$$

In closed-loop, we will have the following transfer function

$$G_f(s) = \frac{G_{PI}(s) \times G_o(s)}{1 + G_{PI}(s) \times G_o(s)} = \frac{k_p s + k_i}{s^2 + k_p s + k_i} \tag{2.73}$$

where $G_o$the open loop transfer is function of the current and G_{PI} the PI controller transfer function.

In applying pole imposition method we will have:

$$\begin{Bmatrix} k_p = 2\zeta\omega_o \\ k_i = \omega_o^2 \end{Bmatrix} \tag{2.74}$$

2.3.3.1 Determination of the internal variable η

We know that the internal variable η is such that:

$$\frac{\partial \eta}{\partial X} \times G(x) = 0 \leftrightarrow \left[\frac{\partial \eta}{\partial X_1} \quad \frac{\partial \eta}{\partial X_2}\right] \times \begin{bmatrix} -\frac{L_c}{X_3} & 0 \\ 0 & -\frac{L_c}{X_3} \end{bmatrix} = 0 \tag{2.75}$$

Since $-\frac{X_3}{L_c} \neq 0$, so we have

$$\begin{Bmatrix} \frac{\partial \eta}{\partial X_1} = 0 \\ \frac{\partial \eta}{\partial X_2} = 0 \end{Bmatrix} \tag{2.76}$$

Which means that the internal variable does not depend on the state variables X_1 and X_2, which is normal, because these state variables are already selected as outputs of the system.
In this case, it remains that:

$$\boldsymbol{\eta = X_3}$$

The internal dynamics is written as:

$$\dot{\eta} = \dot{X}_3 = \frac{1}{C} d_{nd} X_1 + \frac{1}{C} d_{nq} X_2 \tag{2.77}$$

The zero dynamics implies $X_1 = X_2 = 0$ and then the internal dynamics becomes:

$$\dot{\eta} = 0$$

2.3.3.2 Stability study of the internal dynamics

To determine whether the internal dynamics is stable or unstable, a linearization is performed around the equilibrium point ($\eta_o = 0$)

$$\Delta\dot{\eta} = \frac{\partial f(\eta)}{\partial \eta}\,\Delta\eta$$

$$\Delta\eta = \eta - \eta_o \; with \; f(\eta) = \dot{\eta} = 0 \rightarrow \frac{\partial f(\eta)}{\partial \eta} = 0 \tag{2.78}$$

We have: $\Delta\dot{\eta} = 0 \times \Delta\eta$: Linearization of internal dynamics

The matrix A is therefore: $A = [0]$. We determine the poles of the matrix $[sI - A]$

$$(sI - A) = (s - 0) = 0 \rightarrow s = 0$$

Since $s = 0$ which is a pole at the origin then the internal dynamics is marginally stable. This is abnormal because the internal dynamics must be asymptotically stable.

To overcome the problem, one can do either:

- A measured and controlled internal dynamic, where V_{dc} is measured and controlled. Hence the closed-loop poles are chosen to be stable, on the left side of the imaginary/real axis, and it becomes asymptotically stable.
- Add a resistance in parallel with the capacitor and rewrite the dynamics of the voltage across the capacitor.

Here, to overcome this problem a resistance is added as per safety regulations for industrial applications. Consequently, the current flowing through the capacitor is written as:

$$i_c = C\frac{dv_{dc}}{dt} = d_{nd}i_d + d_{nq}i_q - \frac{1}{R}\,v_{dc} \tag{2.79}$$

With the state variables, this expression becomes:

$$\dot{X}_3 = \frac{1}{C} d_{nd} X_1 + \frac{1}{C} d_{nq} X_2 - \frac{1}{RC} X_3 \tag{2.80}$$

Therefore the internal dynamics becomes:

$$\dot{\eta} = \frac{1}{C} d_{nd} X_1 + \frac{1}{C} d_{nq} X_2 - \frac{1}{RC} X_3 \tag{2.81}$$

By applying the zero dynamics, we have:

$$\begin{gathered} \dot{\eta} = -\frac{1}{RC} X_3 \\ \leftrightarrow \ \dot{\eta} = -\frac{1}{RC} \eta \qquad because\ X_3 \neq 0 \end{gathered} \tag{2.82}$$

Linearization of the internal dynamics around the equilibrium point

$$\begin{gathered} \Delta\dot{\eta} = \frac{\partial f(\eta)}{\partial \eta}\ \Delta\eta \\ f(\eta) = \ -\frac{1}{RC}\eta \ \rightarrow \ \frac{\partial f(\eta)}{\partial \eta} = \ -\frac{1}{RC} \end{gathered} \tag{2.83}$$

Hence, the linearization of the internal dynamics is:

$$\Delta\dot{\eta} = \ \dot{\eta} = \ -\frac{1}{RC}\Delta\eta \tag{2.84}$$

$$\left\{ \begin{array}{l} d_{nd} = -\frac{L_c}{X_3}\left(U_d + \frac{R_c}{L_c} X_1 - \omega X_2 - \frac{\mathrm{V}_d}{L_c}\right) = \frac{1}{X_3}\left(-L_c U_d - R_c X_1 + \ \omega L_c X_2 + \mathrm{V}_d\right) \\ d_{nq} = -\frac{L_c}{X_3}\left(U_q + \omega X_1 + \frac{R_c}{L_c} X_2 - \frac{\mathrm{V}_q}{L_c}\right) = \frac{1}{X_3}\left(-L_c U_q - \omega L_c X_1 - R_c X_2 + \mathrm{V}_q\right) \end{array} \right\} \tag{2.85}$$

2.4 Anti-windup PI controller scheme

The PI controller used in the control system governing the shunt active filter is considered as an essential component of the system. However, the performance of a typical PI controller is limited by the existence of saturation, which causes what is known as integrator windup. This phenomenon occurs when the input error to the controller is large or the input error remains nonzero for a long time. When this happens the controller may give delayed response to any change in the input. The feedback loop is then broken and the system goes as in open-loop. The integral will also accumulate since the error is zero. In order to overcome this problem, it is necessary to implement an anti-windup scheme to prevent the controller from saturation. There are many ways to avoid windup where they basically diverge to two techniques, that is conditional-integration, where the value of the integrator is frozen when certain conditions are verified, and back-calculation, where the difference between the controller output and the actual process input is fed back to the integral terms (Visioli, 2003). In this thesis, the back-calculation method is considered. Before applying the anti-windup scheme a review of a typical PI controller is presented:

PI controller:

The transfer function of a typical PI controller is expressed as:

$$G_{PI}(s) = K_p + \frac{K_i}{s} \tag{2.86}$$

where K_p is the proportional constant and K_i is the integral constant

The output of the controller y can be expressed as:

$$y = K_p \times e + K_i \int e\,dt \tag{2.87}$$

where e is the input error.

The block diagram of a typical PI controller is given below in figure 2.3:

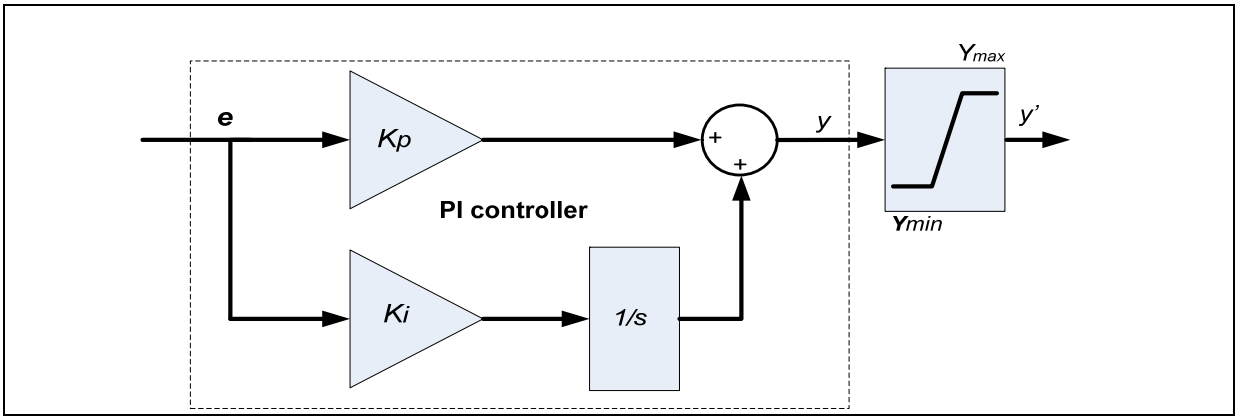

Figure 2.3 Block diagram of a PI controller

2.4.1 Back Calculation method

This technique is shown in Figure 2.4 where the system has an additional feedback path that is created by calculating the real output and developing an error signal as the discrepancy between the output of the controller (y) and the actuator output (y'). The difference is routed to the integrator input over a gain K_{lim}. The difference is zero while there is no saturation and the additional feedback loop has no influence on the system as $y = y'$. Otherwise, once the actuator saturates, the difference is fedback to the integrator in a way that it goes to zero. This suggests that output of the controller is retained near to the saturation limit. The controller output will then change once the error changes sign and integral windup is avoided (Ghoshal et John, 2010).

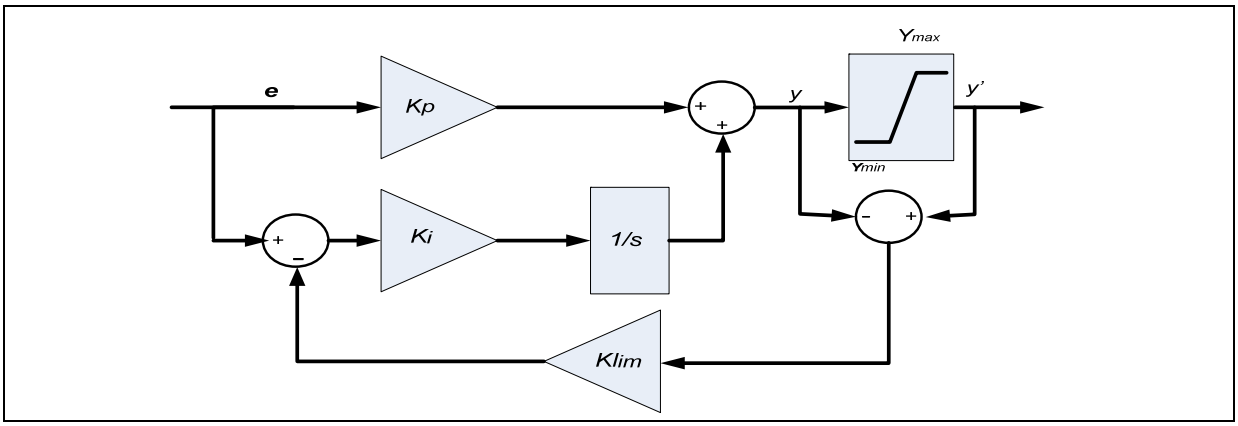

Figure 2.4 PI controller with back calculation anti-windup scheme

The steady state value of output 'y' is of interest for choosing K_{lim}. Considering a situation where $y > Y_{max}$, the following relationships can be derived to get an indication of steady state and dynamic behaviour of the PI controller under saturation with back calculation anti-windup control, where Y_{max} the maximum saturation limit and Y_{min} the minimum saturation limit.

Let us denote the output of integrator as "x", then

$$y = x + K_p \times e \tag{2.88}$$

$$y = \left(e + K_{lim}(y - Y_{max})\right)K_i \, 1/s + K_p \, e \tag{2.89}$$

$$Y(s) = \left(E(s) + K_{lim}(y(s) - Y_{max})\right)K_i + K_p \, E(s) \tag{2.90}$$

$$y = \frac{(K_p s + K_i)}{(s + K_{lim}K_{i)}} E - \frac{K_{lim}K_i}{(s + K_{lim}K_{i)}} Y_{max} \tag{2.91}$$

$$y = \frac{K_i\left(\frac{K_p}{K_i}s + 1\right)}{K_{lim}K_i\left(\frac{s}{K_{lim}K_i} + 1\right)} E - \frac{K_{lim}K_i}{(s + K_{lim}K_i)} Y_{max} \tag{2.92}$$

$$y = \frac{1}{K_{lim}} \frac{(T_1 s + 1)}{(T_2 s + 1)} E - \frac{K_{lim}K_i}{(s + K_{lim}K_i)} Y_{max} \tag{2.93}$$

$$y = \frac{1}{K_{lim}} \left[\frac{T_1}{T_2} + \frac{\left(1 - \frac{T_1}{T_2}\right)}{(T_2 s + 1)}\right] E - \frac{K_{lim}K_i}{(s + K_{lim}K_i)} Y_{max} \tag{2.94}$$

Assuming the initial conditions are zero, the solution of the above equation is obtained

$$y = \frac{E}{K_{lim}} \left(1 + \left(\frac{T_1}{T_2} - 1\right) e^{-\frac{t}{T_2}}\right) - K_{lim}K_i Y_{max} \left(1 + e^{-\frac{t}{T_2}}\right) \tag{2.95}$$

If the steady-state value of 'y' is Y_{ss}, then

$$Y_{ss} = \frac{E}{K_{lim}} - K_i K_{lim} Y_{max} = -K_i K_{lim}\left(-\frac{E}{K_i K_{lim}^{\,2}} + Y_{max}\right) \tag{2.96}$$

To keep the output of the PI controller less than the maximum of the saturation block, then the following is considered:

$$K_i K_{lim} = -1 \rightarrow \begin{Bmatrix} K_{lim} & = -10 \\ K_i = & 0.1 \end{Bmatrix} \tag{2.97}$$

Consequently, when $E > 0$ the ratio $-\frac{E}{K_i K_{lim}^{\,2}} < 0$ guarantees that the steady state output Y_{ss} will be less than Y_{max}.

In order to test the performance of the anti-windup PI controller, an example of a second order system as shown in figure 2.5 is simulated and the simulation results are presented in figure 2.6.

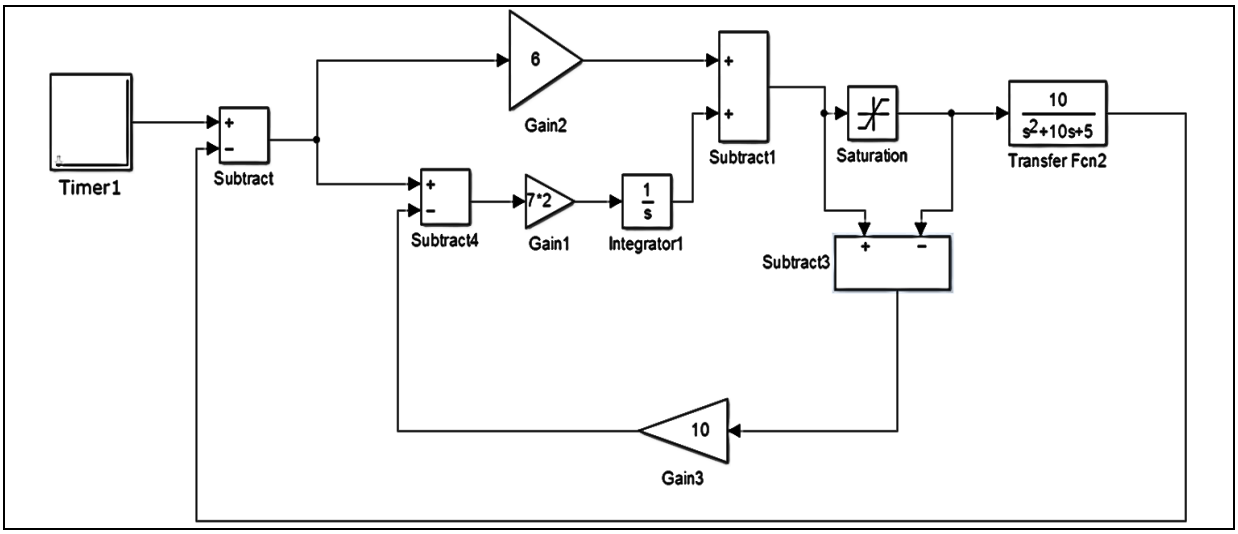

Figure 2.5 PI controller with anti-windup scheme

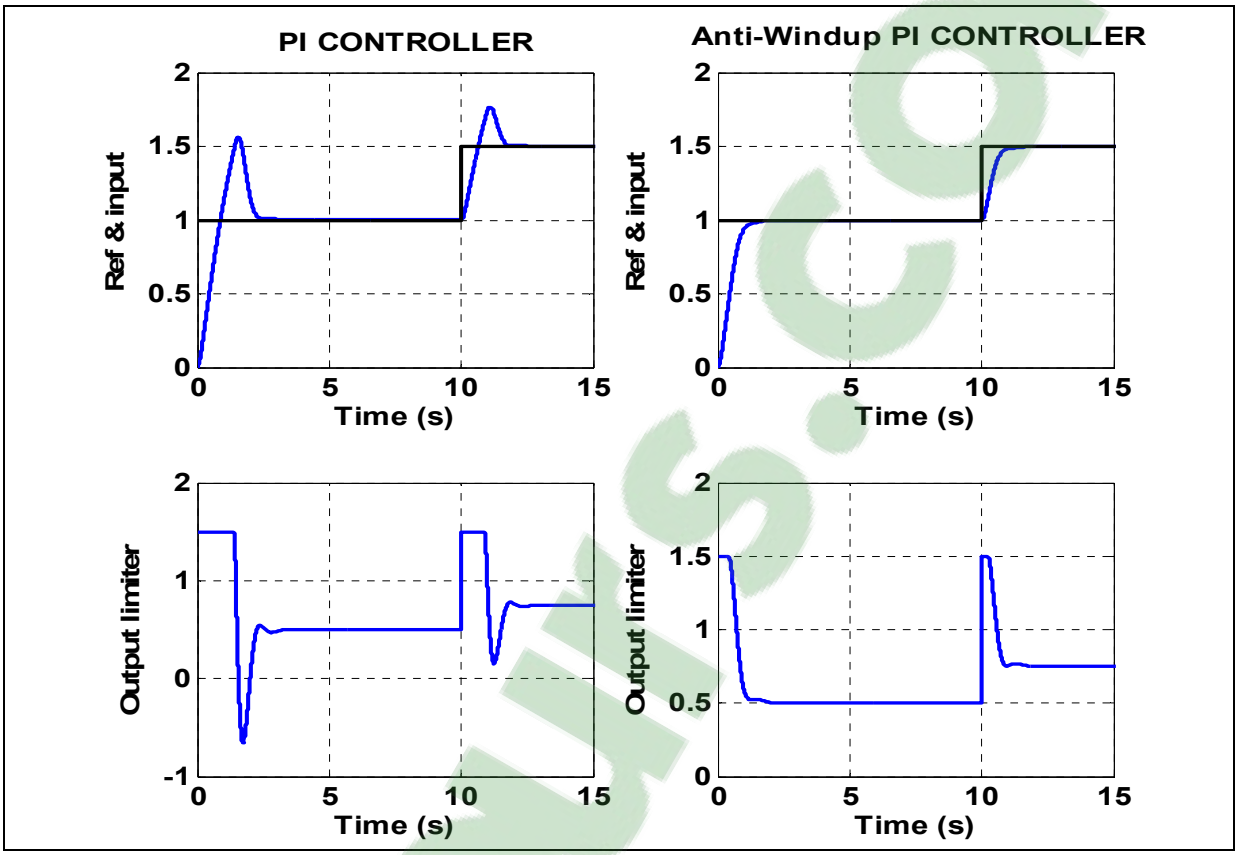

Figure 2.6 Simulation of windup (left) and anti-windup (right)

The simulation results show the windup effect when using a typical PI controller without an anti-windup control. When the input error changes a response delay is produced and the controller output is saturated. However, when an anti-windup PI control is applied, the performance is much improved in terms of faster response time and, the large overshoot is avoided.

CHAPITRE 3

DESIGN OF THREE PHASE THREE WIRE SHUNT ACTIVE POWER FILTER

3.1 Introduction

The power circuit of the SAPF consists of a three-phase voltage source inverter and a harmonic producing load (represented by a bridge rectifier with diodes feeding RL load) as shown in Figure. 3.1. a. A three-phase supply is modeled by three sinusoidal voltage sources in series with an inductance L_s. An additional inductance L_c is connected to the bridge rectifier input in order to limit the di_L/dt gradients at the starting conduction of diodes.

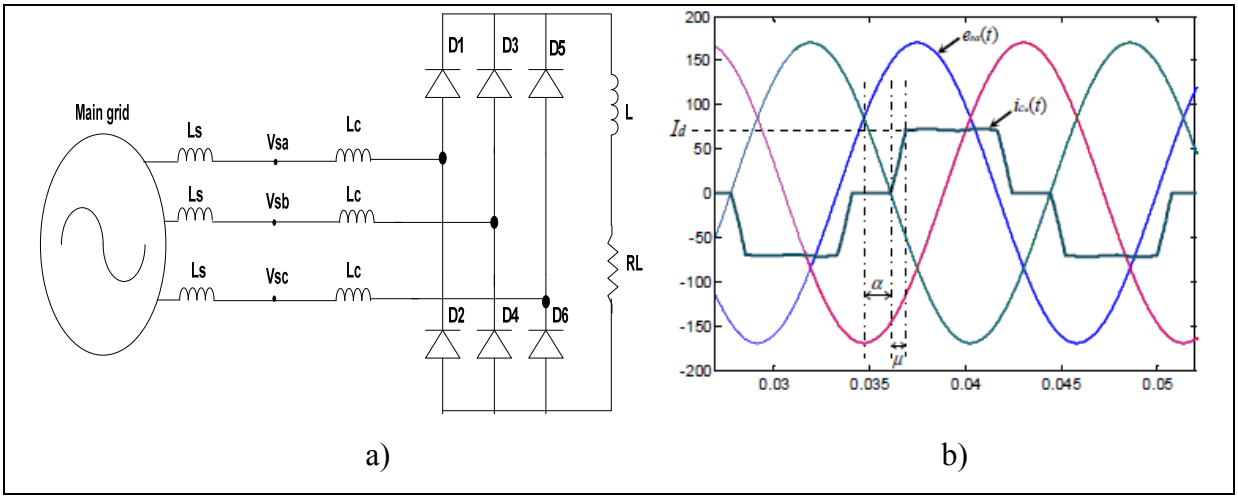

Figure 3.1 Bridge rectifier with diodes feeding RL loads

Consequently, the switching of the diodes cannot be considered as instantaneous and allows an overlap of the conduction intervals of the semiconductors to appear, assuming that the DC side inductance is very large, enabling the converter to supply a perfectly smoothed rectified current I_d. The voltages $v_{sa}(t)$, $v_{sb}(t)$ and $v_{sc}(t)$ form a balanced three-phase system. Considering that the current varies linearly during switching phases, which leads to a trapezoidal alternating current pattern as shown in figure 3.1.b. The parameters of the system are shown in table 3.1.

Table 3.1 System design parameters

Description	Value
Apparent power (S_L)	$S_L = 27\ kVA$
RMS Line voltage (V_{SL})	208 V
RMS load current (I_{La})	$\frac{S_L}{3*V_{Sa}} = 75A$
Frequency source (f_S)	60 Hz
DC load current (I_{dc})	$\frac{I_{La}}{\sqrt{\left(\frac{2}{3}\right)}} = \frac{75}{\sqrt{\left(\frac{2}{3}\right)}} = 91.85\ A$
Fundamental load current (I_{La1})	$I_{dc}\frac{\sqrt{6}}{\pi} = 71.61\ A$
THD of the load current (THD)	$\sqrt{\left(\frac{I_{La}}{I_{La1}}\right)^2 - 1} = 31\%$
Load active power (P_L)	$3 * Vs * I_{La1} * \cos(\varphi_1) = 23\ kW$
RMS fundamental active load current (I_{La1_active})	$\frac{23000}{3*120} = 64.44\ A$
RMS active filter current (I_{comp})	$\sqrt{I_{La}^2 - I_{La1\_active}^2} = 38.35\ A$
Series inductor with the three-phase rectifier diodes (L_{series})	$L_{series} = 0.58\ mH$

The series inductor of the three-phase diode rectifier is calculated using the base impedance given by:

$$Z_{base} = \frac{V_b}{I_b} = \frac{208}{75} = 2.77\ \Omega \tag{3.1}$$

The series inductor is selected to be in the range of 5% - 10% of the base impedance, hence the value of the inductor is:

$$Z_{series} = 8\% \times Z_b = 0.08 \times 2.77 = 0.22\ \Omega$$
$$L_{series} = \frac{Z_{series}}{2 \times \pi \times f} \frac{0.22}{2 \times 3.14 \times 60} = 0.58\ mH \quad (3.2)$$

3.2 Estimation of filter parameters

Several control systems have been developed in recent years for active power filtering. The parameters of the SAPF are often deemed properly estimated, or at least they do not affect the control system performance. The first step in the SAPF design is to select appropriate parameters, in order to reduce the cost, avoid control problems and achieve satisfying filtering performance. However, the value selection of the coupling inductance (L_f) and the capacitance (C) is subjected to several constraints, such as harmonic distortion and reactive power compensation (Chaoui, 2010).

Knowing that SAPF behaves like a controlled current source that acts on the mains current to improve its characteristics in terms of harmonics disturbance and phase shift, the current generated by the SAPF is distorted, which imposes a controllability constraint on the coupling inductor value (L_f). Similarly, for selecting the capacitor values (C) and its reference voltage (V_{dcref}), which are not only related to the demand for reactive power but also to the fluctuations, which are a result of the change and unbalances in the load. The selection of DC bus capacitor (C), DC reference voltage (V_{dcref}) and the coupling inductor (L_f) are three key parameters that must be considered in the design of the SAPF power circuit to ensure adequate control and good filtering quality. In addition, the design of these components will be based on the following assumptions:

- The source voltage is sinusoidal.
- The PWM converter is assumed to operate in the linear modulation mode i.e. ($0 \leq ma \leq 1$).

3.3 Estimation of DC bus reference voltage (V_{dcref})

3.3.1 First method

According to (Ponnaluri et Brickwedde, 2001b);(Al-Zamil et Torrey, 2001), and in order to ensure the controllability of the active filter current, the authors advised that the DC bus nominal voltage (V_{dc}) must be greater than the maximum value (peak value) of the AC side voltage of the inverter and can be deduced by the following relation:

$$m_{a\,\max}\frac{V_{dcref}}{\sqrt{3}} > V_{s\,\max} \tag{3.3}$$

where $m_{a\,\max}$: is the maximum value of the modulation coefficient,
and $V_{s\,\max}$: is the maximum value of the phase output voltage of the grid.

3.3.2 Second method

The authors (Benchaita, Saadate et nia, 1999);(Emadi, Nasiri et Bekiarov, 2004) are particularly interested in compensating current harmonics during switching in a fully controlled bridge rectifier, where during these intervals that the active filter may not be able to compensate for these existing harmonics. In fact, the change in currents to be compensated is very rapid during commutations and this may be incompatible with that of the currents generated by the active filter. From an analysis of current variations, the value of the DC bus voltage was deduced as follows:

$$V_{dcref} \geq \sqrt{\sqrt{3}\pi}\, V_s \sqrt{\cos(\alpha)^2 + [(k+1)\sin(\alpha) + \delta k]^2}$$

$$k = \frac{L_f}{L_c} \quad , \quad \delta = \frac{\sqrt{6} L_c\, \omega\, I_d}{\pi\, V_s} \tag{3.4}$$

The determination of (V_{dcref}) in this method is dependent on the prior knowledge of the nonlinear load and the inductance value L_f.

3.3.3 Third method

In this article (Rastogi, Naik et Mohan, 1994), the authors introduced a new hypothesis, based generally on the fact that the practical value of the inductance L_f is small, due to the selection of a high switching frequency for the SAPF. This makes the voltage of the inverter V_f approximately equal to the voltage source V_s. So, for maximum modulation (ma = 1), the expression of V_{dcref} is written as:

$$V_{dcref} = 2\sqrt{2}\ V_s \tag{3.5}$$

Additionally, assuming that the voltage V_{dcref} must be regulated to be 10% higher than the maximum input voltage of the inverter, then:

$$V_{dcref} = 1.1 \cdot 2\sqrt{2}\, V_s \tag{3.6}$$

However, V_{dcref} may be decreased if the PWM sinusoidal reference is modulated with the third and ninth harmonics. So in that case, the minimum voltage value of the V_{dcref} may be expressed as a function of the source voltage as:

$$V_{dcref} = \frac{2\sqrt{2}}{1.155} V_s \tag{3.7}$$

This last method allows estimating the (V_{dcref}) without prior knowledge of other parameters or simulation. Thus, in addition to its simplicity, the third method offers the possibility to calculate the (V_{dcref}) which presents the best quality of energy. However, it remains to verify the impact of the reference change as a function of the DC bus voltage, in steady state and transient conditions.

3.3.4 Proposed DC bus reference voltage estimation method

The selection of reference DC voltage (V_{dc}) essentially influences the shunt active power filter performance. In fact, an ideal choice of V_{dc} enhances the filter performance, prevents power loss and harmonic generation. The best value of V_{dc} might be established by applying the concept in the work of (Ladoux et Ollé, 2002), where the selection of the DC bus reference voltage (V_{dcref}) is a function of the load-rated power and the maximum harmonic order to be compensated. Therefore, neglecting the resistance of the SAF, the output voltage of the inverter is written as:

$$V_f(t) = v_s(t) + L_f \frac{di_f(t)}{dt} \tag{3.8}$$

where i_f represents the current supplied by the inverter and corresponds to the harmonic component of the load current which is of a current source type of nonlinear load consisting of the three-phase bridge rectifier and an RL load.

So $i_f(t)$ can be developed by:

$$i_L = i_{L1} + \sum_{h=3}^{n} \left[a_n \cos\left(n\omega t - \varphi_n\right) + b_n \sin\left(n\omega t - \varphi_n\right) \right] \tag{3.9}$$

$$\begin{aligned} a_n &= \frac{2}{2\pi}\int_0^{2\pi} i_{ch}\cos(\mathrm{n}\omega t)\,d\omega t = \frac{1}{\pi}\left(\int_{\frac{\pi}{6}}^{\frac{5\pi}{6}} I_d\cos(\mathrm{n}\omega t)\,d\omega t + \int_{\frac{7\pi}{6}}^{\frac{11\pi}{6}} (-I_d)\cos(\mathrm{n}\omega t)\,d\omega t\right) \\ &= \frac{I_d}{\pi}\left(\left[\frac{1}{n}\sin(\mathrm{n}\omega t)\right]_{\frac{\pi}{6}}^{\frac{5\pi}{6}} - \left[\frac{1}{n}\sin(\mathrm{n}\omega t)\right]_{\frac{7\pi}{6}}^{\frac{11\pi}{6}}\right) = \frac{I_d}{n\pi}\left[\sin(\mathrm{n}\frac{5\pi}{6}) - \sin(\mathrm{n}\frac{\pi}{6}) - \sin(\mathrm{n}\frac{11\pi}{6}) + \sin(\mathrm{n}\frac{7\pi}{6})\right] \end{aligned} \tag{3.10}$$

$$\begin{aligned} b_n &= \frac{2}{2\pi}\int_0^{2\pi} i_{ch}\sin(\mathrm{n}\omega t)\,d\omega t = \frac{1}{\pi}\left(\int_{\frac{\pi}{6}}^{\frac{5\pi}{6}} I_d\sin(\mathrm{n}\omega t)\,d\omega t + \int_{\frac{7\pi}{6}}^{\frac{11\pi}{6}} (-I_d)\sin(\mathrm{n}\omega t)\,d\omega t\right) \\ &= \frac{I_d}{\pi}\left(\left[-\frac{1}{n}\cos(\mathrm{n}\omega t)\right]_{\frac{\pi}{6}}^{\frac{5\pi}{6}} - \left[-\frac{1}{n}\cos(\mathrm{n}\omega t)\right]_{\frac{7\pi}{6}}^{\frac{11\pi}{6}}\right) = \frac{I_d}{n\pi}\left[-\cos(\mathrm{n}\frac{5\pi}{6}) + \cos(\mathrm{n}\frac{\pi}{6}) + \cos(\mathrm{n}\frac{11\pi}{6}) - \cos(\mathrm{n}\frac{7\pi}{6})\right] \end{aligned} \tag{3.11}$$

Table 3.2 Coefficients of FFT load current

n	**1**	**2**	**3**	**4**	**5**	**7**	**11**	**13**
a_n	0	0	0	0	0	0	0	0
b_n	$\frac{2\sqrt{3}}{\pi}I_d$	0	0	0	$-\frac{1}{5}\frac{2\sqrt{3}}{\pi}I_d$	$-\frac{1}{7}\frac{2\sqrt{3}}{\pi}I_d$	$\frac{1}{11}\frac{2\sqrt{3}}{\pi}I_d$	$\frac{1}{13}\frac{2\sqrt{3}}{\pi}I_d$

The angle is expressed as:

$$\varphi_1 = \tan^{-1}(\frac{a_1}{b_1}) = 0 \qquad \varphi_2 = \tan^{-1}(\frac{a_2}{b_2}) = 0$$

,

$$\varphi_1 = \varphi_2 = \varphi_n = 0$$

The maximum magnitude of the fundamental load current is given by:

$$I_{L1\max} = \sqrt{a_1^2 + b_1^2} = \frac{2\sqrt{3}}{\pi} I_d \tag{3.12}$$

The Fourier development of the load current is given by:

$$i_L = i_{L1} + \sum_{h=3}^{n} b_n \sin\left(n\omega t - \varphi_n\right) \tag{3.13}$$

$$i_L = i_{L1} + \sum_{h=5}^{n} I_{Lh} = \frac{2\sqrt{3}}{\pi} I_d \sin(\omega t - \phi_1) + \sum_{h=5}^{n} \frac{2\sqrt{3}}{h\pi} I_d \sin(h\omega t - \phi_h) \tag{3.14}$$

$$i_{Lh} = i_{L1} - \frac{2\sqrt{3}}{\pi} I_d \sin(\omega t - \phi_1) = -\frac{2\sqrt{3}}{5\pi} I_d \sin(5\omega t - \phi_5) - \frac{2\sqrt{3}}{7\pi} I_d \sin(7\omega t - \phi_7) + \frac{2\sqrt{3}}{11\pi} I_d \sin(11\omega t - \phi_{11}) + \frac{2\sqrt{3}}{13\pi} I_d \sin(13\omega t - \phi_{13}) + .. \tag{3.15}$$

Considering the term i_f representing the load harmonic, one deduces that:

$$\frac{di_f}{dt} = \frac{di_{Lh}}{dt} = -\frac{2\sqrt{3}}{\pi} I_d 5\omega \cos(5\omega t - \phi_5) - \frac{2\sqrt{3}}{\pi} I_d 7\omega \cos(7\omega t - \phi_7) + \frac{2\sqrt{3}}{\pi} I_d 11\omega \cos(11\omega t - \phi_{11}) + \frac{2\sqrt{3}}{\pi} I_d 13\omega \cos(13\omega t - \phi_{13}) + .. \tag{3.16}$$

Using the equation (3.8), one can also deduce that:

$$v_F = V_{s\max}\sin(\omega t) - L_F 5\omega\frac{2\sqrt{3}}{\pi}I_d\cos(5\omega t-\phi_5) - L_F 7\omega\frac{2\sqrt{3}}{\pi}I_d\cos(7\omega t-\phi_7)+ \quad (3.17)$$
$$L_F 11\omega\frac{2\sqrt{3}}{\pi}I_d\cos(11\omega t-\phi_{11}) + L_F 13\omega\frac{2\sqrt{3}}{\pi}I_d\cos(13\omega t-\phi_{13})+..$$

$$v_F = V_{s\max}\sin(\omega t)+L_F\omega\frac{2\sqrt{3}}{\pi}I_d\left[-5\cos(5\omega t-\phi_5)-7\cos(7\omega t-\phi_7)+11\cos(11\omega t-\phi_{11})+13\cos(13\omega t-\phi_{13})+.\right] \quad (3.18)$$

Knowing that the DC bus voltage reference is determined using the equation below:

$$V_{dcref} = 2\frac{V_{s\max}}{m_a} \quad with \quad 0\le m_a\le 1 \quad (3.19)$$

then

$$V_{f\max} = \sqrt{{V_{s\max}}^2 + \sum_{h=5}^{n} h\left(L_f\omega\frac{2\sqrt{3}}{\pi}I_d\right)^2} \quad (3.20)$$

From (3.20) the maximum voltage of the active filter is greater than the maximum source voltage, hence, the DC bus voltage reference with modulation index m_a =1 is given by:

$$V_{dcref} = 2kV_{\mathrm{F}\max} \quad (3.21)$$

where k < 1.

Table 3.3 shows the ideal selected value for K which corresponds to 298V of $V_{dcref.}$ This ensures V_{fmax} > 170V and the THD of the source current to be less than 5% as shown in figure 3.2.

Table 3.3 Calculation of V_{inv} for different K values

K	V_{invmax}	V_{inv}
0.9	$\sqrt{{V_{f-fund}}^2+{V_{fh\max}}^2}$	$179.23\,V$
0.85	$\sqrt{{V_{f-fund}}^2+{V_{fh\max}}^2}$	$172.8\,V$
0.8	$\sqrt{{V_{f-fund}}^2+{V_{fh\max}}^2}$	$164.35\,V$

The DC bus voltage reference is then given by:

$$V_{dcref} = 2k * \sqrt{{V_{s\max}}^2 + \sum_{h=5}^{n} h\left(L_f \omega \frac{2\sqrt{3}}{\pi} I_d \right)^2} \qquad (3.22)$$

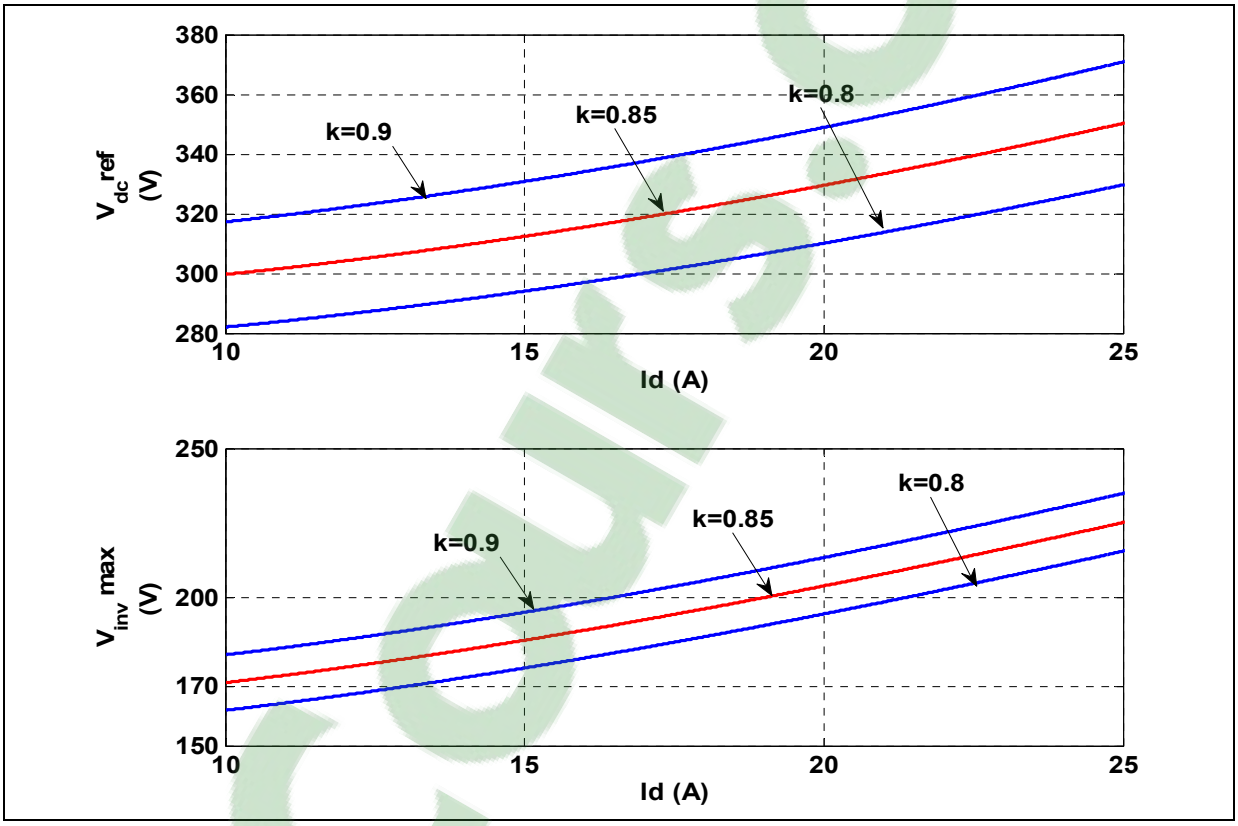

Figure 3.2 Simulation results of the validation of V_{dcref} estimation method

Figure 3.2 shows V_{dcref} versus the DC current of the three-phase diode rectifier (top) and V_{invmax} versus the DC current of the three-phase diode rectifier (bottom). The minimum DC bus voltage is found to be V_{dcref_min} = 298 V. The figure also shows that the DC bus voltage reference is a function of the DC load current. In practice, the load power demand is often subjected to variations. Hence, it is necessary to examine the performance of the system under such variations as shown in figure 3.3.

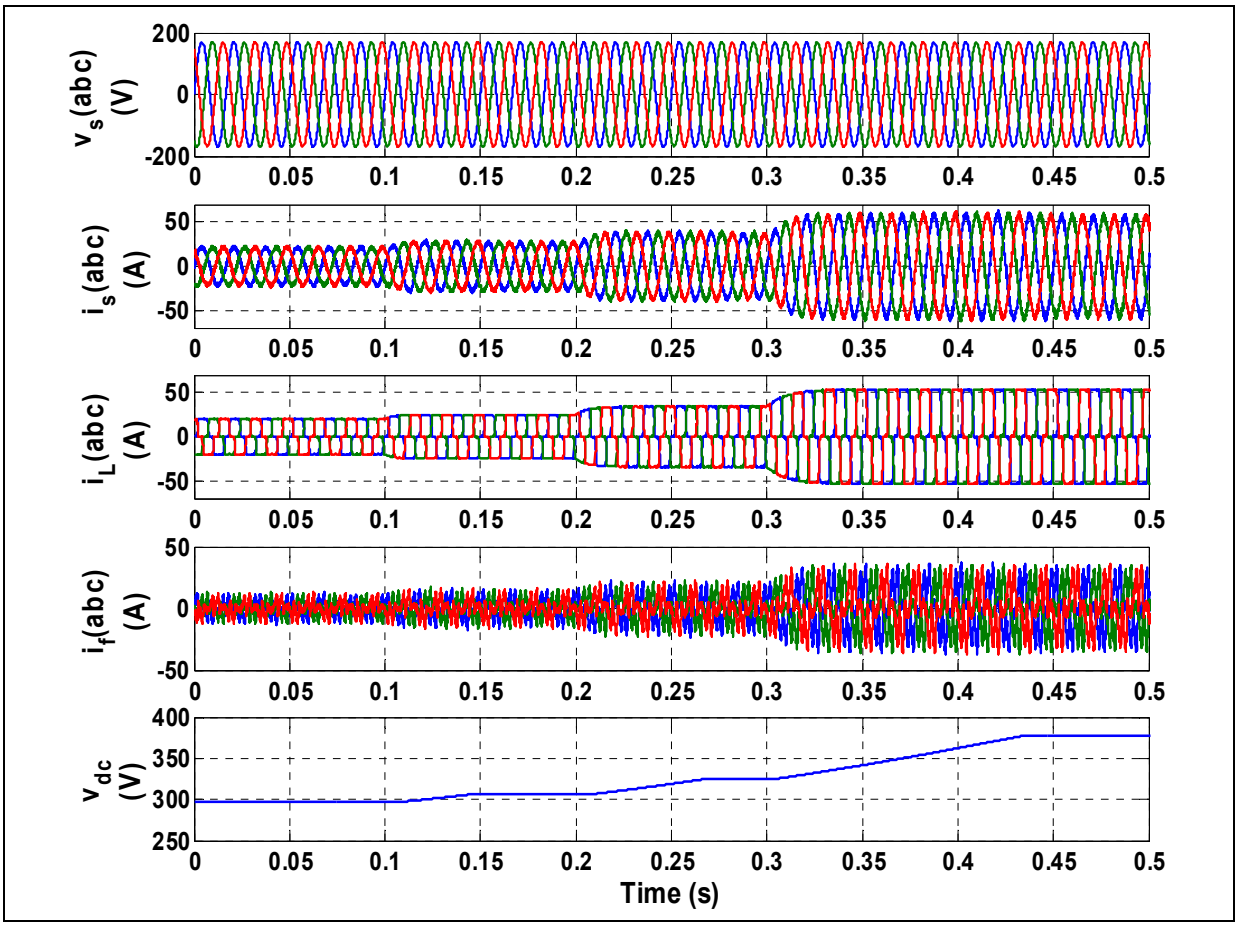

Figure 3.3 Proposed DC bus voltage reference under load variations

The results shown in figure 3.3 demonstrate the good performance of the proposed method during variations of the load current. Thus, the proposed model offers better compensation performance whenever the load changes, adapting DC bus voltage, and the THD for the source current at different variations of the load is less than 5% as shown in figure 3.4.

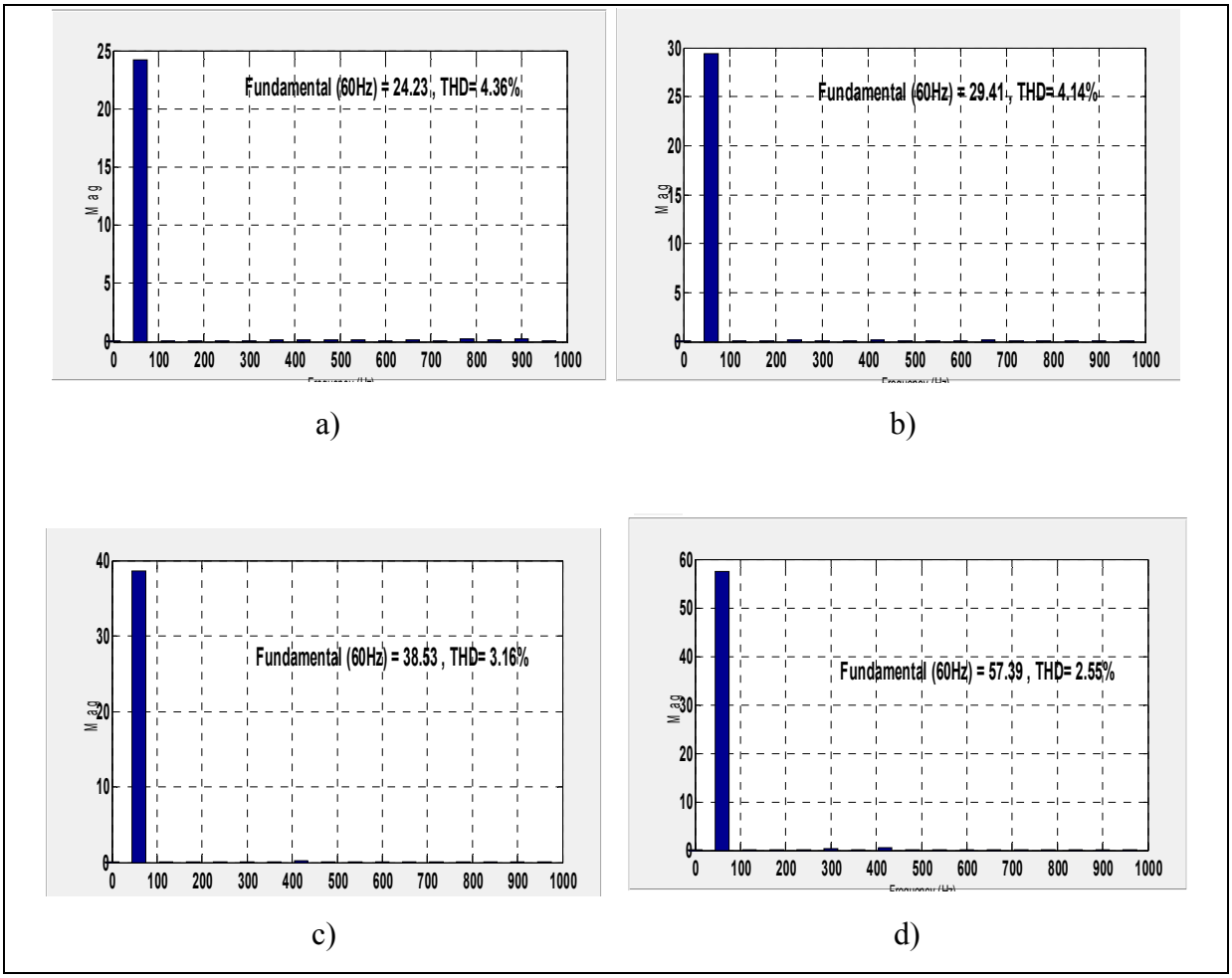

Figure 3.4 Source current harmonic spectrum at different V_{dcref}

To validate the feasibility of the proposed method, sag and swell voltage of (±20%) is generated on the grid side. Figure 3.5 shows the simulation results where the DC bus voltage reference is optimally estimated and the grid current is adequately compensated with a THD less than IEEE-519 standard requirement.

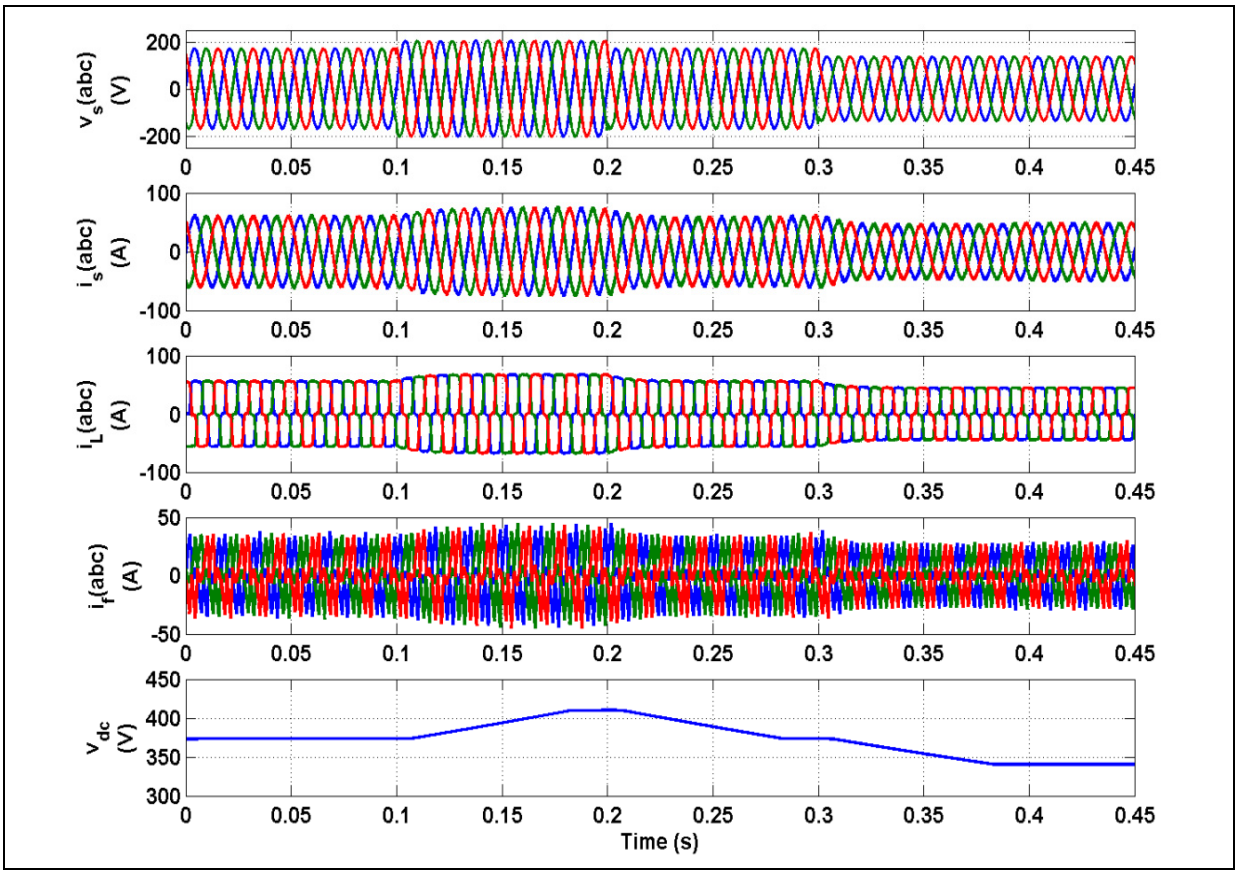

Figure 3.5 Simulation results of sag and swell voltage

3.3.5 Adaptive DC bus voltage reference

The second proposed approach is realized using the model of the SAF, and the output voltage of the active filter is estimated by regulating the output variables of the model. The model of the SAF is given by:

$$L_f \frac{di_{fd}}{dt} = L_f \omega i_{fq} - v_{fd} + v_{sd}$$
$$L_f \frac{di_{fq}}{dt} = -L_f \omega i_{fd} - v_{fq} + v_{sq} \quad (3.23)$$

The objective is to estimate the DC bus voltage reference by regulating the output variables i_d and i_q to their references. The estimated inverter output voltage is then given in dq reference frame using a PI controller.

$$L_f \frac{di_{fd}}{dt} = L_f \omega i_{fq} - v_{fd} + v_{sd} = u_d$$
$$L_f \frac{di_{fq}}{dt} = -L_f \omega i_{fd} - v_{fq} + v_{sq} = u_q \tag{3.24}$$

The filter estimated voltages are given by:

$$v_{fd} = L_f \omega i_{fq} + v_{sd} - u_d$$
$$v_{fq} = -L_f \omega i_{fd} + v_{sq} - u_q \tag{3.25}$$

The maximum filter voltage is determined by:

$$V_{inv}(\max) = \sqrt{v_{fd}^{\,2} + v_{fq}^{\,2}} \tag{3.26}$$

The DC bus voltage reference is given by:

$$V_{dcref} = 1.7\sqrt{v_{fd}^{\,2} + v_{fq}^{\,2}} \tag{3.27}$$

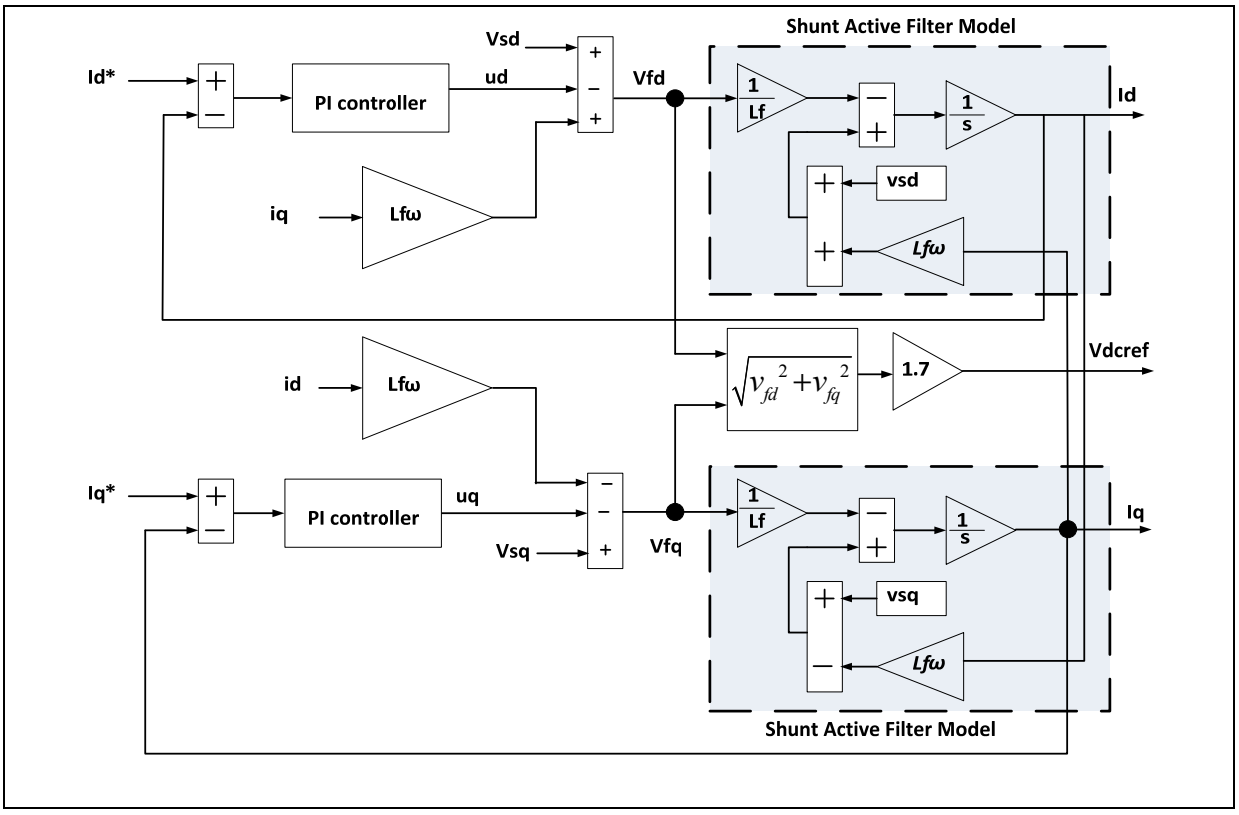

Figure 3.6 Block diagram of the DC bus reference voltage generation

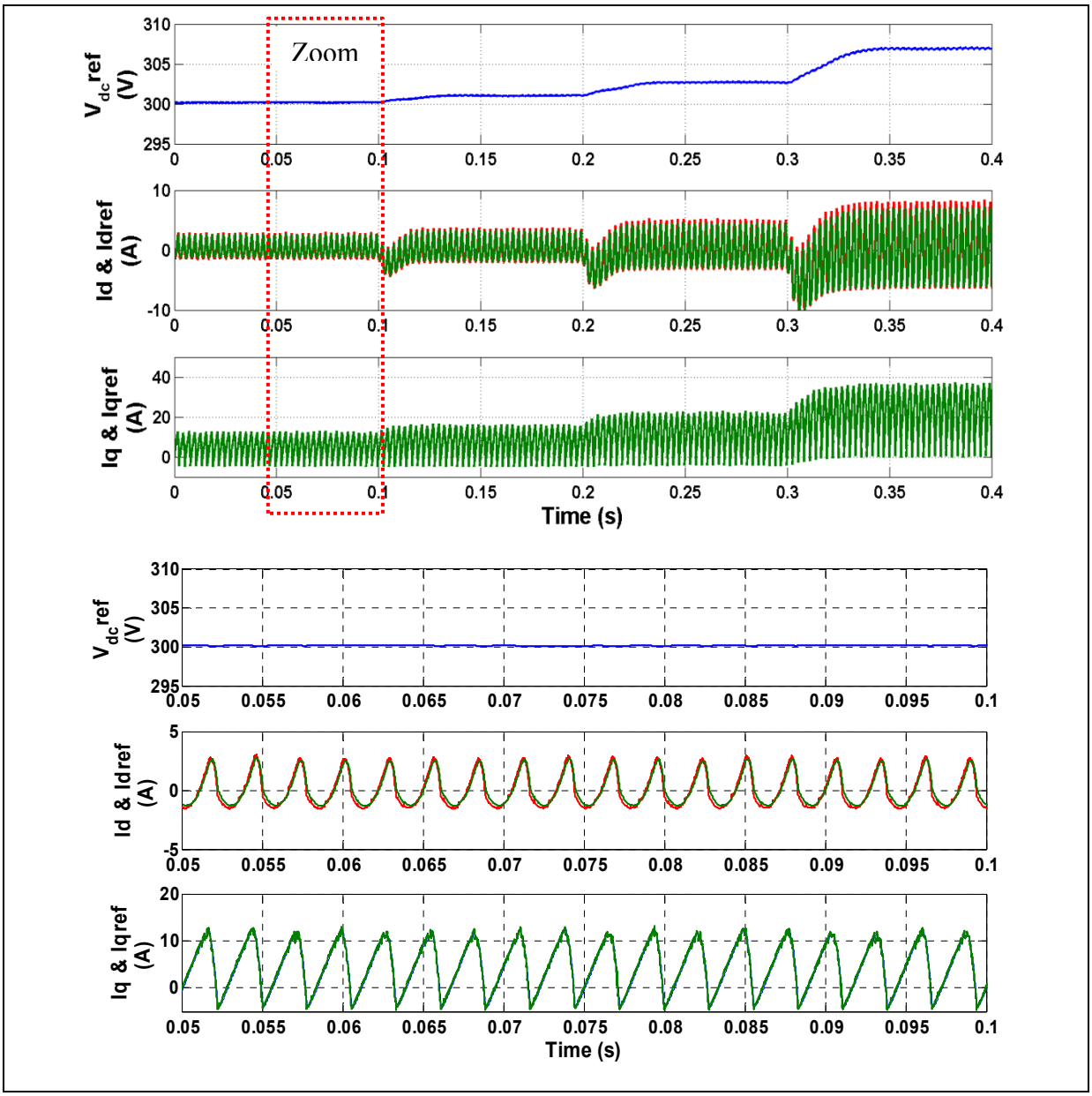

Figure 3.7 DC bus voltage reference using the SAF model

Comparing the waveform results of both V_{dcref} estimation methods, it is evident that V_{dcref} obtained using the filter model gives an optimal value of V_{dc} compared to the previous method, where V_{dc} vary relatively when load current varies considerably. In addition, when sag and swell were introduced in the grid voltage, the DC bus voltage can efficiently adapt to the variation by maintaining the required voltage as shown in figures 3.8 and 3.9.

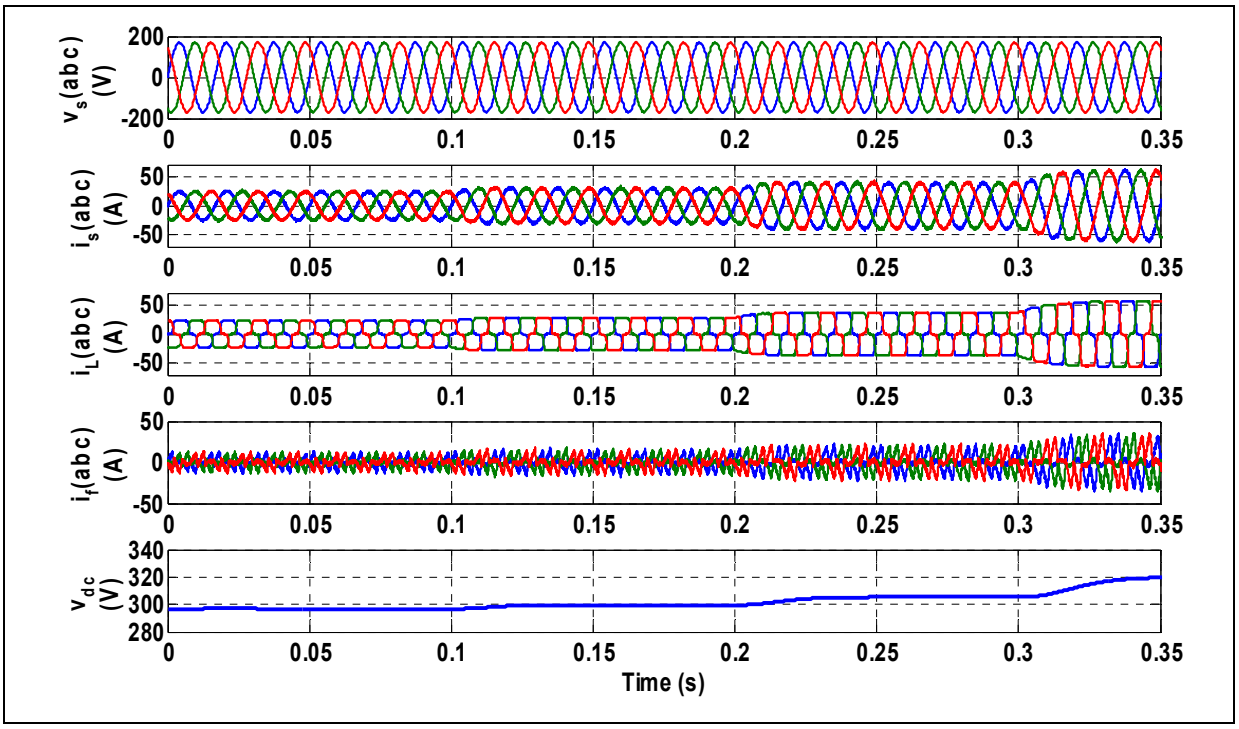

Figure 3.8 System waveforms using DC bus reference voltage generation

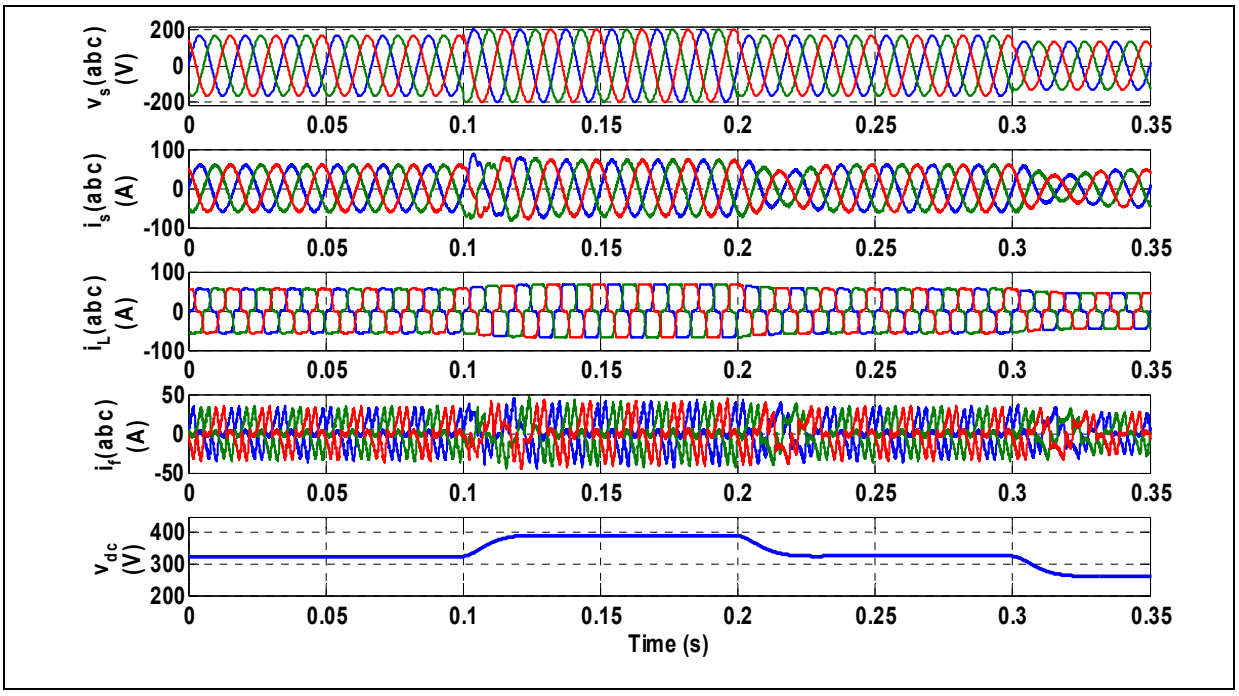

Figure 3.9 Waveforms of the system during sag and swell grid voltage

3.4 Estimation of the coupling inductor

The coupling inductor is an essential element in the SAPF, it ensures the transfer of energy between the point of common coupling (PCC) and the inverter. Therefore, several requirements have to be imposed for estimation of this inductance L_f. First ensuring the dynamics of all current harmonics generated by the inverter and control, secondly guarantee the filtering of current harmonics at a certain level of quality and finally limit the voltage drop to a value less than 20% of the voltage source. Based on these criteria, some techniques are developed in order to calculate the value of the inductance.

3.4.1 First method

In the references (Ponnaluri et Brickwedde, 2001b);(Ponnaluri et Brickwedde, 2001a), the peak ripple current is chosen as sizing criteria of the inductance. To calculate the ripple current, it is considered that there is no load and the resistance effect of the inductance is negligible. Under these conditions, the inverter reference voltage is equal to the voltage source. The peak to peak ripple value of the filter current obtained from the development in (Holmes et Lipo, 2003) is then written as:

$$\Delta I_{f(p-p)max} = \frac{m_a V_{dc}}{8\sqrt{3} f_s L_f} \tag{3.28}$$

Taking the value $m_a = \frac{2\sqrt{2}V_s}{V_{dc}}$

$$L_f = \frac{V_s}{2\sqrt{6} f_s \Delta I_{f(p-p)max}} \tag{3.29}$$

The authors proposed a value of $\left(\Delta I_{f(p-p)max} = 15\%\ I_{fmax}\right)$.

3.4.2 Second method

In (Azevedo et al., 2003), the inductance value is limited by a maximum (*Lfmax*) and a minimum (*Lfmin*) bounds. To keep the ripple current at a reduced level, the inductance value must not be less than (*Lfmin*). One possibility of estimating this minimum value from the maximum current (*Ifmax*) that the SAPF must supply in order to compensate for a totally inductive load is by using the following relationship:

$$L_{fmin} = \frac{\Delta V}{\omega\, I_{fmax}} \tag{3.30}$$

Such as ΔV represents the potential difference between the voltage source and the inverter voltage, which is dependent on the DC bus voltage and the modulation index. For the role of the SAPF, the value of the inductance must be bounded by maximum value to produce the necessary quantity of compensation current harmonics. For this purpose, a maximum value (*Lfmax*) is determined, for a given switching frequency on the basis of the constraint that the minimum slope of the filter current must be less than the slope of the triangular carrier signal which defines the switching frequency. (Morán, Dixon et Wallace, 1995);(Rashid, 2007). The slope of the triangular signal, (λ) is defined by:

$$\lambda = 4\, A\, f_m \tag{3.31}$$

where, *A* is the triangular signal amplitude, which must be equal to the maximum allowed current ripples, and f_m is the carrier frequency. The maximum slope of the inductance current is equal to:

$$\frac{di_f}{dt} = \frac{V_s + 0.5V_{dc}}{L_f} \tag{3.32}$$

Knowing the constraint imposed previously, it is then possible to deduce:

$$L_f < \frac{V_s + 0.5V_{dc}}{4\, A\, f_m} = L_{fmax} \tag{3.33}$$

Then, the inductance value estimated by this approach can be limited as follows:

$$\frac{\Delta V}{\omega\, I_{fmax}} < L_f < \frac{V_s + 0.5V_{dc}}{4\, A\, f_m} \tag{3.34}$$

3.4.3 Third method

In (Etxeberria-Otadui, 2003), proposes an inductance value between two constraints. A minimum value (Lf_{min}) which limits the injected ripple current into the network, and a maximum value (Lf_{max}) which allows the generation of all the current harmonics stated by the specification. The maximum ripple current neglecting the resistance of the inductance can be calculated from the approximate expression of the derivative of the current:

$$\Delta I_f = \frac{\Delta V}{L_f}\Delta t \tag{3.35}$$

By considering a PWM modulation, in each half period of the modulation, the average value of the inverter output voltage will be equal to its set-point. Assuming that the inverter tries to accurately reproduce the mains voltage, the positive *(T+)* and negative *(T-)* voltage application interval of the inverter can be calculated using:

$$T_+(\omega t) = \frac{T_s}{2}\left(\frac{2V_s(\omega t) + V_{dc}}{2V_{dc}}\right)$$
$$T_-(\omega t) = \frac{T_s}{2}\left(\frac{-2V_s(\omega t) + V_{dc}}{2V_{dc}}\right) \tag{3.36}$$

Thus, the current variation between each interval can be calculated from (3.35):

$$\Delta I_f^+(\omega t) = \frac{T_+}{L_f}\left(\frac{V_{dc}}{2} - V_s(\omega t)\right) = \frac{T_s}{8L_fV_{dc}}\left({V_{dc}}^2 - 4{V_s}^2(\omega t)\right)$$
$$\Delta I_f^-(\omega t) = \frac{T_-}{L_f}\left(\frac{V_{dc}}{2} + V_s(\omega t)\right) = \frac{T_s}{8L_fV_{dc}}\left({V_{dc}}^2 - 4{V_s}^2(\omega t)\right) \tag{3.37}$$

It is clear that the two variations are identical, so the peak-peak maximum ripple will be:

$$\Delta I_{fmax} = \frac{T_s\, V_{dc}}{8\, L_f} \tag{3.38}$$

Hence the minimum value of the inductance is obtained:

$$L_{fmin} = \frac{T_s V_{dc}}{8\,\Delta I_{fmax}} \tag{3.39}$$

Once the minimum value is calculated to minimize the ripple current, it is necessary to analyze the system ability to generate the desired harmonics. Thus, from the knowledge of the harmonic current type, one can calculate the limit inductor value, which enables their generation from:

$$i_{ch}(t) = \sum_{h=0}^{\infty} \sqrt{2}\, I_{ch} \cos(h\omega t + \varphi_h) \tag{3.40}$$

where $\left(i_{ch}(t)\right)$ represents the current harmonics to be compensated

The voltage drop across the inductor will be:

$$\Delta V = \sqrt{2}\, L_f\, \omega \sum_{h=0}^{\infty} h\ I_{ch} \cos(h\omega t + \varphi_h) \tag{3.41}$$

In the worst case, all the harmonics will be in phase and thus the maximum rms value of the voltage to be generated by the inverter will be (neglecting the fundamental term of the current):

$$V_{fmax} = \sqrt{2}V_s + \sum_{h=0}^{\infty} L_f\, \omega\, h\ I_{ch}\sqrt{2} \tag{3.42}$$

Considering a PWM modulation, the value of the inductance must be less than:

$$L_{fmax} = \frac{V_{dc} - 2\sqrt{2}V_s}{2\sum_{h=0}^{\infty} \omega\ h\ I_{ch}\sqrt{2}} \tag{3.43}$$

Finally, the value of the inductance can be estimated by:

$$\frac{T_s V_{dc}}{8\,\Delta I_{fmax}} < L_f < \frac{V_{dc} - 2\sqrt{2}V_s}{2\sum_{h=0}^{\infty} \omega\ h\ I_{ch}\sqrt{2}} \tag{3.44}$$

3.4.4 Fourth method

By neglecting the resistance value of the inductance, the equation of the SAPF can be written as follows (Chaoui, 2010):

$$L_f \frac{di_f(t)}{dt} = v_s(t) - u_{abc}(t)V_{dc}$$
$$C_{dc} \frac{dV_{dc}}{dt} = u_{abc}(t)^T \, i_f(t) \tag{3.45}$$

The use of PWM techniques to obtain the reference values (u^*_{abc}) causes ripple current, which must be kept below a maximum accepted value ($\Delta I_{f(p-p)max}$), in order to limit the distortions at high frequency. Then, it is possible to write:

$$i_f(t) = i^*_f(t) + \Delta i_f(t)$$
$$u_{abc}(t) = u^*_{abc}(t) + \Delta u_{abc}(t) \tag{3.46}$$

where * indicates reference values and Δ the ripple caused by the PWM technique. Substituting (3.46) into (3.45), one obtains:

$$L_f \frac{d\Delta i_f(t)}{dt} = -\Delta u_{abc}(t)V_{dc} \tag{3.47}$$

The worst case of ripple occurs when (u^*_{abc}) is in the middle of a portion of the hexagon, as shown in figure 3.10.

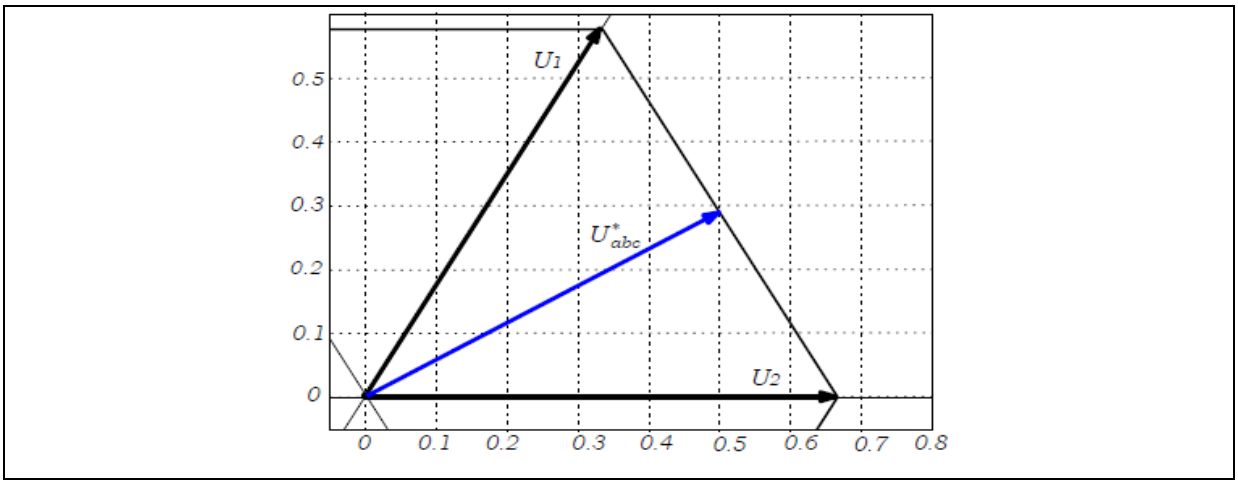

Figure 3.10 Position of the reference vector for the worst case of ripple currents

In this situation, and according to (Ronchi et Tilli, 2002a) assuming that the value of the DC bus voltage is constant over a switching period (*Ts*), the peak to peak ripple current is written as:

$$\Delta I_{f(p-p)} = \int_{t0}^{t0+Ts/2} \left[\frac{d\Delta f(t)}{dt}\right]_{U1} dt = \frac{V_{dc}}{6\, L_f f_s} \tag{3.48}$$

The maximum current must be less than the maximum ripple chosen $\Delta I_{f(p-p)max}$ from which the inductance value for their limitation is obtained as in (Rastogi, Naik et Mohan, 1994); (Mohan, Robbins et Undeland, 1995); (Bruyant, 1999):

$$\Delta I_{f(p-p)} < \Delta I_{f(p-p)max} \rightarrow L_f = \frac{V_{dc}}{6\, \Delta I_{f(p-p)max}\, f_s} \tag{3.49}$$

3.5 Design of active filter inductor based on the slope of the load current

3.5.1 Introduction

The analysis to determine the inductor value of the SAPF in the previous methods has overlooked the slope of the load current when designing the filter inductor. Figure 3.11 shows that the inductor value of the shunt active filter is directly related to the power quality of the source current. Using an inductor of $5mH$, one can observe that the source current is not properly filtered, unlike when using a $2mH$ inductor, which offers a better compensation performance. This issue is mainly caused due to the slope of the filter current as being not fast enough to keep up with the load current slope. Additionally, the magnitude of the active filter ripple current may also slightly affect the performance of the compensation.

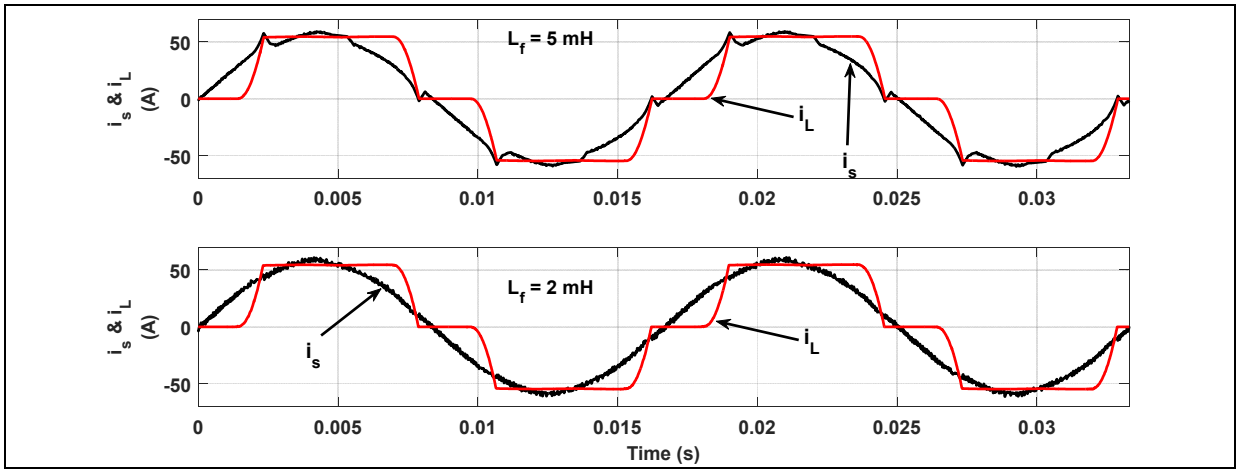

Figure 3.11 Source current with two different shunt active filter inductor

Hence, to select the inductor of the active filter, the slope of the load current and the maximum ripple active filter current are taken into consideration. From analyzing the simulation, it is found that minimum active filter slope current occurs when (t_{on}) or (t_{off}) is maximum and these maximum values are around $0.7*T_{sw}$ as shown in Figure 3.12.

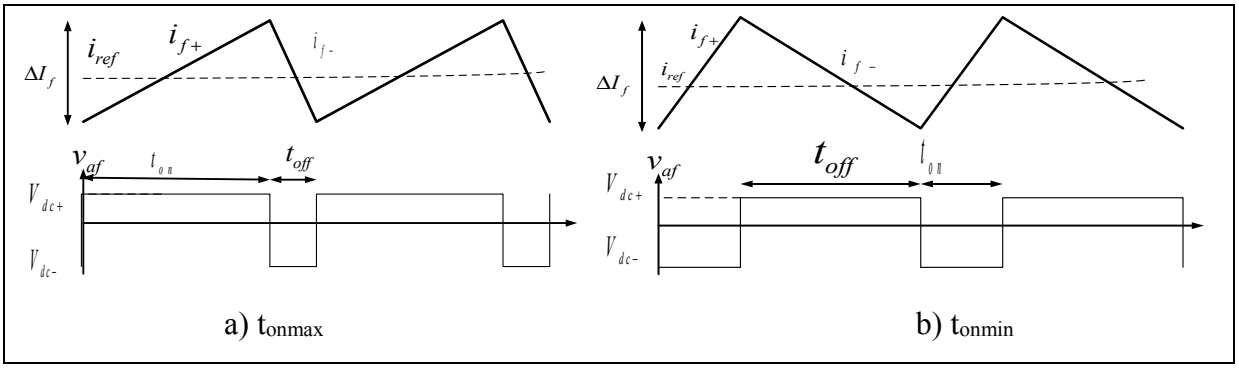

Figure 3.12 Ripple current and voltage of shunt active filter

For proper operation, the slope of the active filter current should satisfy the following equation given by:

$$\frac{di_{f1}}{dt}=\frac{\Delta I_f}{t_{on}}>\frac{di_{L1}}{dt} \text{ or } \frac{di_{f1}}{dt}=\frac{\Delta I_f}{t_{off}}>\frac{di_{L1}}{dt}$$

$$\frac{di_{f1}}{dt}=\frac{\Delta I_{f\max}}{t_{on}}>40000 \text{ A/s} \rightarrow t_{on}<\frac{\Delta I_{f\max}}{40\ 000}=\frac{0.15*27}{40\ 000}=101.25\ \mu\text{s} \quad (3.50)$$

The selected switching period is T_{sw} =166.67 μs, therefore 101.25 μs represents a duty cycle of (D < 61%). To ensure the condition is fulfilled, the duty cycle should be less than 61%. The inductor value should also be chosen to guarantee that the slope of the active filter current is always greater than the slope of the load current. With t_{on} = (0.7*T_{sw}), the slope of the active filter current can be deduced by the following equation:

$$\frac{di_{f1}}{dt}(\min)=\frac{\Delta I_f}{t_{on(\max)}}=\frac{\Delta I_f}{0.7*T_s} \quad (3.51)$$

3.5.2 Determination of load current slope

The slope of the load current is calculated as illustrated in Figure 3.13.

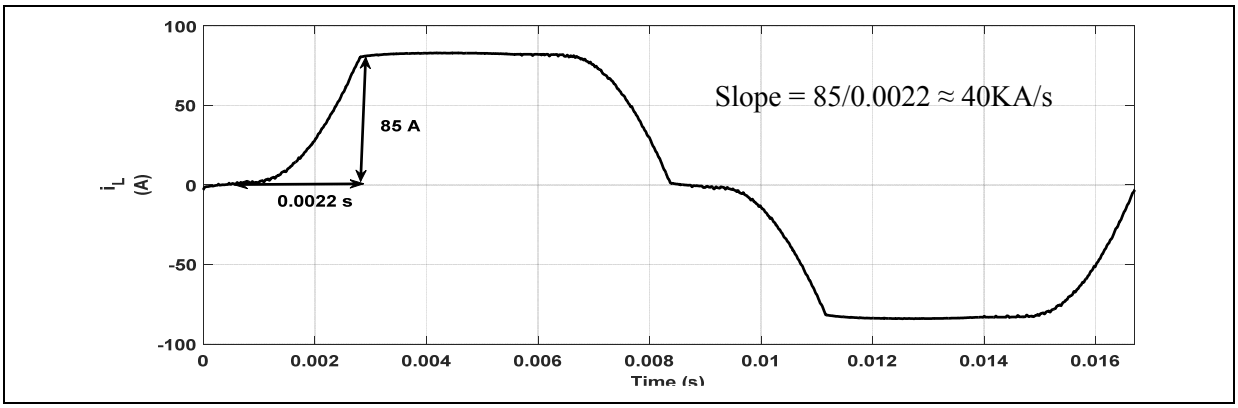

Figure 3.13 Slope of the load current

3.5.3 Comparison of coupling inductor estimation methods

The simulated comparison in figure 3.14 is made with the parameters given below:

$V_{dc} \geq 2\hat{V}_s = 2 \times 170 = 340V$, $V_{dc} = 340 + (0.1 \times 340) = 374V$ at f_{sw} of 6 kHz.

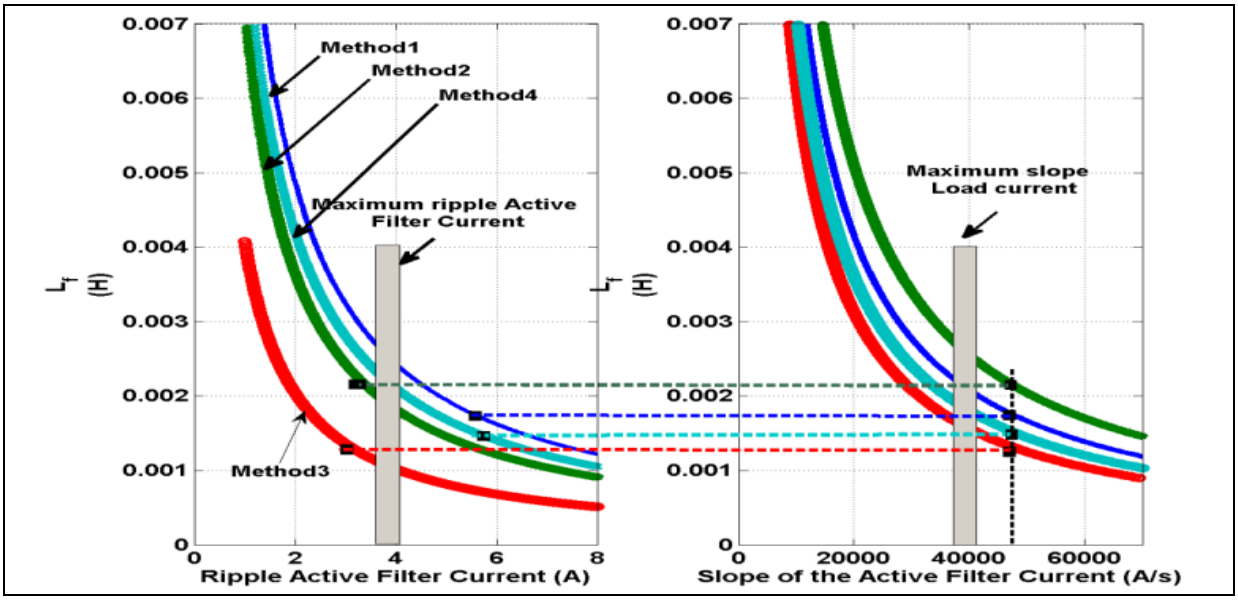

Figure 3.14 Comparison of different methods based on the minimum filter slope current

Figure 3.14 shows the comparison of the different methods to estimate the inductor value of the shunt active filter. From this figure, it is important to select the slope of the active filter current to be greater than the slope of the load current. One can realize from the figure that only in two cases the maximum ripple current and the maximum slope is achieved. In addition, the third method offers the best approach to determine the inductor value of the shunt active filter based on the equation (3.39).

3.5.4 Validation of the third method

Based on the above hypothesis and in order to validate the analysis in method 3, the slope of the active filter current (di_f/dt) is simulated with two different inductor values (1.2mH, 2.6mH) at a fixed switching frequency as shown in figure 3.15. Consequently, the selection of the active filter inductor value depends on the slope of the shunt active filter current to be greater than the slope of the load current $(di_f/dt) > (di_L/dt)$, and the maximum ripple of the shunt active filter current to be (15% of I_{fmax}).

Verification of the two cases:

Case 1: If $di_L/dt = 40000\ A/s$ and $L_f = 2.6mH$, the slope of the shunt active filter current is found to be: $di_f/dt \approx 25000\ A/s$, and the filter ripple current is optimal (≤ 1V).

Case 2: If di_L/dt = 40000 A/s and $L_f = 1.2mH$, the slope of the shunt active filter current is found to be: $di_f/dt \approx 45000\ A/s$, and the filter ripple current is (≤ 3V). The simulation results of the two cases are given in figures 3.15 and 3.16.

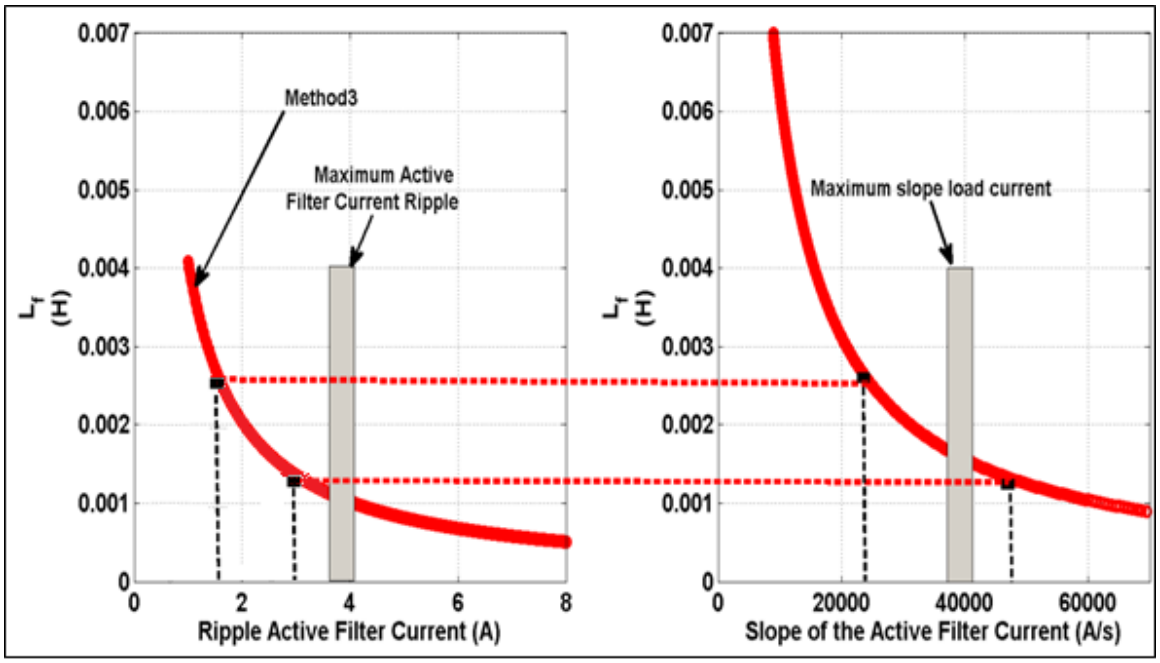

Figure 3.15 Slope of the active filter current

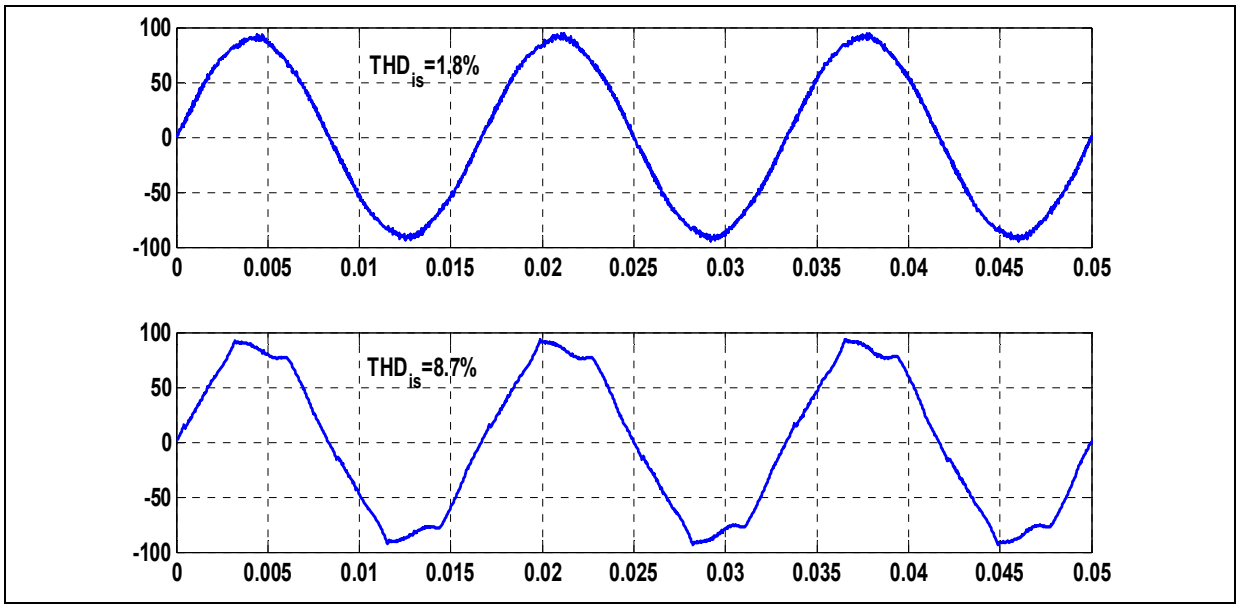

Figure 3.16 Waveform of source current for two different inductor values

From figure 3.16, it is evident that when the filter current slope is less than the load current slope, the waveform of the grid current is distorted with THD = 8.7%, despite the fact that the ripple active filter current is less than the maximum set-point.

3.5.5 Test of the third method for different switching frequencies

The following is a simulation of the third method for different switching frequencies at a fixed ripple current, which offers different inductor values.

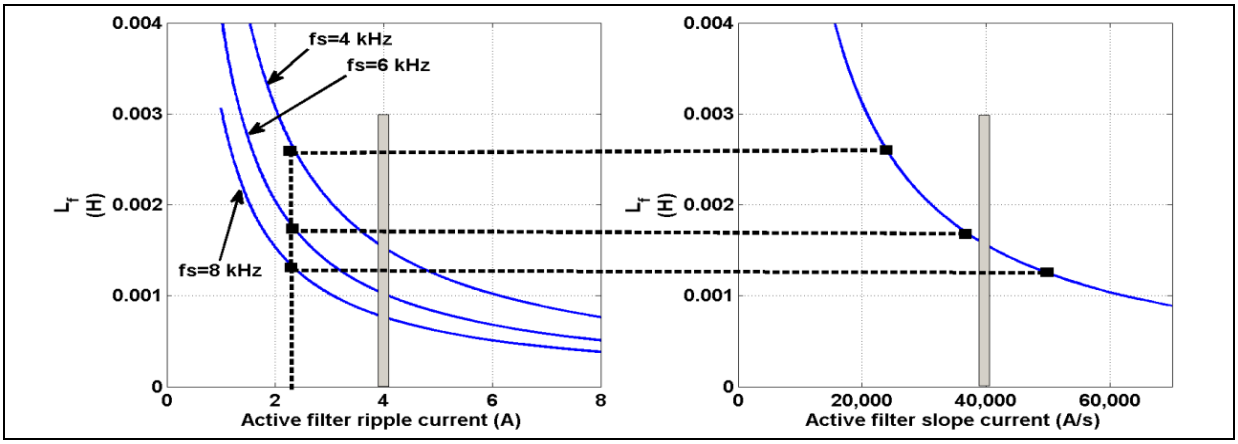

Figure 3.17 L_f at fixed ripple current and slope of filter current using different f_{sw}

From figure 3.17, it is clear that increasing the switching frequency results in reducing the inductor value and increases the slope of the filter current which validates the good performance of compensation. While using a fixed L_f of $1.2mH$, only 6 kHz and 8 kHz switching frequencies offer good compensation performance as shown in figure 3.18.

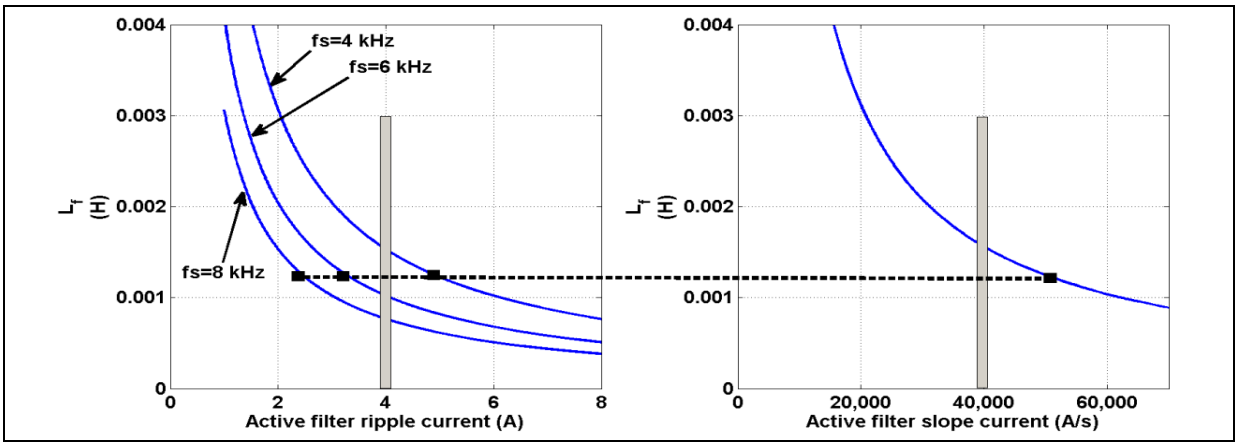

Figure 3.18 Fixed L_f at different current ripple and slope of filter current using different f_{sw}

3.6 Estimation of DC bus capacitor (C)

The determination of the capacitance value of the energy storage capacitor (C) can be made based on the principle of instantaneous exchange of power necessary to support the step increase or decrease of power consumed by the load using the theory of power balance, or by the mitigation of the DC bus voltage oscillations V_{dc} imposed by the lower order harmonics of the nonlinear load, or the unbalance of the linear/nonlinear loads in steady state.

3.6.1 First method

This approach is based on the role of the DC bus capacitor which may have to consume or supply the power demand by the load during transient conditions. In (Ronchi et Tilli, 2002a) and (Chatterjee, Fernandes et Dubey, 1999), the calculation of the capacitor value is based on the production of the maximum load power over a period of the voltage source. On the basis of the maximum real power of the load (P_{max}), the capacitor value which is to supply the equivalent power in the worst case of the transient is given by:

$$C = \frac{2 \cdot P_{max}}{V_{dc}^2(1-k^2)} \quad \text{where } k = \frac{V_{dcmin}}{V_{dc}} \tag{3.52}$$

The voltage V_{dcmin} must be chosen carefully to ensure the controllability of current at all operating points. Based on the same findings, the authors (Singh et al., 2004) suggest that the SAPF must have the necessary energy to manage the loads locally and instantaneously without disturbing the source. This indicates that its response time is of the control algorithm computation time order. In this case, the capacitance values are small and do not allow a good attenuation of voltage oscillations V_{dc}. A choice between three capacitor values has been cited in (Hsu et Wu, 1996). The first value (C_1) is due to step increase in the real fundamental component of the load current given by:

$$C_1 = \frac{V_m \cdot \Delta I_{c1} \cdot T}{V_{dc}^2 - V_{dcmin}^2} \tag{3.53}$$

The second value corresponds to step decrease in the real fundamental component of the load current given by:

$$C_2 = \frac{V_m \cdot \Delta I_{c1} \cdot T}{V_{dcmax}^2 - V_{dc}^2} \tag{3.54}$$

However, during the steady state, the reactive components and current harmonic charges and discharges the energy storage capacitor. Consequently, using the concept of power balance, it is possible to have:

$$C_3 = \frac{V_m \cdot \Delta I_c \cdot (T/2)}{|V_{dc\Delta}^2 - V_{dc}^2|} \tag{3.55}$$

where:

(ΔI_c) is the ripple rms value of the reactive current and the nonlinear load harmonic;

($V_{dc\Delta}$) is the ripple voltage across the capacitor;

(T/2) corresponds to the maximum time of charge/discharge of the reactive components and current harmonic.

If the sinusoidal current waveform of the mains is to be maintained during transients, the highest value of the three capacitances must be selected.

3.6.2 Second method

This method does not consider the transient in load condition but takes into account the steady state of an unbalanced load (Jain et Agarwal, 2003);(Chiang et Chang, 1999). The authors consider that the idea of fluctuations due to change of load cannot be taken as a design method for the capacitor, because the ripple in voltage amplitude V_{dc} ($Vdcmin$, V_{dcmax}), considered in such methods for calculating the capacitance value, can be reduced by an appropriate choice of DC bus control loop parameters. Following this analysis, the selection of the capacitance value of the capacitor C is governed by the reduction of the worst case of voltage ripple at (2ω), caused by the unbalanced load. Based on the principle of instantaneous powers flow on both sides of the inverter in the stationary frame ($\alpha\beta$):

$$P_{dc/ac}^{\alpha\beta} = V_{dc} i_{dc} = v_{f\alpha}(t)\, i_{f\alpha}(t) + v_{f\beta}(t)\, i_{f\beta}(t) = \sqrt{2} V_{f\beta} * \sin(\omega t)\sqrt{2}\, I_{f\beta}\ \sin(\omega t - \varphi\beta) + \sqrt{2} V_{f\alpha} \cos(\omega t)\, \sqrt{2} I_{f\alpha}\ \cos(\omega t - \varphi\alpha) \quad (3.56)$$

This last expression can be written in the form:

$$P_{dc/ac}^{\alpha\beta} = V_{f\beta} I_{f\beta}\, [\cos(\varphi\beta) - \cos(2\omega t - \varphi\beta)] + V_{f\alpha} I_{f\alpha} [\cos(\varphi\alpha) + \cos(2\omega t - \varphi\alpha)] \quad (3.57)$$

Comparatively to the conditions of the load, the following two cases are considered:

- If the three-phase load is balanced, then $V_{f\beta} = V_{f\alpha} = V_f$, $I_{f\beta} = I_{f\alpha} = I_f$ and $\varphi\beta = \varphi\alpha = \varphi$ then relation (3.57) can be written as:

$$P_{dc/ac}^{\alpha\beta} = V_{dc} i_{dc} = 2 V_f I_f \cos(\varphi) \quad (3.58)$$

It can be seen that the DC bus contains no oscillations.

- If the three-phase load is unbalanced, then

$$P_{dc/ac}^{\alpha\beta} = V_{dc} i_{dc} = \left[V_{f\beta} I_{f\beta}\ \cos(\varphi\beta) + V_{f\alpha} I_{f\alpha} \cos(\varphi\alpha)\right] + \left[-V_{f\beta} I_{f\beta} \cos(2\omega t - \varphi\beta) + V_{f\alpha} I_{f\alpha} \cos(2\omega t - \varphi\alpha)\right] \quad (3.59)$$

It appears that the first term of the power equation (3.59) is constant and corresponds to the value that the SAPF must supply to keep the DC bus voltage constant, whereas the second term is a second harmonic power produced by the SAPF to compensate for the power of the unbalanced load. The alternating term of the power will cause oscillations of the second harmonic of the voltage superimposed on the continuous term of the DC bus voltage.

Taking, for example, the extreme case of unbalance where:

$$\varphi\beta = \varphi\alpha - \pi\,, V_{f\beta} = V_{f\alpha} = \frac{V_{dc}}{2}\,, I_{f\beta} = 0, \frac{I_{f\alpha}}{2} = I_{dc}$$

Therefore, equation (3.59) becomes:

$$P_{dc/ac}^{\alpha\beta} = V_{dc} i_{dc} = \left[\frac{V_{dc}}{2} I_{f\alpha} \cos(\varphi\alpha)\right] + \left[\frac{V_{dc}}{2} I_{f\alpha} \cos(2\omega t - \varphi\alpha)\right]$$
$$i_{dc} = \ [I_{dc} \cos(\varphi\alpha)] + [I_{dc} \cos(2\omega t - \varphi\alpha)] \tag{3.60}$$

The peak to peak voltage ripple of the DC bus ($v_{dc(p\text{-}p)max}$) is calculated from the second term of the ripple current at (2ω) which is given by (Mohan, Robbins et Undeland, 1995):

$$v_{dc(p-p)max}(t) = \frac{1}{C} \int I_{dc} \cos(2\omega t - \varphi\alpha) = \frac{I_{dc}}{2\ \omega\ C} \sin(2\omega t - \varphi\alpha) \tag{3.61}$$

The amplitude of the voltage ripple ($v_{dc(p\text{-}p)max}$) is then written as:

$$V_{dc(p-p)max} = \frac{I_{dc}}{2\ \omega\ C} \ \rightarrow \ C = \frac{I_{dc}}{2\ \omega\ V_{dc(p-p)max}} \tag{3.62}$$

3.6.3 Third method

Form the work of (Alali et al., 2000), which is based on the measurement of current harmonic I_h of the lowest harmonic order, the value of the capacitance is calculated as follows:

$$C = \frac{I_h}{\omega_h \varepsilon_v V_{dc}} \tag{3.63}$$

where ω_h corresponds to the frequency of the lowest harmonic order to be compensated.

In summary, the analysis determines that the capacitor values obtained from the different estimation methods do not converge to a single result, and hence the change in the capacitor value has no remarkable effect on the quality of the current and voltage source signals.

3.7 Simulation of shunt active power filter

The following figure contains the parameters used in the simulation of the shunt active filter based on the previously validated design methods of the filter's various components. The shunt active filter was simulated under balanced and unbalanced load variations to verify the compensation performance of the SAPF. Simulation results are presented in figures 3.20 and 3.21 respectively. The block diagram of the shunt active filter is also shown in figure 3.19.

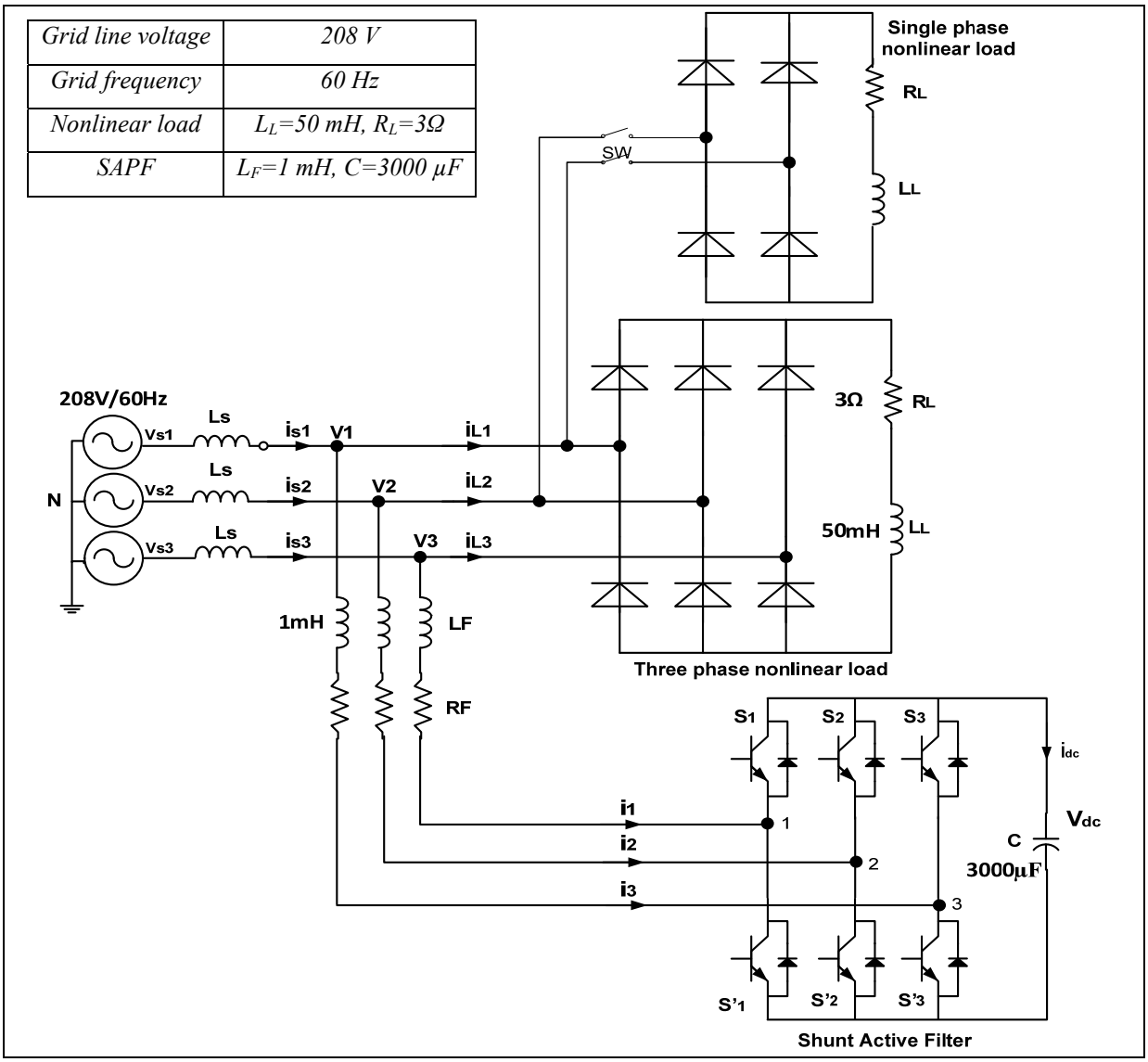

Figure 3.19 SAPF scheme with unbalanced nonlinear load

In the figure 3.20 the balanced load current is increased at (t=0.05s) resulting in a slight decrease in the transient DC bus voltage (V_{dc}), after that the DC bus voltage recovers back to 350V until the load current is decreased at (t=0.15s), that's when the DC bus voltage demonstrates an overshoot for a short time, afterwards it regulates itself and maintains a 350Vdc.

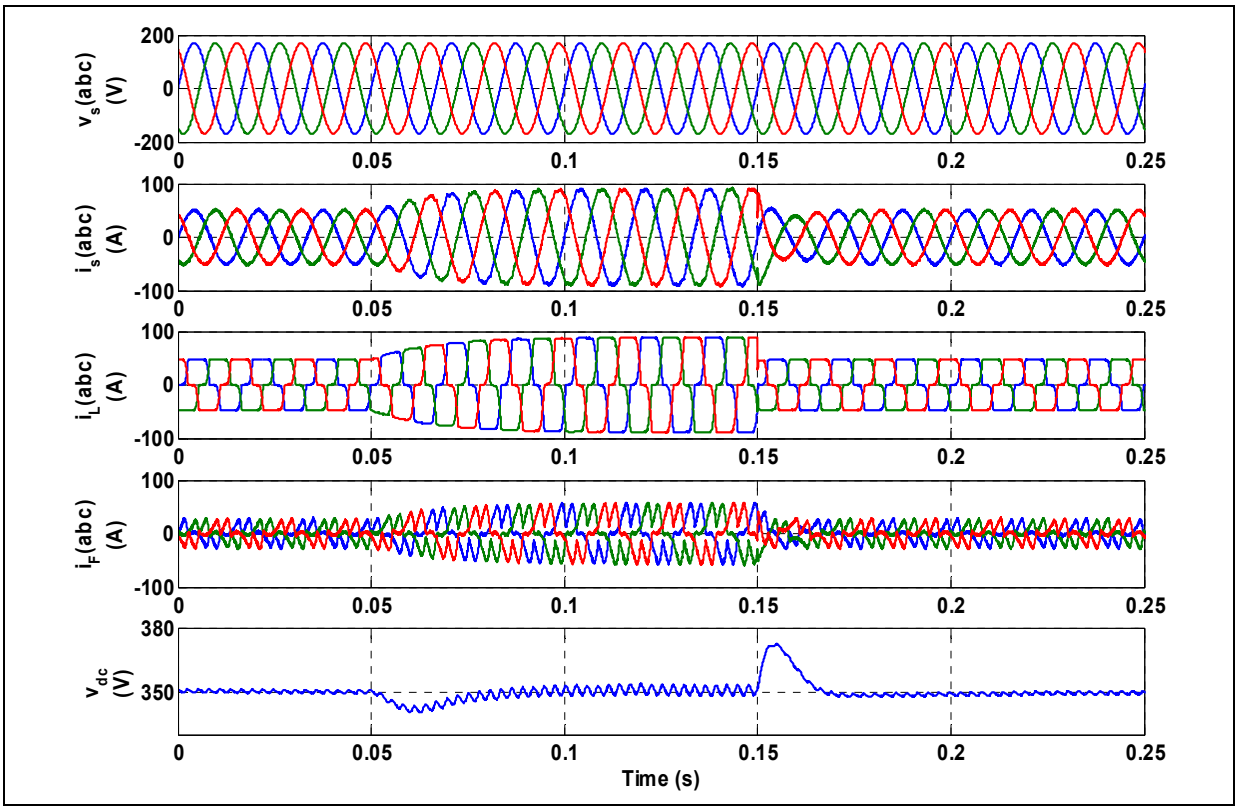

Figure 3.20 Dynamic response of the SAF during balanced load variation

While in figure 3.21 unbalanced load is connected and the load current is increasingly varied just after (t=0.05s) resulting in a fluctuation of the DC bus voltage (V_{dc}) with higher ripple voltage, after that the DC bus voltage recovers to maintain the 350V until the load current is decreased at around (t=0.15s), that's when the DC bus voltage increases in amplitude. At (t=0.2s) the DC bus voltage starts to gradually regulate itself and maintains a 350Vdc. In this case, when an unbalanced load is connected, the quality of the source current is ideal with THD less than 5% as shown in figure 3.22, which validates the good performance of the system.

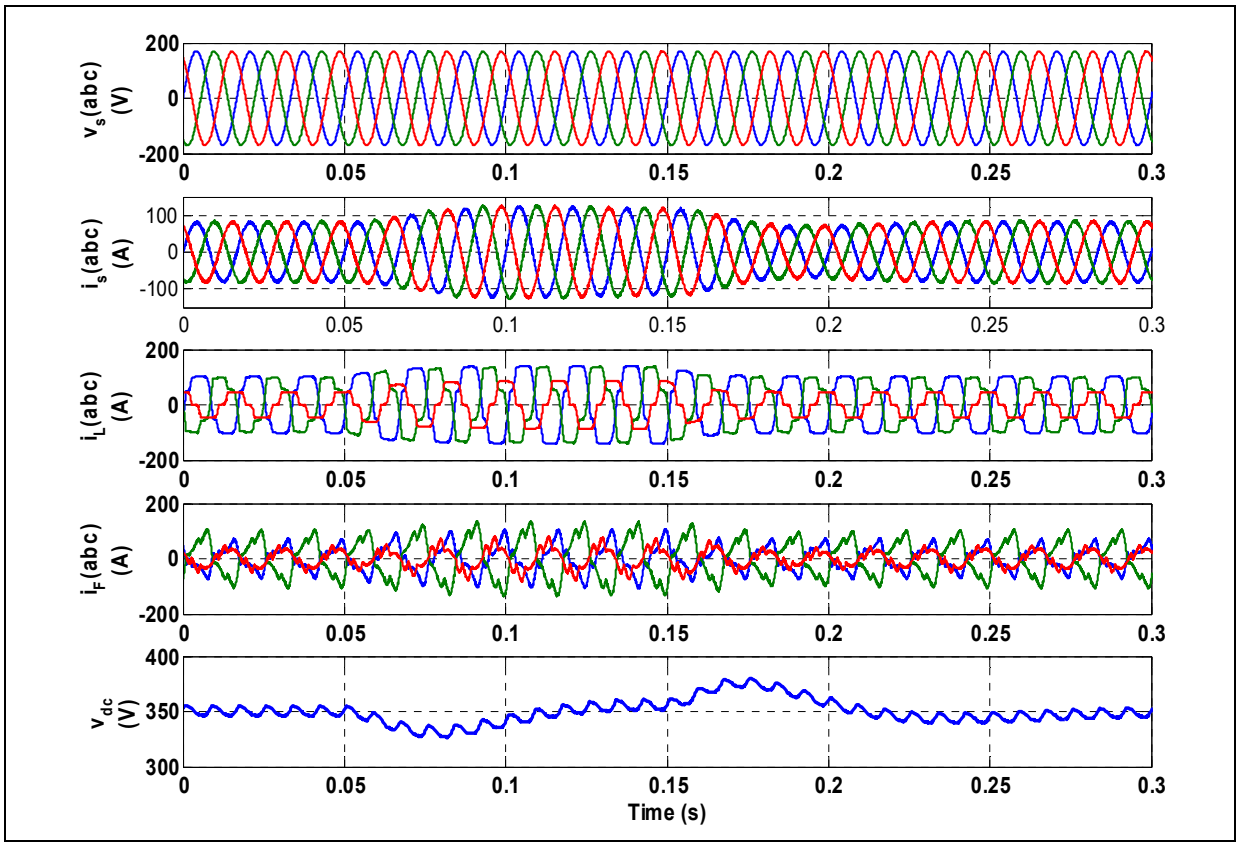

Figure 3.21 Dynamic response of the SAF during unbalanced load variation

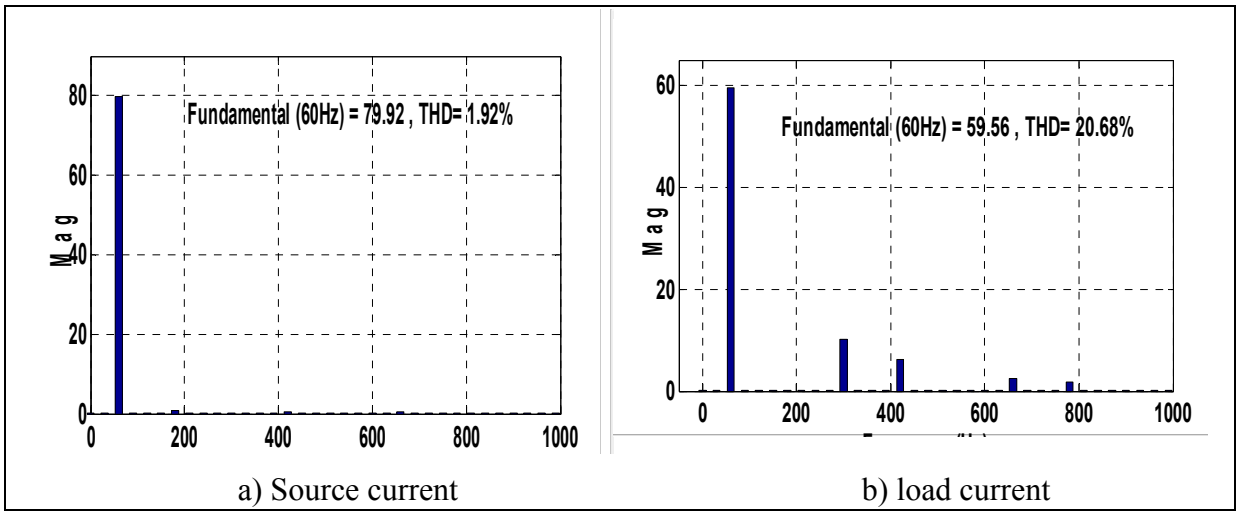

a) Source current b) load current

Figure 3.22 Harmonic spectrum

CHAPITRE 4

PROTECTION INVESTIGATION OF THE ACTIVE POWER FILTER

4.1 Introduction

Stability and protection of systems are amongst the major concerns in the operation of power systems. Several modeling software and tools are developed to enable the simulation of power systems under various operating conditions. MATLAB is the most commonly used tool for educational and industrial applications. However, currently, MATLAB power system library does not have tools for power system protection (Aman et al., 2012). In this chapter, various protection measures are developed and tested to improve the safe operation of shunt active power filters. The fault protection scheme includes the detection of positive phase sequence, soft start and stop of the filter, preloading, DC capacitor discharge, regulation of frequency deviation, and suppression of voltage transients.

4.2 Voltage/current phase sequence detection

Detection of phase sequence and phase reversal of a three-phase AC supply is essential for the proper performance of three-phase active power filters. The fundamental concept to determine the phase sequence is mainly based on the calculation of the zero crossing. In ideal operating conditions, the power system is regarded as a symmetrical system, hence only the positive sequence voltages and currents exist. In the case of a fault in the power system, the positive, negative and probably zero sequence currents and voltages exist. The protection relays employ these sequence components together with phase current and/or voltage data as the input to protective elements. The sequence currents or voltages from a three-phase unbalanced set can be calculated using the following equations:

$$\text{Zero sequence component: } \mathrm{V_0} = \frac{1}{3}\,(V_a + V_b + V_c) \tag{4.1}$$

$$\text{Positive sequence component: } \mathrm{V_p} = \frac{1}{3}\,(V_a + aV_b + a^2V_c) \tag{4.2}$$

$$\text{Negative sequence component: } \mathrm{V_n} = \frac{1}{3}\,(V_a + a^2V_b + aV_c) \tag{4.3}$$

where $(V_a; V_{b;}V_c)$ are the voltage phasors at the specified frequency.

and

$$a = e^{j120^\circ} = 1\angle 120^\circ .$$

Thus, the symmetric components in the (**ABC)** sequence can be calculated as follows:

$$\begin{aligned}
V_p &= \frac{1}{3}\left(V_m e^0 + e^{j120^\circ}V_m e^{-j120^\circ} + e^{j240^\circ}V_m e^{j120^\circ}\right) = \frac{V_m}{3}\left(e^0 + e^0 + e^{j360^\circ}\right) = \frac{V_m}{3}(1+1+1) = V_m \\
V_n &= \frac{V_m}{3}\left(1 + (-\frac{1}{2} + j\frac{\sqrt{3}}{2}) + (-\frac{1}{2} - j\frac{\sqrt{3}}{2})\right) = \frac{V_m}{3}(1-1) = 0 \\
V_{zero} &= \frac{V_m}{3}\left(1 + (-\mathrm{j}\frac{\sqrt{3}}{2} - \frac{1}{2}) + (\mathrm{j}\frac{\sqrt{3}}{2} - \frac{1}{2})\right) = \frac{V_m}{3}(1-1) = 0
\end{aligned} \tag{4.4}$$

The symmetric components in the (**ACB)** sequence can be calculated as follows:

$$\begin{aligned}
V_p &= \frac{1}{3}\left(V_m e^0 + e^{j120^\circ}V_m e^{j120^\circ} + e^{j240^\circ}V_m e^{-j120^\circ}\right) = \frac{V_m}{3}\left(1 + (-\frac{1}{2} + j\frac{\sqrt{3}}{2}) + (-\frac{1}{2} - j\frac{\sqrt{3}}{2})\right) = 0 \\
V_n &= \frac{1}{3}\left(V_m e^0 + e^{j240^\circ}V_m e^{j120^\circ} + e^{j120^\circ}V_m e^{-j120^\circ}\right) = \frac{V_m}{3}(1+1+1) = V_m \\
V_{zero} &= \frac{1}{3}\left(V_m e^0 + V_m e^{j120^\circ} + V_m e^{-j120^\circ}\right) = \frac{V_m}{3}\left(1 + (-\mathrm{j}\frac{\sqrt{3}}{2} - \frac{1}{2}) + (\mathrm{j}\frac{\sqrt{3}}{2} - \frac{1}{2})\right) = 0
\end{aligned} \tag{4.5}$$

Using these calculations, a program is written in Matlab to find the right phase sequence.

Table 4.1 Phase sequence combinations

Sequences	**ABC**	**ACB**	**A -B C**	**A -B -C**	**A B -C**	**A -C B**	**A C -B**	**A -C -B**
Symmetric component	V,0,0	0,V,0	V , (-V+V*j) , -V	-V,V,V	V , (-V-V*j) , -V	(-V-V*j) , (V-V*j) , (-V+V*j)	-V , (V-V*j) , (-V-V *j)	V,-V,V

The control scheme to automatically adapt the right phase sequence is given in figure 4.1. The positive, negative and zero sequence symmetrical components are calculated using the circuits given in figure 4.2. The calculations given in figure 4.2 provide positive, negative and complex parts which are very important to select and identify the measured sequences. As for the sequences A(-B)C, AB(-C), (A-CB) and (AC-B) which yield similar components, they can be identified using the complex part of each sequence as shown in table 4.1.

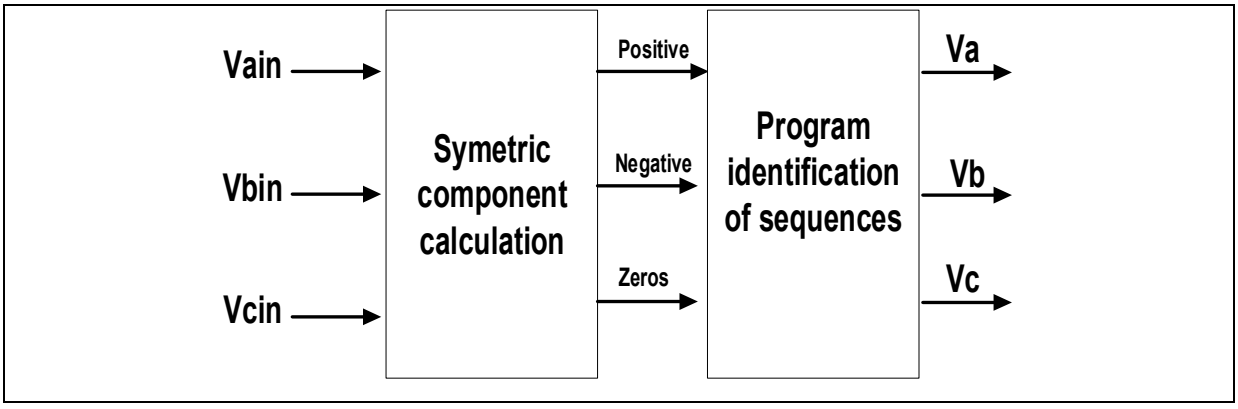

Figure 4.1 Automatic detection scheme of voltage phase sequence

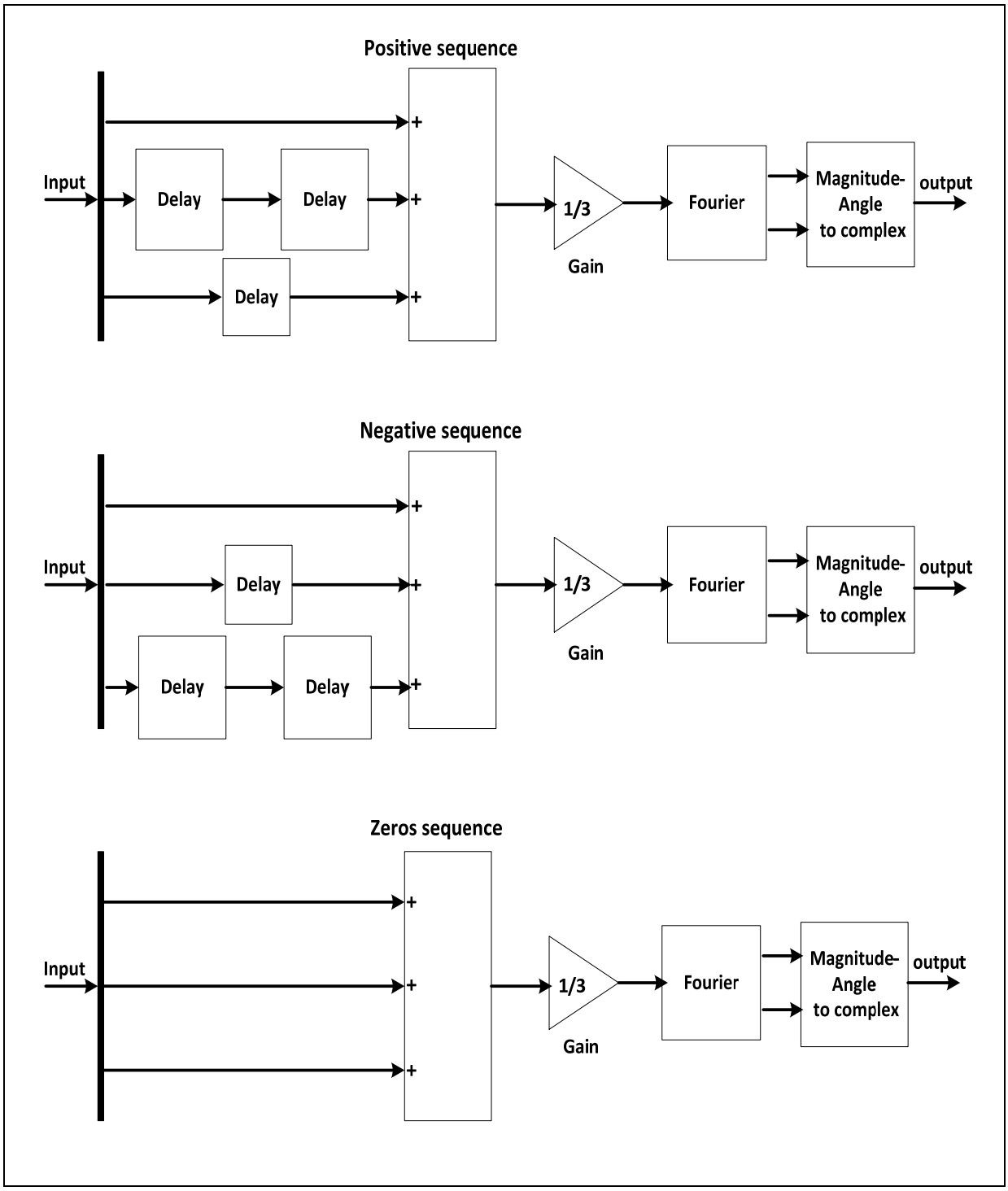

Figure 4.2 Calculations of symmetric components

4.2.1.1 Simulation results

The simulation results below demonstrate that the voltage sequence components can be efficiently identified using the automatic detection scheme.

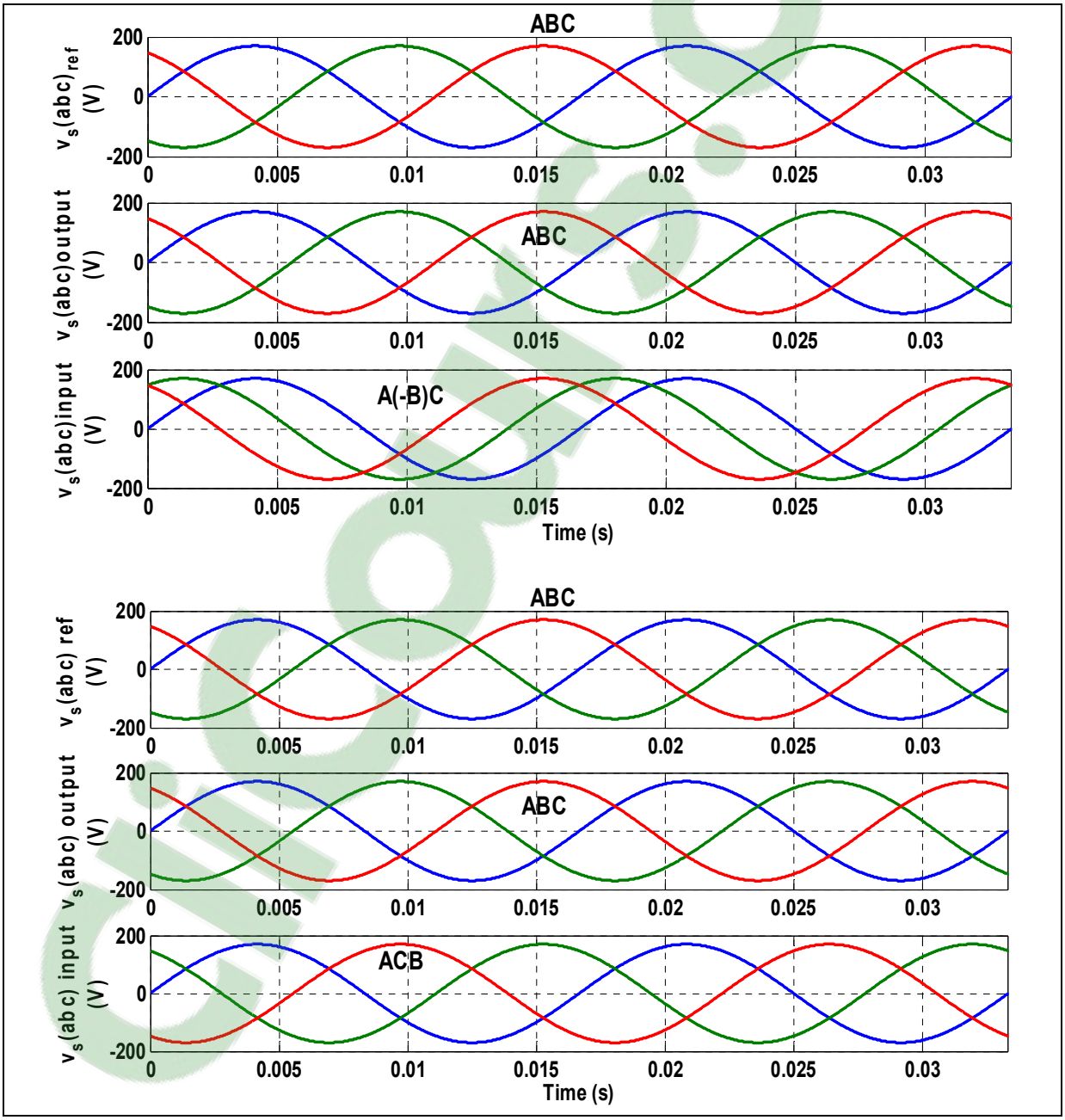

Figure 4.3 Simulation results of voltage sequences detection

4.3 Operation of the Shunt Active Filter

The mechanism to start and stop the shunt active filter is shown in figure 4.4. In this configuration, three relays are used. The charge relay is used to charge the DC bus capacitor from the 208V grid, while discharge relay is used to discharge the capacitor when the shunt active filter is stopped, and active filter relay is used to start or to stop the shunt active filter.

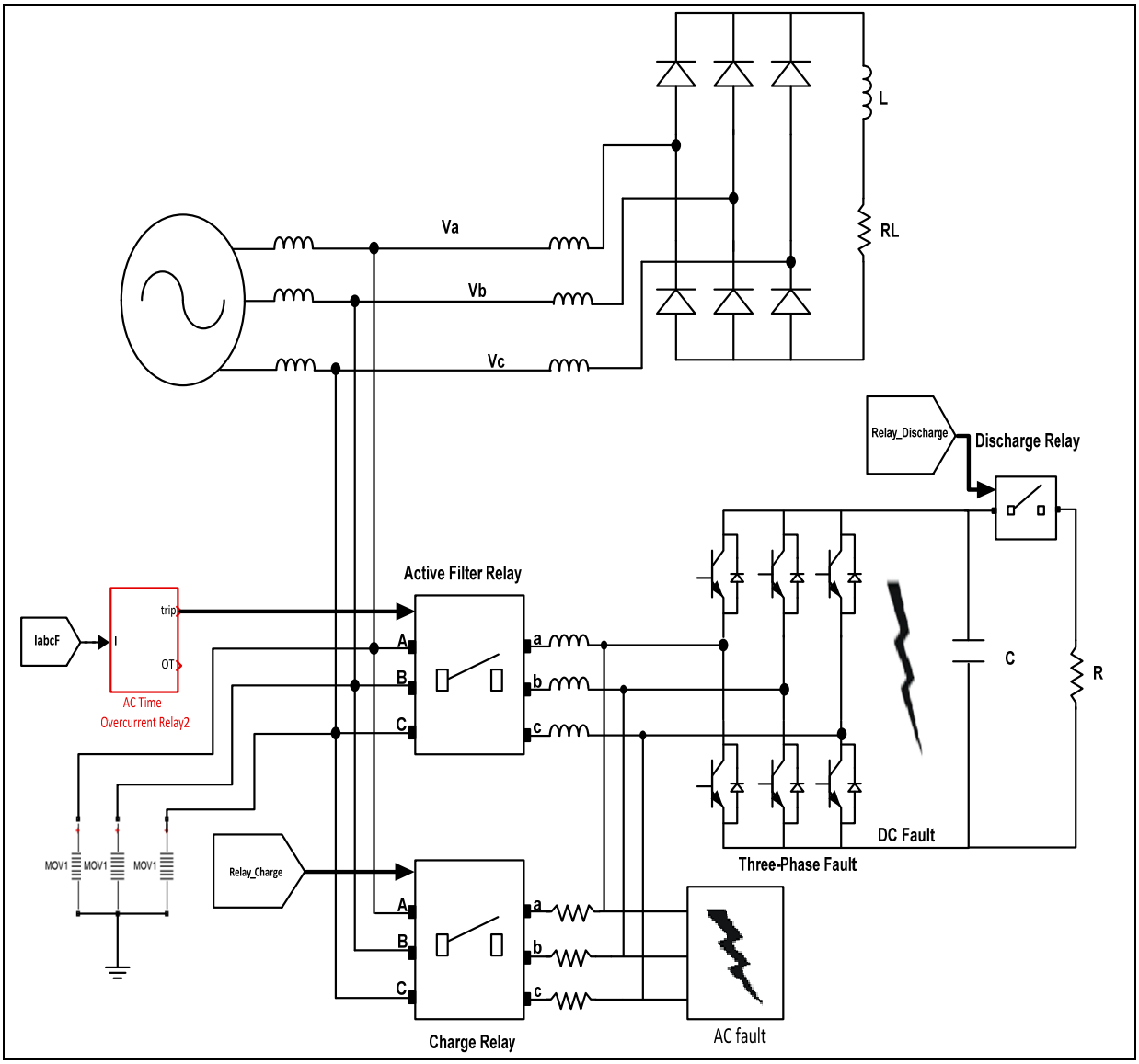

Figure 4.4 Active filter with protection scheme

4.3.1 Principle of operation

The principle to safely control the startup and the shutdown of the shunt active filter is based on controlling the slope of the DC bus voltage during starting and stopping of the active filter. The control of the slope can softly start the active filter without overcurrent. The sequence of starting or stopping the shunt active filter is given as follows:

1- The sequence of preloading the filter is initiated by charging the capacitor from the grid by setting the charge relay to on.

2- After the capacitor is fully charged, the charge relay is set to zero.

3- The control gating signals and the relay of the filter are instantaneously set to on, and the shunt active filter is started.

4- To stop the shunt active filter, the DC bus voltage capacitor has to be discharged to a certain level, then the active filter current is reduced and the filter relay is set to zero. Then the process of discharging the capacitor through the resistor is initiated by activating the discharge relay. The control scheme is given in figure 4.5.

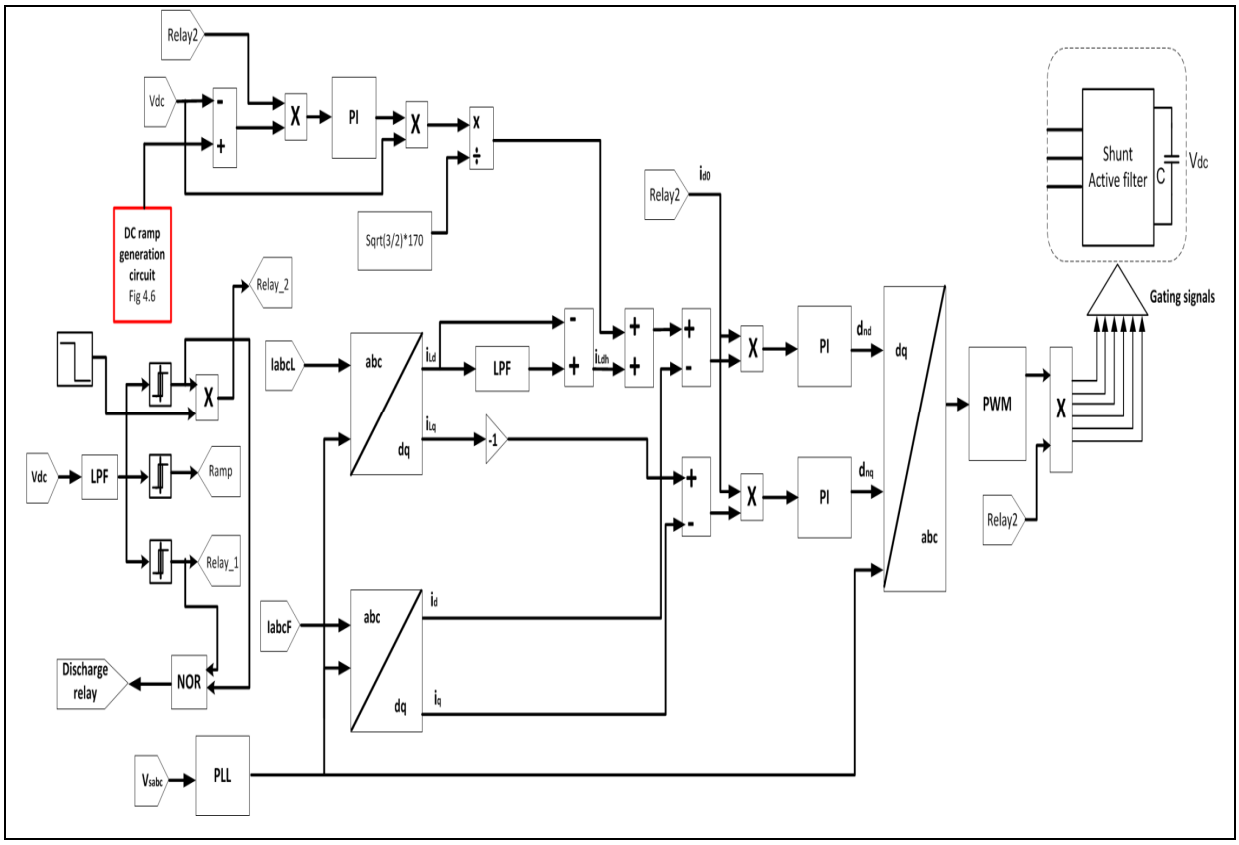

Figure 4.5 Integrated protection in the control of the active filter

4.3.1.1 Charging the DC Bus Capacitor

The problem of starting a three-phase shunt active power filter without initially charging the capacitor may damage the inverter. To charge the capacitor, charge relay is used along with a resistor to limit the charging current. Initially, the gating signals are off and filter relay is open. To charge the DC bus capacitor, charge relay has to be closed to allow the supply voltage to charge the capacitor through the freewheeling diodes at the desired current. The voltage level across the DC bus of the active filter can be calculated using the equation

$$V_{dc} = (3\sqrt{3}\, V_{smax})/\pi \qquad (4.6)$$

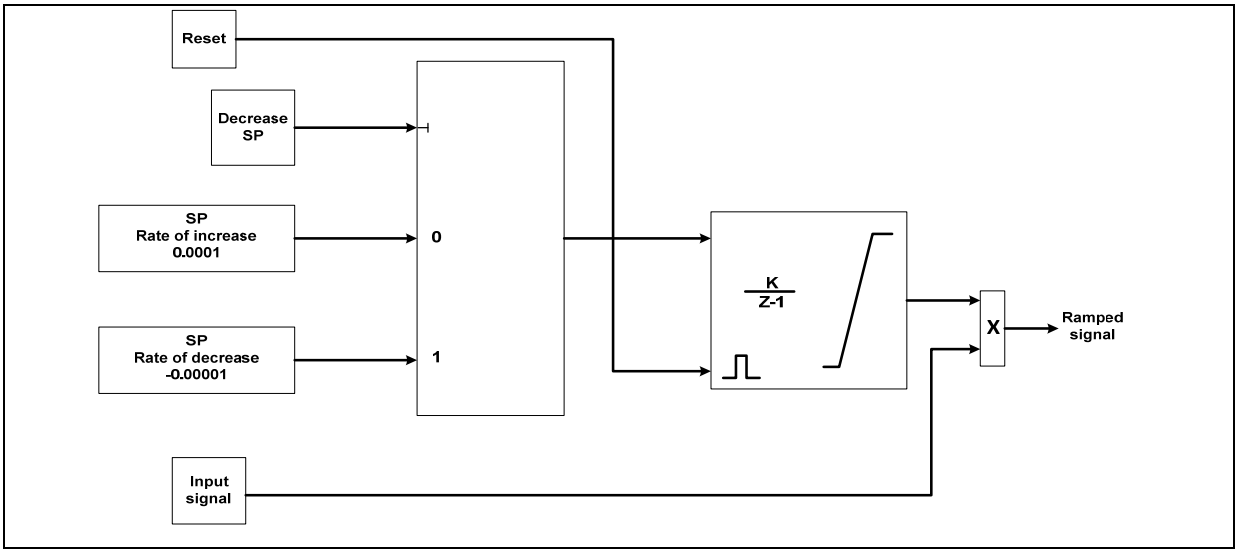

Figure 4.6 Ramp generation for DC bus voltage

4.3.1.2 Startup of the shunt active filter

Initially, the DC capacitor is supposed to be charged through the control circuit, where filter relay is closed and the gating pulses are on. The active filter can then be started smoothly and safely without overcurrent being produced. The DC bus voltage is then increased following a predetermined slope as shown in figure 4.6.

4.3.2 Frequency Deviation

Grid frequency is an important parameter in the control and protection of power systems. For power converters, the estimation of grid frequency is of major importance to ensure the proper operation and synchronization of these converters. Frequency variations may cause undesired disturbances which account for the difficulties to indicate the frequency of various signals that are needed to be defined in order to provide an accurate control system. Nowadays, signal frequency can be measured by a number of methods. In the work of (Aman et al., 2012) a digital frequency relay is developed to detect the frequency variations.

It is comprised of a frequency measuring unit and a frequency detection element. The frequency is measured by calculating the difference in time between two consecutive zero crossing (T_1 & T_2) as shown in figure 4.7.a below.

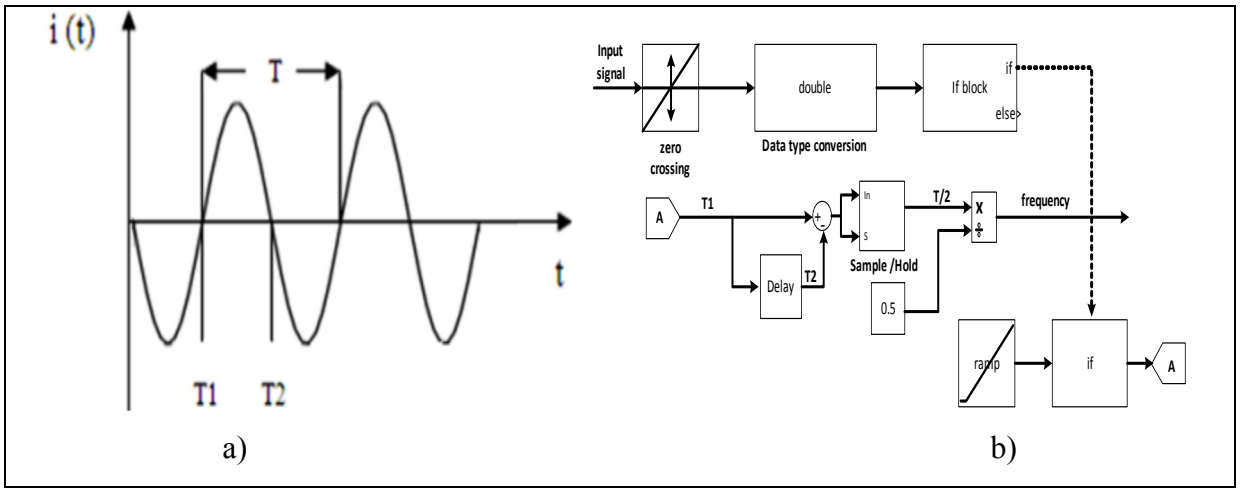

Figure 4.7 Measuring frequency of voltage signal

However, to measure the total time of a complete waveform, the difference between T_1 and T_2 is multiplied by a factor of 2, as shown in the following equation:

$$T = 2 \times (T_2 - T_1)\,, \qquad F = \frac{1}{T} = \frac{1}{2(T_2 - T_1)} \tag{4.7}$$

The hit crossing block in figure 4.7.b is applied for the detection of the zero crossing. At the instant of zero crossings, the block passes the input signal to the following if block, which in turn starts to send ramp signal to the output. Once the time extent of the ramp is measured then it could be stored in a variable called (A). Hence, the time of the next zero crossing is measured by feeding the variable (A) through a delay. A sample and hold block is also used to hold the value of time period (T/2) given by subtracting both entries of (A). After doing the required calculations, the instantaneous frequency is obtained. In case of a fault, the measured frequency sends to the frequency detection element for necessary tripping action.

4.3.2.1 Frequency Detection Element

The frequency detection element is used to perform the required action in the event of frequency variations. The output from over frequency and under frequency blocks are logically connected to an AND gate. The output of the frequency relay is set at either 1 (normal operation), or 0 (for tripping). The block diagram of the frequency detection element is shown in Figure 4.8.

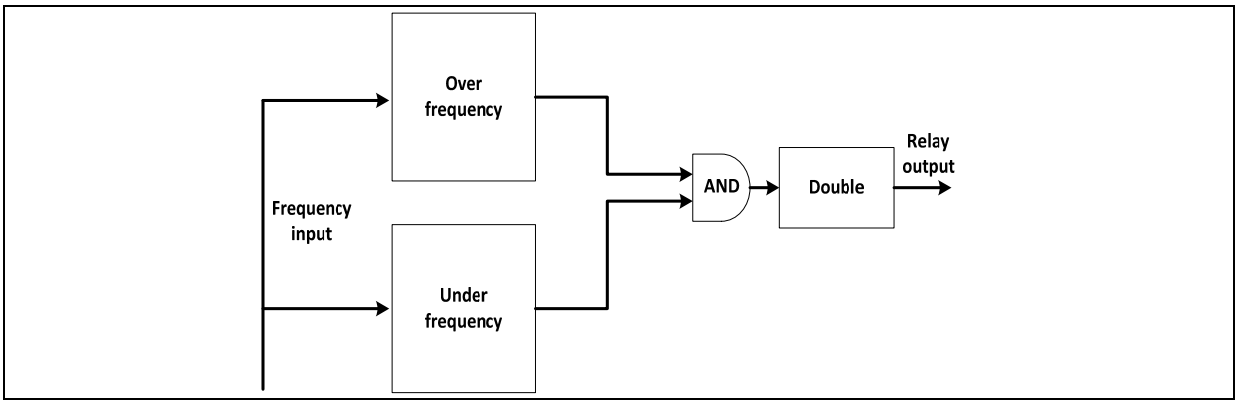

Figure 4.8 Frequency detection scheme

The frequency measurement scheme is tested under different conditions with a 60Hz grid frequency and a limit of ±3%. In the figures below the behavior of the system is observed under different load conditions. In figure 4.9 no frequency control is used in the simulation. At (t=0.15s) the grid frequency is changed to 61.8Hz, which caused the active filter to shut down and the DC bus voltage to collapse. On the other hand, when the frequency measurement scheme is applied and grid frequency is also changed to 61.8Hz, the system adapts to the variation in frequency and the performance of the active filter is stably maintained as clearly demonstrated in figure 4.10. However, if the grid frequency varies beyond the ±3% limit, the system cannot operate efficiently.

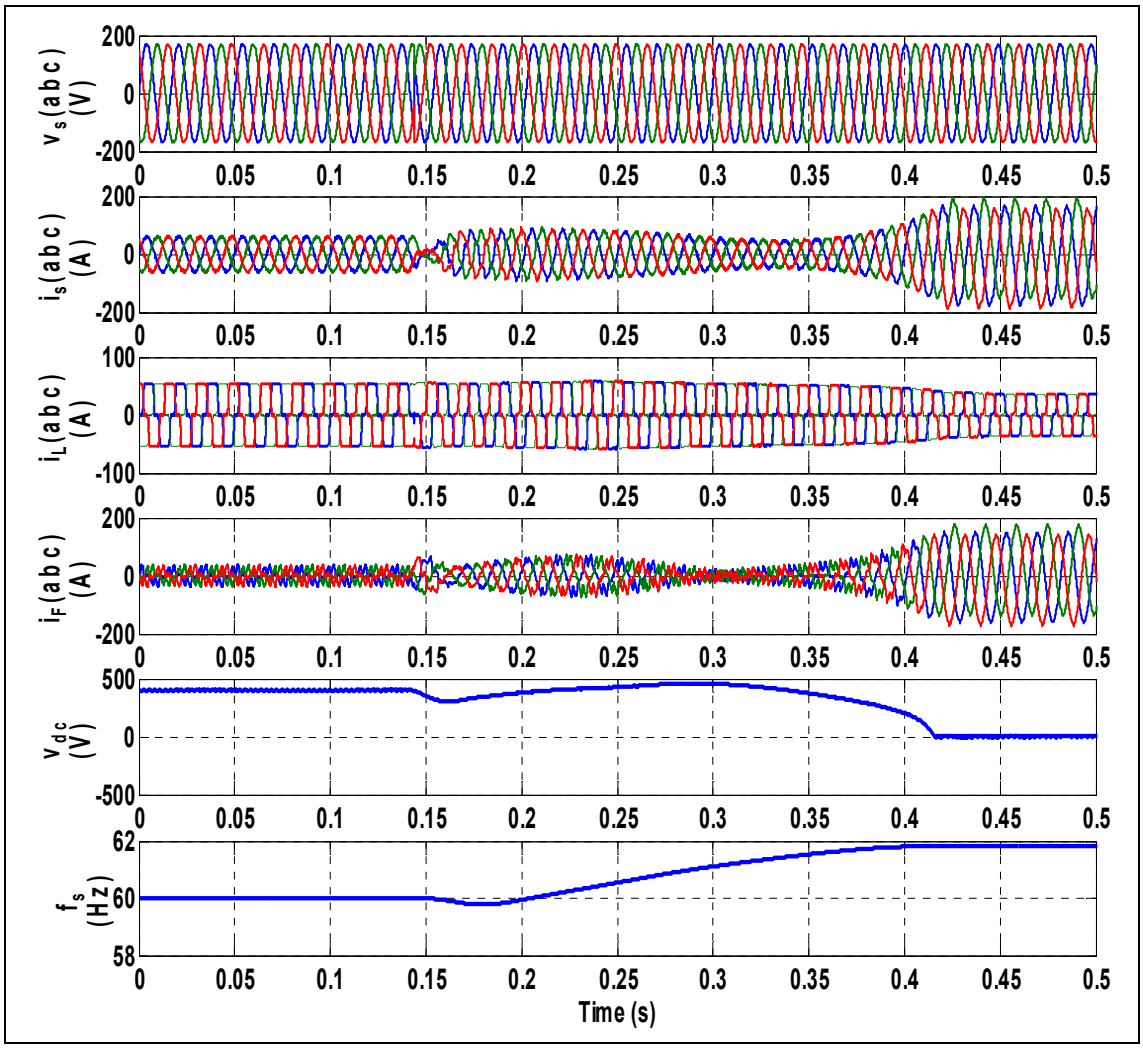

Figure 4.9 Impact of grid frequency variation without frequency measurement

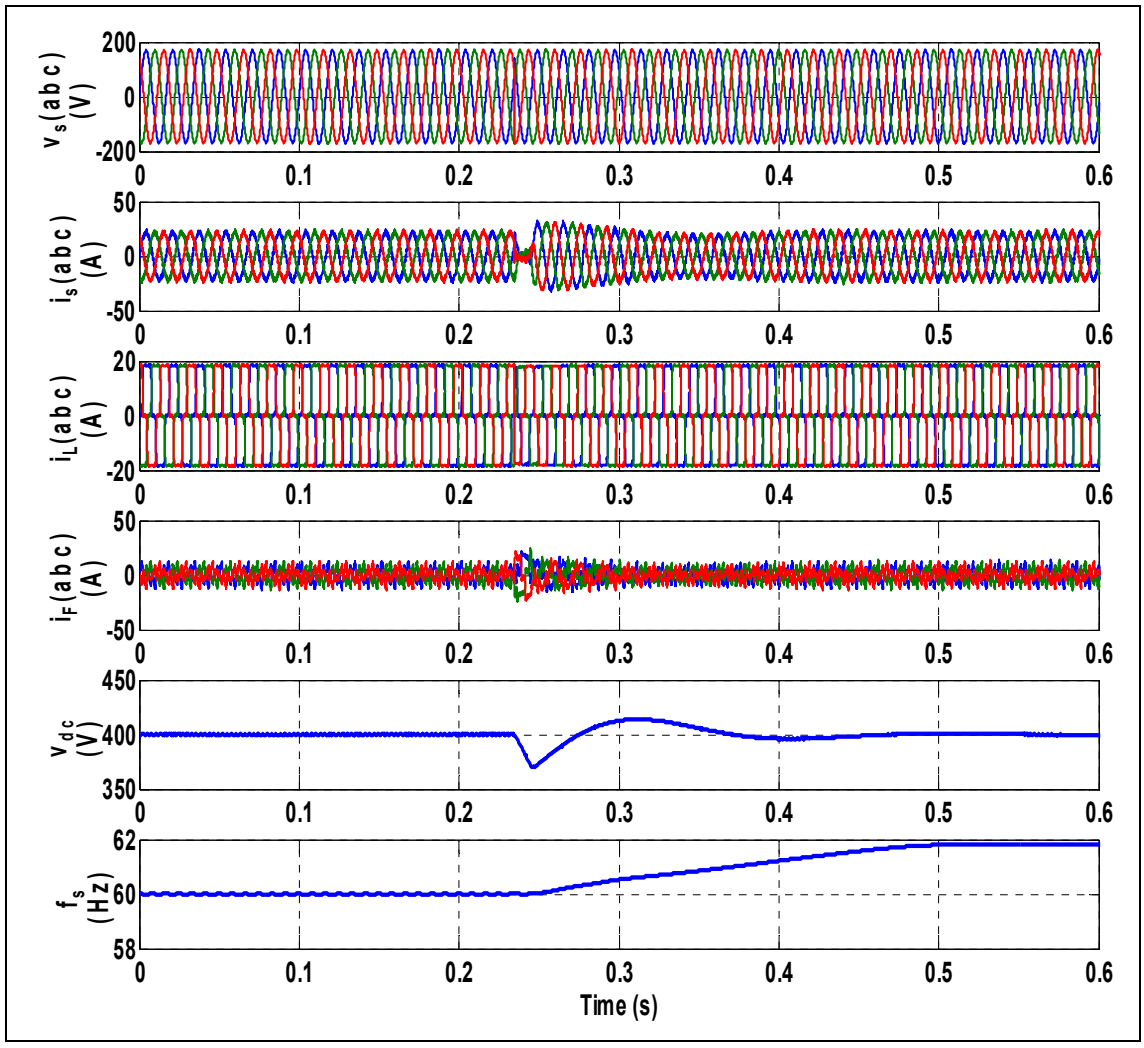

Figure 4.10 Impact of grid frequency variation with frequency measurement

4.3.3 Validation of the protection scheme using Matlab Simpower system/Simulink

The parameters used in simulation to validate the proposed protection scheme of the three-phase shunt active filter under different operating conditions are given in table 3.1. The following procedures and faults are tested to confirm the reliability of the protection scheme.

4.3.3.1 Simulation results during startup of the active filter

Figure 4.11 shows the source currents and voltages, load current, filter current and DC bus voltage, which represent the complete process of starting up, brief operation and shutting down the shunt active filter operating under normal load conditions. In the following figures zoomed segments of this figure is individually demonstrated and described.

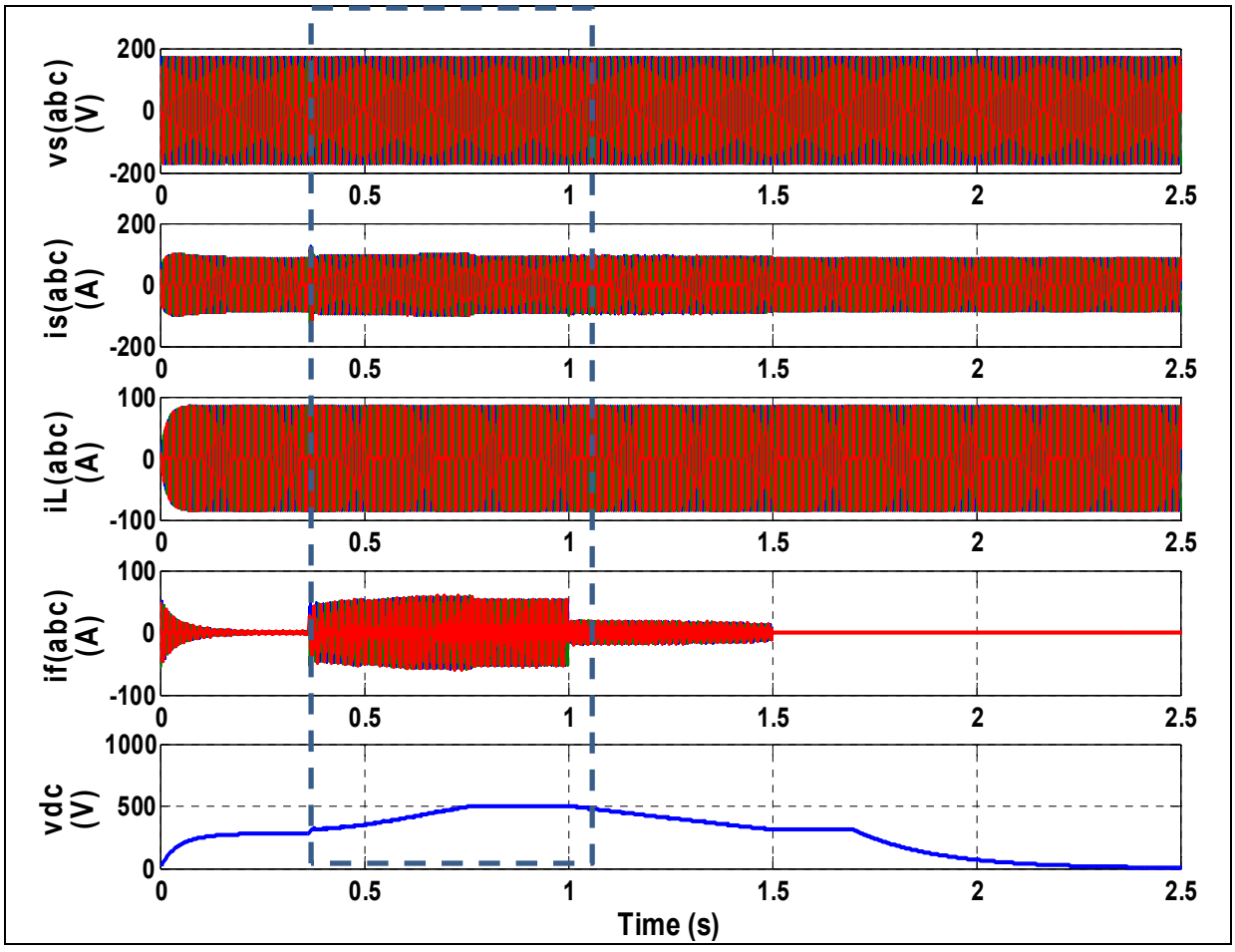

Figure 4.11 Simulation result during start and stop operation of SAF

In Figure 4.12 below, the process of preloading the active filter is shown before the filter is started at (t ≈ 0.37s), where the DC bus voltage is showing a steady charging progress.

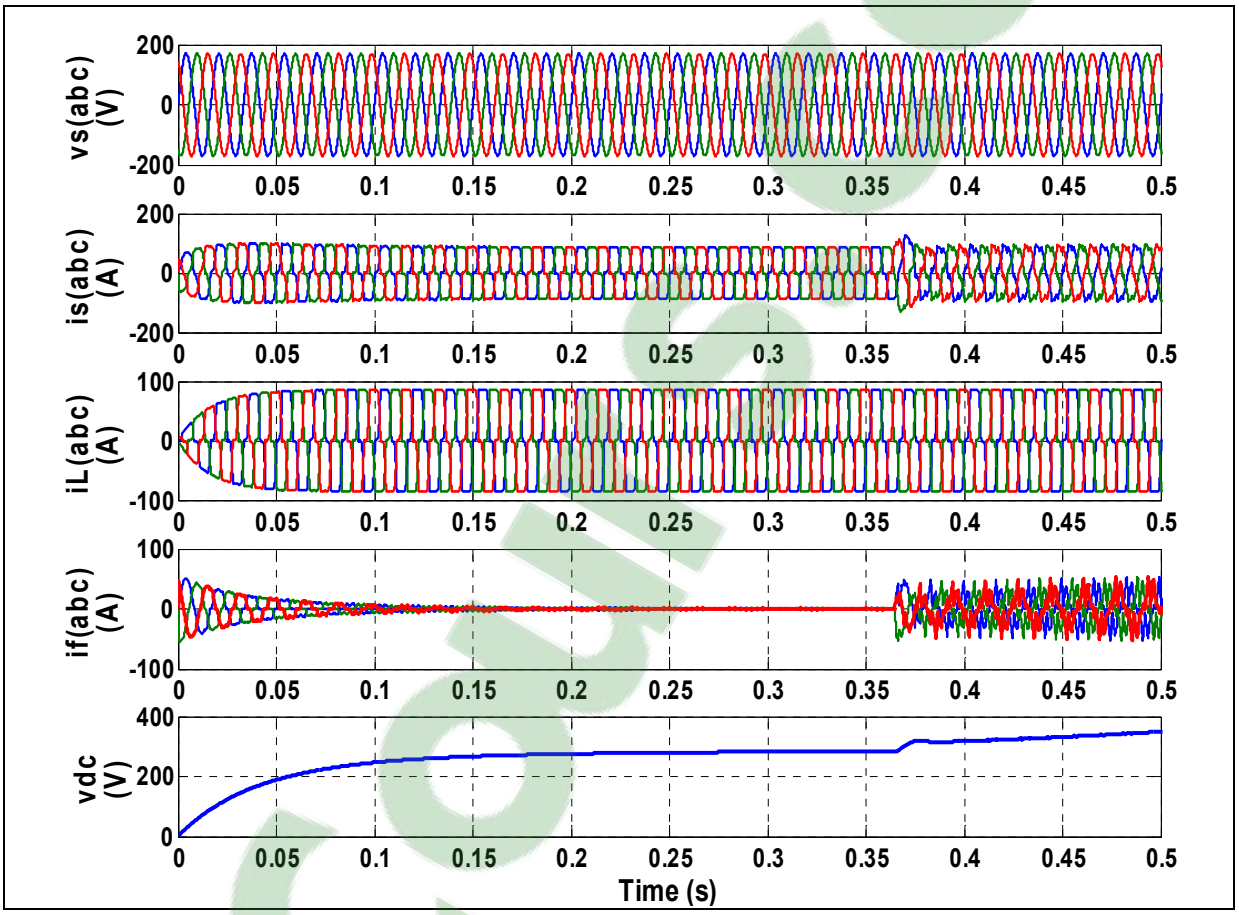

Figure 4.12 Active filter during start-up operation (Zoom1)

Following the start of the active filter at (t≈0.37s), the DC voltage (V_{dc}) reaches the reference voltage of 500V_{dc} at (t=0.75s), where the filter current (I_{Fabc}) starts to display a good compensation performance and in turn the source current (I_{Sabc}) is becoming less distorted as shown in Figure 4.13.

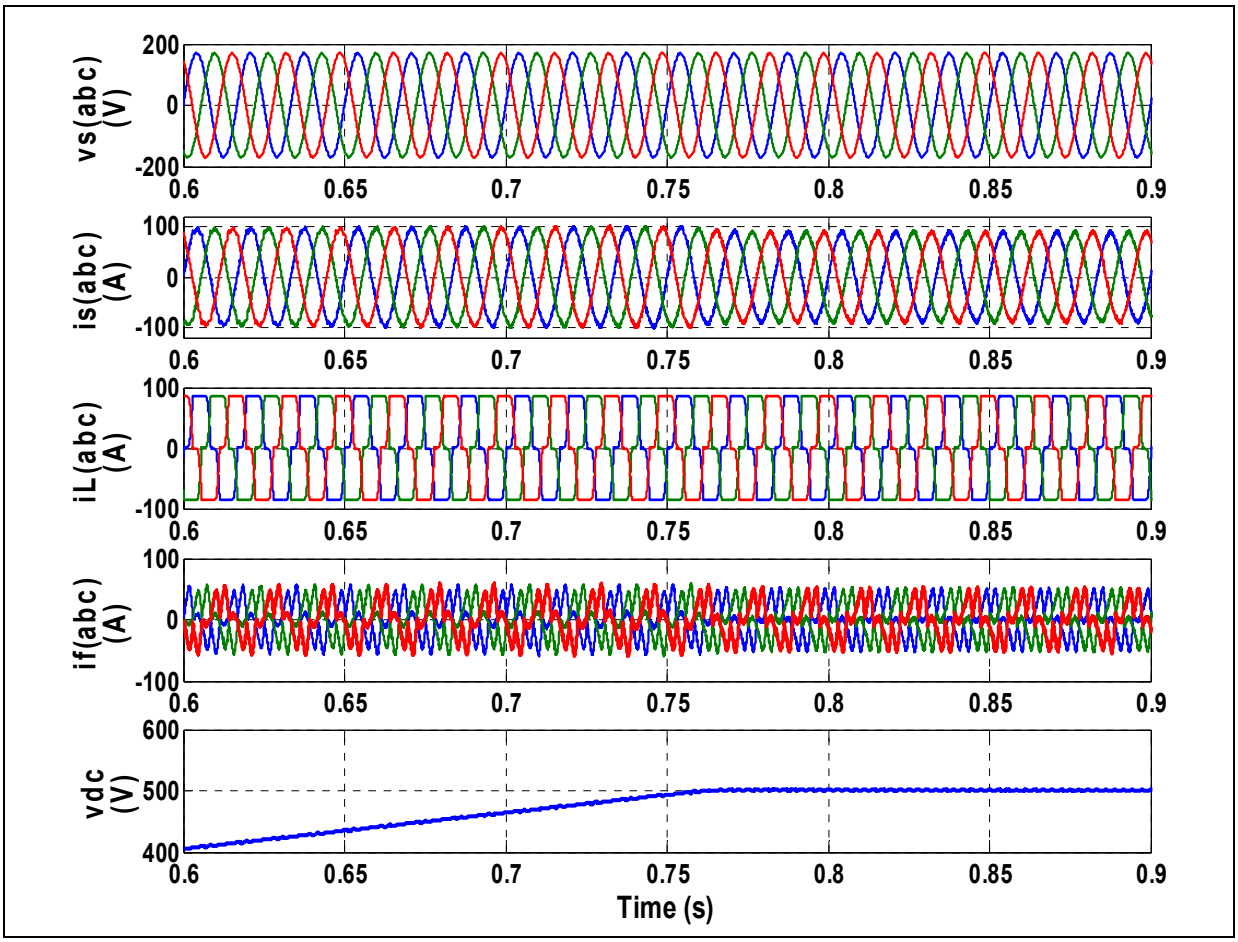

Figure 4.13 Active filter during start-up operation (Zoom2)

4.3.3.2 Simulation results during stop of the active filter

In Figure 4.14, the active filter is stopped at (t=1s), which initiates the DC voltage ramp slope control causing the DC bus voltage to decline and the filter current to decrease in order to allow for the smooth disconnection of the active filter. As a result, the filter relay is opened at (t=1.5s) as shown in figure 4.15. The process to discharge *C* starts at (t=1.7s) by closing the discharge relay as shown in Figure 4.16 allowing V_{dc} to decline to zero and eventually the safe shutdown of the active filter.

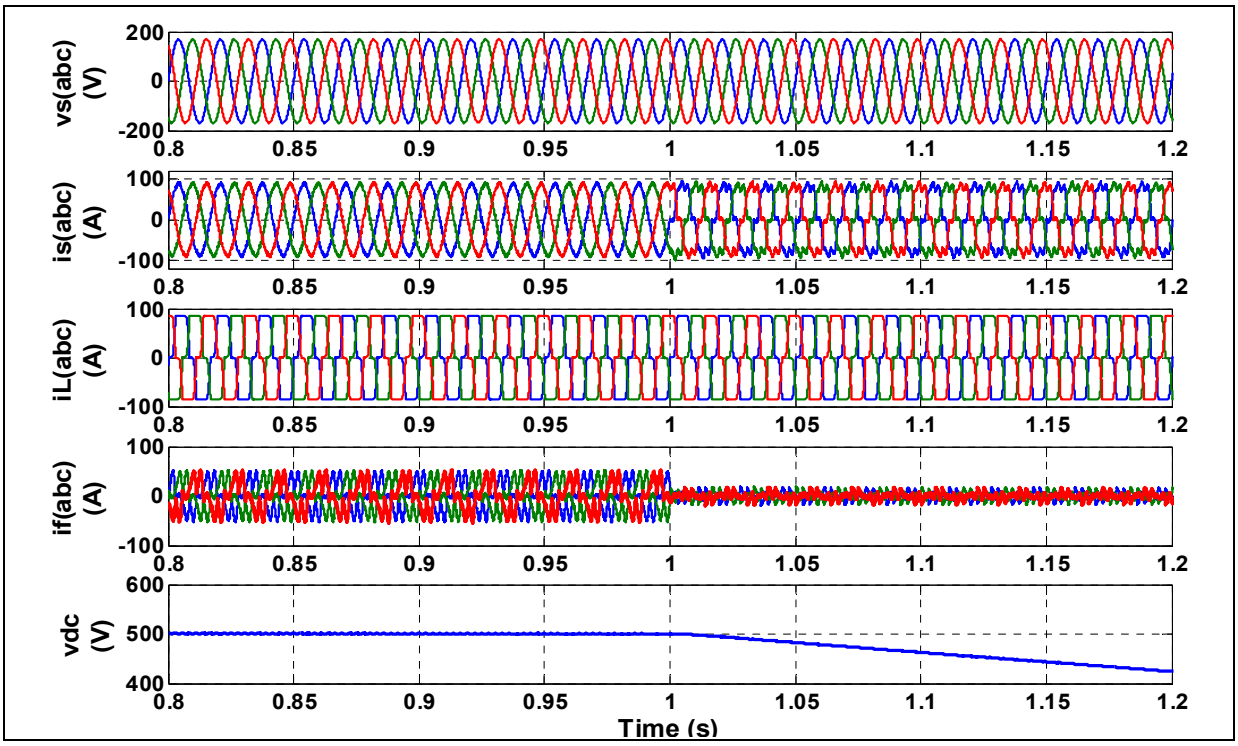

Figure 4.14 Active filter during stop operation

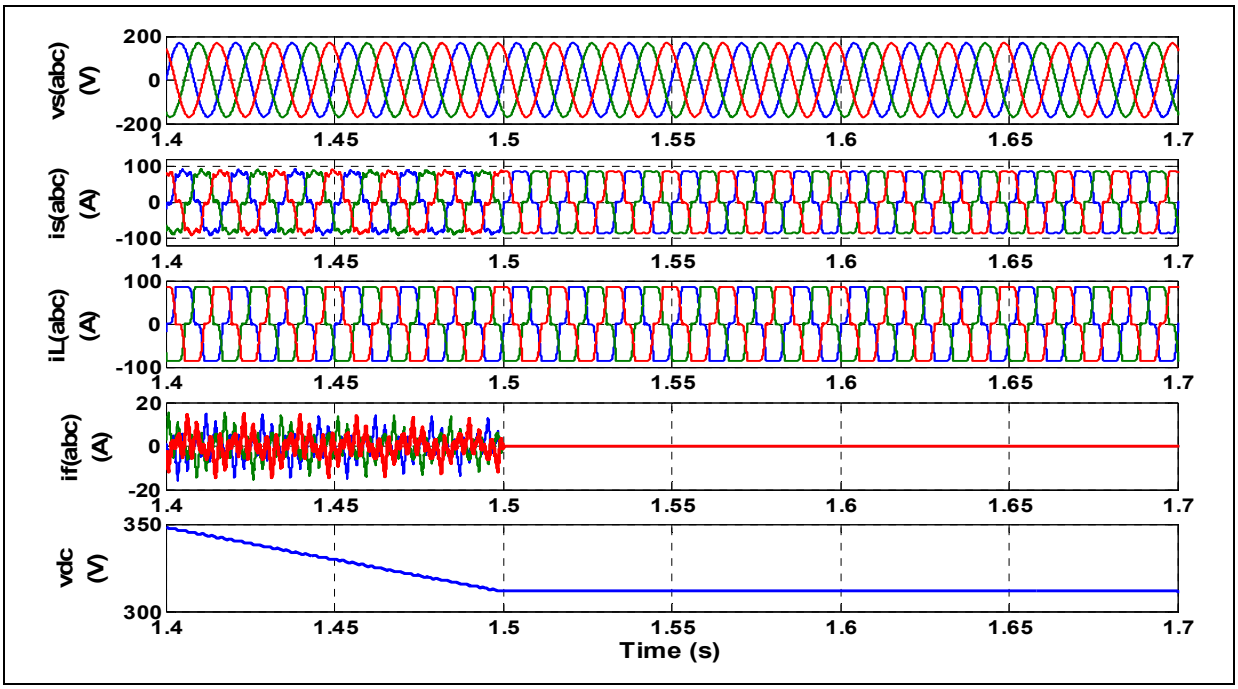

Figure 4.15 Active filter during stop operation (Zoom1)

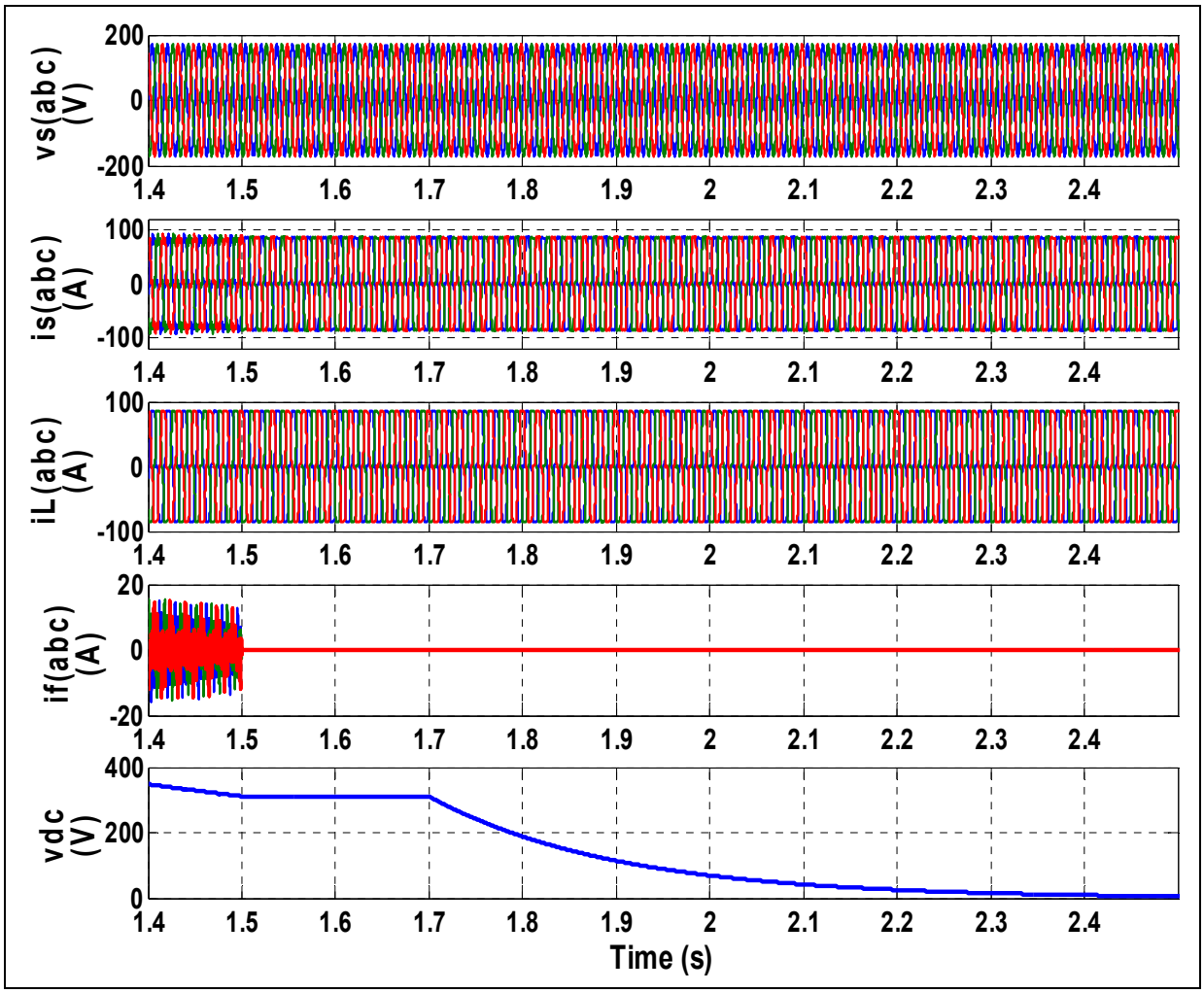

Figure 4.16 Active filter during stop operation (Zoom2)

4.3.3.3 Simulation results during AC fault

The performance of the active filter is observed under a three-phase AC fault using an extremely inverse overcurrent protection relay as shown below in figure 4.17. At (t=1s) a three-phase AC fault is introduced causing overcurrent in source current, filter current and a surge in source voltage. After a preset time delay, the OCR is activated to clear the fault and stop the shunt active filter from the operation.

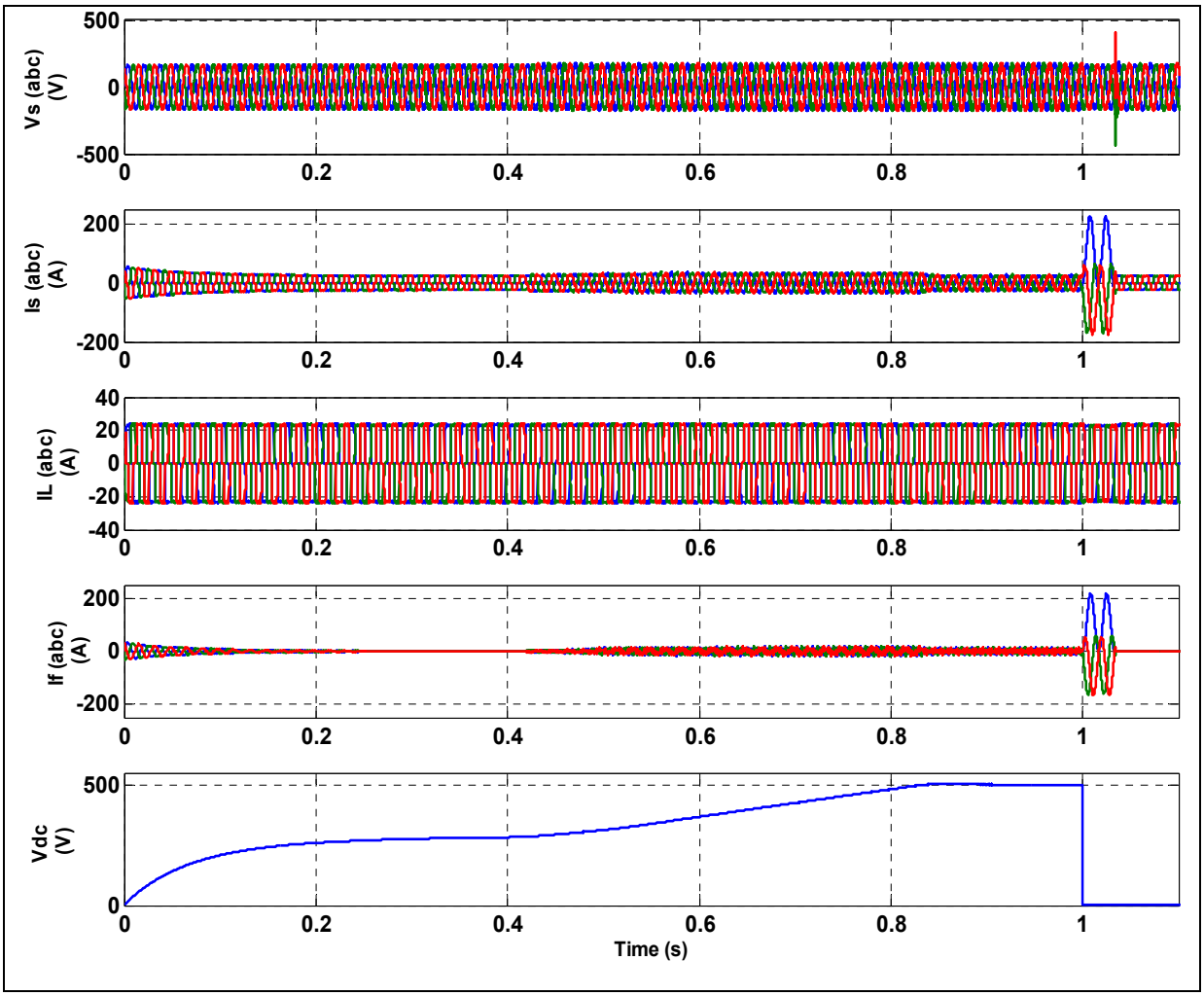

Figure 4.17 Active filter during AC fault using extremely inverse OCR

As a result of the three-phase AC fault on the filter, voltage transients appeared in the source voltages. Thus a MOV protection device is used in order to eliminate these voltage transients. Figure 4.18 is a zoomed segment of the fault in Figure 4.17. It can be seen that transients are effectively reduced to a value substantially less than the potential peak voltage that would occur if the voltage suppressing device was not used.

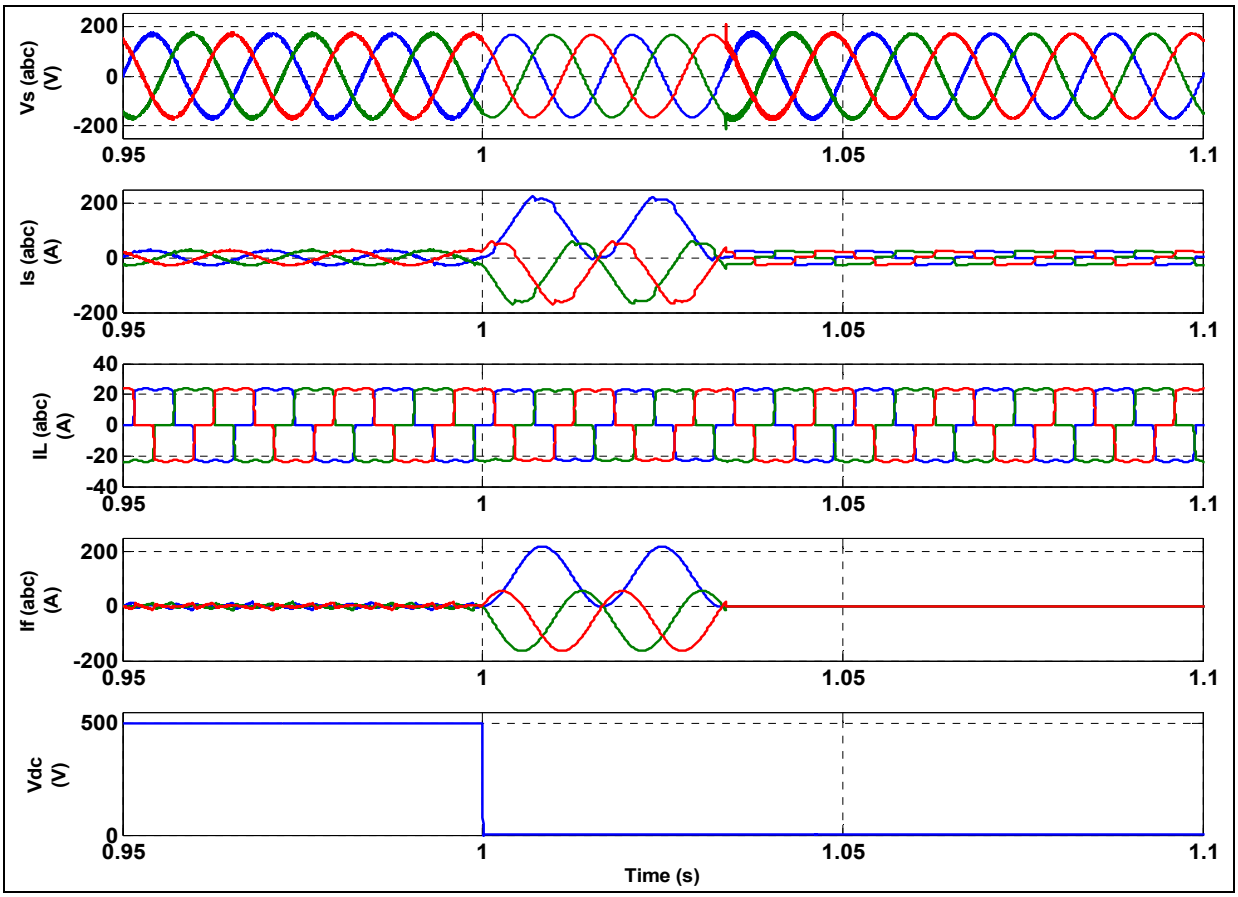

Figure 4.18 Active filter during AC fault operation using (MOV) voltage protection

4.3.3.4 Simulation results during DC fault

In this figure, the active filter is subjected to a DC fault on the DC bus. Employing the same overcurrent protection relay, the following simulation result was obtained as shown below in figure 4.19. At (t=1s) a DC fault is introduced which produced an overcurrent in source current, filter current and a surge in source voltage. In due time, the OCR is triggered, and the fault is cleared and the shunt active filter is disconnected from the operation. As for the voltage transients in the source voltages, a MOV protection device is used effectively again to remove the voltage transients.

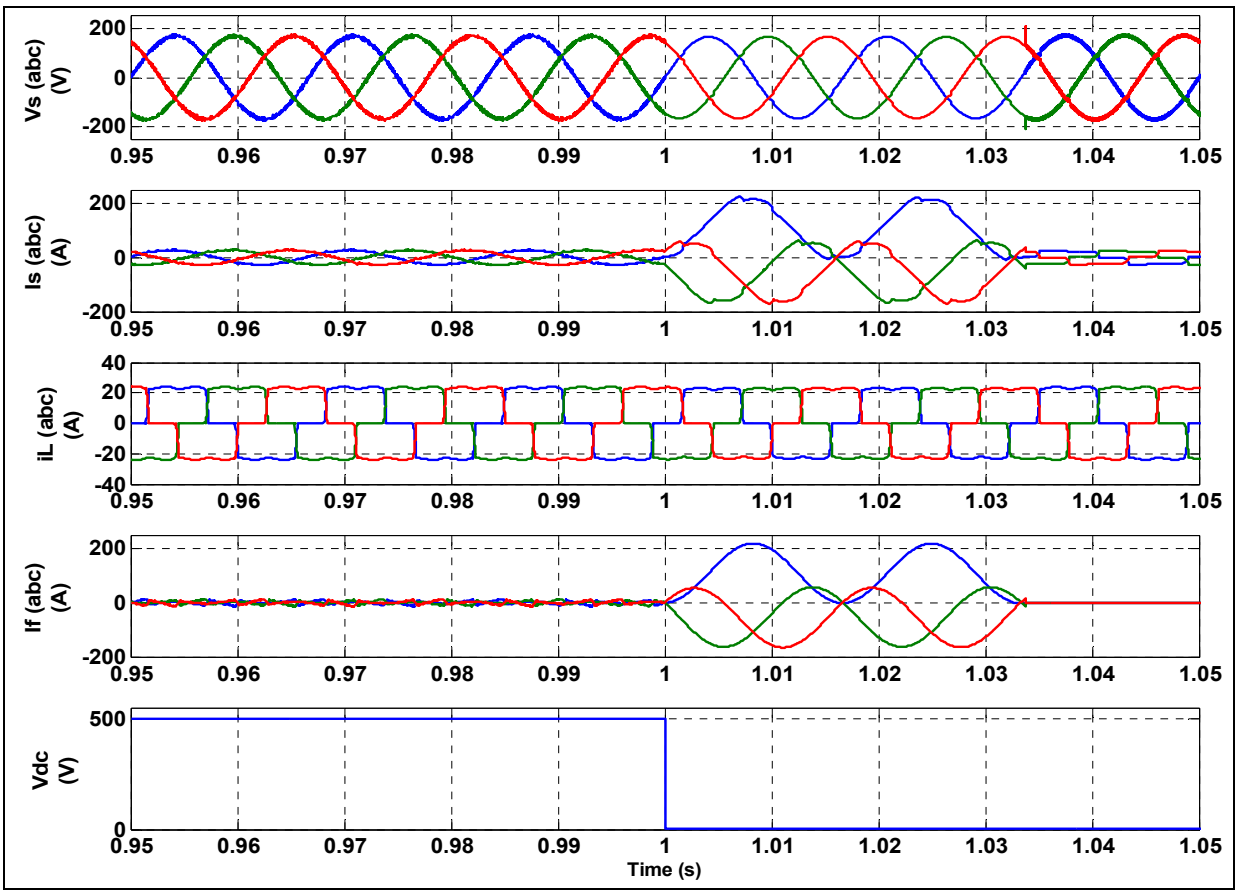

Figure 4.19 Active filter during DC fault using OCR and MOV

CONCLUSION

In the course of this research, a study was dedicated to improvements in performance and protection of shunt active filters by developing a control and protection system. The application of the active filter allows compensating for harmonic currents and reactive power, while the protection scheme offers a protection against faults occurring in the distribution power system.

In order to test the performance of the system in terms of compensation and regulation of the DC bus voltage, a nonlinear control approach was introduced and analyzed to improve harmonic compensation performance. A complementary study on the stability of the system was conducted and the steady-state error of the used PI controller is avoided by developing an anti-windup scheme. Moreover, the design factors and ratings of the shunt active filter's components are presented. We have studied different methods for the estimation of V_{dcref}, L_f and DC capacitor. A comparative study between the estimation methods of L_f and V_{dcref} in terms of compensation performance and V_{dc} regulation showed that the three estimation methods of V_{dcref} are effective in regulating the voltage V_{dc} at the output of the active filter. However, more accurate methods were proposed for determining the optimal value of DC bus voltage. Similarly, the inductor value estimation methods offered relatively good compensation performance. However, the application of the proposed load current slope based method demonstrated an improved performance and quality of source current THD.

To improve the safe operation of the shunt active filter, a protection scheme using overcurrent relays, MOVs, grid frequency variation measurement and voltage phase sequence detection was developed. It has shown that the proposed protection devices were capable to enhance the operation performance. Furthermore, a soft-start and stop mechanism is also presented to improve the initial start-up and shutdown of the filter.

The simulations carried out using the Matlab/Simulink software enabled validation and verified the feasibility of the proposed control and protection scheme.

BIBLIOGRAPHY

Akagi, H. 2005. « Active Harmonic Filters ». *Proceedings of the IEEE,* vol. 93, nº 12, p. 2128-2141.

Akagi, Hirofumi, Yoshihira Kanazawa et Akira Nabae. 1983. « Generalized theory of the instantaneous reactive power in three-phase circuits ». In *IPEC*. Vol. 83, p. 1375-1386. Tokyo.

Al-Zamil, A. M., et D. A. Torrey. 2001. « A passive series, active shunt filter for high power applications ». *IEEE Transactions on Power Electronics,* vol. 16, nº 1, p. 101-109.

Alali, MAE, S Saadate, YA Chapuis et F Braun. 2000. « Energetic study of a shunt active conditioner compensating current harmonics, power factor and unbalanced ». In *Proceedings of the International Conference on Power Electronics and Motion Control (EPE-PEMC)*. Vol. 4, p. 211-216.

Almas, M. S., R. Leelaruji et L. Vanfretti. 2012. « Over-current relay model implementation for real time simulation & Hardware-in-the-Loop (HIL) validation ». In *IECON 2012 - 38th Annual Conference on IEEE Industrial Electronics Society*. (25-28 Oct. 2012), p. 4789-4796.

Aman, Muhammad Mohsin, Ghauth Bin Jasmon, Hazlie Bin Mokhlis, Qadeer Ahmed Khan, Ab Halim Bin Abu Bakar et Mazaher Karimi. 2012. « Modeling and simulation of digital frequency relay for generator protection ». In *Power and Energy (PECon), 2012 IEEE International Conference on*. p. 701-706. IEEE.

Anderson, Paul M (1330). 1998. *Power system protection. Volume 4 of IEEE press Series on Power Engineering*. Wiley.

The Authoritative Dictionary of IEEE Standards Terms, Seventh Edition. 2000. *IEEE Std 100-2000*, p. 1-1362.

Axente, I., M. Basu, M. F. Conlon et K. Gaughan. 2010. « Protection of unified power quality conditioner against the load side short circuits ». *IET Power Electronics,* vol. 3, nº 4, p. 542-551.

Azevedo, Hélder, José Ferreira, António José de Pina Martins et Adriano da Silva Carvalho. 2003. « Direct current control of an active power filter for harmonic elimination, power factor correction and load unbalancing compensation ». *Proceedings of the EPE 2003*.

Benchaita, L., S. Saadate et A. Salem nia. 1999. « A comparison of voltage source and current source shunt active filter by simulation and experimentation ». *IEEE Transactions on Power Systems,* vol. 14, nº 2, p. 642-647.

Beom-Seok, Chae, Lee Woo-Cheol, Lee Taeck-Kie et Hyun Dong-Seok. 2001. « A fault protection scheme for unified power quality conditioners ». In *4th IEEE International Conference on Power Electronics and Drive Systems. IEEE PEDS 2001 - Indonesia. Proceedings (Cat. No.01TH8594)*. (22-25 Oct. 2001) Vol. 1, p. 66-71 vol.1.

Bhattacharya, S. 2003. *High power active filter systems*. Thesis. University of Wisconsin--Madison.

Blackburn, J Lewis, et Thomas J Domin. 2015. « Protective relaying: principles and applications ». Fourth edition, p. 695 CRC press.

Boussaid, Abdlfettah, Yassine Maouche, Ahmed Lokmane Nemmour et Abdelmalek Khezzar. 2013. « A positive and negative sequences detecting method based on an improved PQ theory for power grid synchronization ». In *Electrical and Electronics Engineering (ELECO), 2013 8th International Conference on*. p. 181-185. IEEE.

Bruyant, Nicolas. 1999. Thesis. « Etude et commande généralisées de filtres actifs parallèles. Compensation globale ou sélective des harmoniques. Régime équilibré ou déséquilibré ».

Buso, Simone, Luigi Malesani et Paolo Mattavelli. 1998. « Comparison of current control techniques for active filter applications ». *IEEE transactions on industrial electronics,* vol. 45, nº 5, p. 722-729.

Chaoui, Abdelmadjid. 2010. Thesis « Filtrage actif triphasé pour charges non linéaires ». École nationale supérieure d'ingénieurs.

Chatterjee, Kishore, BG Fernandes et Gopal K Dubey. 1999. « An instantaneous reactive volt-ampere compensator and harmonic suppressor system ». *IEEE Transactions on Power Electronics,* vol. 14, nº 2, p. 381-392.

Chiang, SJ, et JM Chang. 1999. « Design and implementation of the parallelable active power filter ». In *Power Electronics Specialists Conference, 1999. PESC 99. 30th Annual IEEE*. Vol. 1, p. 406-411. IEEE.

Drabkin, MM. 2002. « Surge protection of low-voltage AC power by MOV-based SPDs ». In *Harmonics and Quality of Power, 2002. 10th International Conference on*. Vol. 1, p. 13-16. IEEE.

Emadi, Ali, Abdolhosein Nasiri et Stoyan B. Bekiarov. 2005. *Uninterruptible power supplies and active filters*. Coll. « Power electronics and applications series ». Boca Raton, Fla.: CRC Press,, 276 p.

Etxeberria-Otadui, Ion. 2003. « Sur les systèmes de l'électronique de puissance dédiés à la distribution électrique–Application à la qualité de l'énergie ». Institut National Polytechnique de Grenoble-INPG.

Ghoshal, Anirban, et Vinod John. 2010. « Anti-windup schemes for proportional integral and proportional resonant controller » In: National Power Electronics Conference, 10 - 13th June of 2010, Roorkee..

Gotherwal, Niharika, Soumyadeep Ray, Nitin Gupta et Dipti Saxena. 2016. « Performance comparison of PI and fuzzy controller for indirect current control based shunt active power filter ». In *Power Electronics, Intelligent Control and Energy Systems (ICPEICES), IEEE International Conference on*. p. 1-6. IEEE.

Haddad, Kévork. 1996. Thesis « Design and implementation of three-phase four-wire active filters ». Concordia University.

Hao, Tianqu, Li Ran, Zheng Zeng et Wei Lai. 2016. « Fast extraction of positive and negative sequence voltage components for inverter control ». In *Power Electronics, Machines and Drives (PEMD 2016), 8th IET International Conference on*. p. 1-6. IET.

Hasan, Md, et Foisal Mahedi. 2013. Thesis « A shunt active filter for distorted voltage conditions ». The Petroleum Institute (United Arab Emirates).

Holmes, D Grahame, et Thomas A Lipo. 2003. *Pulse width modulation for power converters: principles and practice*, 18. John Wiley & Sons.

Hsu, Chin-Yuan, et Horng-Yuan Wu. 1996. « A new single-phase active power filter with reduced energy-storage capacity ». *IEE Proceedings-Electric Power Applications,* vol. 143, n^{o} 1, p. 25-30.

IEEE Recommended Practices and Requirements for Harmonic Control in Electrical Power Systems. 1993. « ». *IEEE Std 519-1992*, p. 1-112.

Jain, Shailendra Kumar, et Pramod Agarwal. 2003. « Design simulation and experimental investigations, on a shunt active power filter for harmonics, and reactive power compensation ». *Electric Power Components and Systems,* vol. 31, n^{o} 7, p. 671-692.

Jamarani, Mohammad, Adib Abrishamifar, Mohammad Pichan et Mehdi Fazeli. 2014.
« Evaluation of different positive sequence detection structures applied to grid-connected systems ». In *Power Electronics, Drive Systems and Technologies Conference (PEDSTC), 2014 5th*. p. 126-130. IEEE.

James, Sisira. 2014. Thesis « Investigation of surge propagation in transient voltage surge suppressors and experimental verification ». University of Waikato.

Khadkikar, Vinod. 2008. « Power quality enhancement at distribution level utilizing the unified power quality conditioner (UPQC) ». Thèse (PhD). Montréal, École de technologie supérieure.

Kim, Sangsun. 2002. *New Approaches to Mitigate Harmonics: Development of Active Power Filters and Converters Embedded with Harmonic Filtering Functions*. Thesis (Ph.D) Texas A&M University.

Ladoux, P, et G Ollé. 2002. « Compensateur d'harmoniques et de puissance réactive ». *Système didactique, Publication RESELEC* (laboratoire d'électrotechnique et d'électronique industrielle) de Toulouse.

Lanfang, Li, Ma Hui, Xu Xiaogang, Chen Xiaoke, Sun Biaoguang et Xie Yunxiang. 2016.
« Repetitive control implementation with frequency adaptive algorithm for shunt active power filter ». In *Power Electronics and Motion Control Conference (IPEMC-ECCE Asia), 2016 IEEE 8th International*. p. 1328-1332. IEEE.

Mane, Minarti, et Mini K Namboothiripad. 2016. « Current harmonics reduction using sliding mode control based shunt active power filter ». In *Intelligent Systems and Control (ISCO), 2016 10th International Conference on*. p. 1-6. IEEE.

Mendalek, Nassar. 2003. « Qualité de l'onde électrique et moyens de mitigation ». École de technologie supérieure Thèse (PhD).

Mohan, N., & Undeland, T. M. (2007). Power electronics: converters, applications, and design. John Wiley & Sons.

Moore, PJ, Jost H Allmeling et Allan T Johns. 1996. « Frequency relaying based on instantaneous frequency measurement [power systems] ». *IEEE Transactions on Power Delivery,* vol. 11, nº 4, p. 1737-1742.

Moran, L. A., I. Pastorini, J. Dixon et R. Wallace. 1999. « A fault protection scheme for series active power filters ». *IEEE Transactions on Power Electronics,* vol. 14, nº 5, p. 928-938.

Morán, Luis A, Juan W Dixon et Rogel R Wallace. 1995. « A three-phase active power filter operating with fixed switching frequency for reactive power and current harmonic compensation ». *IEEE Transactions on Industrial Electronics,* vol. 42, nº 4, p. 402-408.

Olm, Josep M, Germán A Ramos, Ramon Costa-Castelló et Rafael Cardoner. 2010. « Odd-harmonic repetitive control of an active filter under varying network frequency: Control design and stability analysis ». In *American Control Conference (ACC), 2010*. p. 1749-1754. IEEE.

Özkaya, Hasan. 2007. « Parallel active filter design, Control, and Implementation ». MSc. Thesis. Citeseer.

Ponnaluri, S., et A. Brickwedde. 2001a. « Generalized system design of active filters ». In *2001 IEEE 32nd Annual Power Electronics Specialists Conference (IEEE Cat. No.01CH37230)*. (2001) Vol. 3, p. 1414-1419 vol. 3.

Ponnaluri, Srinivas, et Axel Brickwedde. 2001b. « System Design of Three phase Active filters using Time domain techniques ». *EPE. Power Electronics In Generation, Transmission And Distribution Of Electrical Energy. Graz, Austria*.

Pregitzer, R., J. G. Pinto, L. F. C. Monteiro et J. L. Afonso. 2007. « Shunt Active Power Filter with Dynamic Output Current Limitation ». In *2007 IEEE International Symposium on Industrial Electronics*. (4-7 June 2007), p. 1021-1026.

Rastogi, Mukul, Rajendra Naik et Ned Mohan. 1994. « A comparative evaluation of harmonic reduction techniques in three-phase utility interface of power electronic loads ». *IEEE Transactions on Industry Applications,* vol. 30, nº 5, p. 1149-1155.

Rohten, Jaime, José Espinoza, Felipe Villarroel, Marcelo Perez, Javier Muñoz, Pedro Melín et Eduardo Espinosa. 2012. « Static power converter synchronization and control under varying frequency conditions ». In *IECON 2012-38th Annual Conference on IEEE Industrial Electronics Society*. p. 786-791. IEEE.

Ronchi, F, et A Tilli. 2002a. « Design Methodology for active filters ». In *EPE-EPMC, 10th International Power Electronics and Motion Central Conference*.

Ronchi, F, et A Tilli. 2002b. « Three-phase positive and negative sequences estimator to generate current reference for selective active filters ». In *Proceedings of the 10th Mediterranean Conference on Control and Automation*. Citeseer.

Samaras, Kostas, Chet Sandberg, Chris J Salmas et Andreas Koulaxouzidis. 2007.
« Electrical surge-protection devices for industrial facilities—A tutorial review ». *IEEE Transactions on Industry Applications,* vol. 43, nº 1, p. 150-161.

Serra, Federico M, Daniel G Forchetti et Cristian H De Angelo. 2010. « Comparison of positive sequence detectors for shunt active filter control ». In *Industry Applications (INDUSCON), 2010 9th IEEE/IAS International Conference on*. p. 1-6. IEEE.

Sheng, Xu. 2016. « An improved current-limiting control strategy for shunt active power filter ». In *2016 IEEE 8th International Power Electronics and Motion Control Conference (IPEMC-ECCE Asia)*. (22-26 May 2016), p. 1306-1311.

Singh, Bhim, Kamal Al-Haddad et Ambrish Chandra. 1999. « A review of active filters for power quality improvement ». *IEEE transactions on industrial electronics,* vol. 46, nº 5, p. 960-971.

Singh, BN, P Rastgoufard, B Singh, Ambrish Chandra et Kamal Al-Haddad. 2004. « Design, simulation and implementation of three-pole/four-pole topologies for active filters ». *IEE Proceedings-Electric Power Applications,* vol. 151, nº 4, p. 467-476.

Slotine, J.J.E., et W. Li. 1991. *Applied Nonlinear Control*. Prentice-Hall.

Standard, IEC. 2004. « 61000-3-2: 2004, Limits for harmonic current emissions ». *International Electromechanical Commission. Geneva*.

Tianyuan, Tan, Jiang Qirong, Ji Jianhui et Yue Jian. 2007. « Design of security and protection system for shunt active power filter ». *Automation of Electric Power Syst,* vol. 13, nº 12, p. 81-85.

Visioli, Antonio. 2003. « Modified anti-windup scheme for PID controllers ». *IEEE Proceedings-Control Theory and Applications,* vol. 150, nº 1, p. 49-54.

Wang, Deqiang, Jing Zhao, Wei Zhang et Yuanjun Zhou. 2013. « Design and analysis of hybrid active power filter based on sliding mode control under variable network frequency ». In *Electrical Machines and Systems (ICEMS), 2013 International Conference on*. p. 1571-1576. IEEE.

Wu, R., F. Blaabjerg, H. Wang, M. Liserre et F. Iannuzzo. 2013. « Catastrophic failure and fault-tolerant design of IGBT power electronic converters - an overview ». In *IECON 2013 - 39th Annual Conference of the IEEE Industrial Electronics Society*. (10-13 Nov. 2013), p. 507-513.

Xu, L., B. R. Andersen et P. Cartwright. 2005. « VSC Transmission Operating Under Unbalanced AC Conditions—Analysis and Control Design ». *IEEE Transactions on Power Delivery,* vol. 20, nº 1, p. 427-434.